UNIVERSITÀ
DEGLI STUDI
DI BRESCIA

DOTTORATO DI RICERCA IN

Technology for Health

settore scientifico disciplinare CHIM/07

CICLO XXXVI

Carbon Capture through Accelerated Carbonation and Enhanced Stabilization of Industrial Alkaline Residues

DOTTORANDO

Giampiero Pasquale Sorrentino

SUPERVISOR

Prof. Elza Bontempi

Abstract

Accelerated carbonation technology (ACT) is a promising technology for mitigating climate change in the short- to medium-term—offering sustainable ways to both harness yet minimize carbon dioxide (CO_2) emissions into the atmosphere. This technology also poses enormous opportunities to exploit billions of metric tons of industrial alkaline residues from the energy sector worldwide that hitherto have been landfilled as hazardous wastes because of harmful leachates including salts, chlorinated and alkaline chemicals, and heavy metals. This study explores the utilization of such alkaline materials, rich in calcium and magnesium, for CO_2 sequestration via ACT. As a controlled and accelerated process that mimics natural weathering processes taking centuries, ACT subjects metal oxides, e.g., from combustion/fly ash residues, to a controlled gas stream of moist CO_2, promoting rapid mineralization to $(Ca,Mg)CO_3$—often within minutes. Foremost, this study aims to improve the feasibility of ACT for industrial applications, focusing on operating time, CO_2 sequestration efficiency, and stabilization of leachable compounds. Mixtures of various industrial alkaline residues—municipal solid waste incineration fly ash (MSWI FA) and bottom ash, coal fly ash (CFA), flue gas desulfurization residues (FGD), and cork fly ash (CkFA)—were reacted with CO_2 under varying conditions of pressure (5-45 bar), temperature (35-75 °C), and water content (0.7-1.2 L/kg). CkFA was included as a potential alternative to CFA and FGD. Carbonation efficiency and heavy metal stabilization were assessed using XRD-Rietveld, SEM-EDS, and ICP-OES techniques. The results demonstrated that mixtures of different residues exhibit superior carbonation performance compared to individual residues, achieving CO_2 uptake from 199-248 kg CO_2/mt MSWI FA under 90 minutes. The presence of water was critical for efficient carbonation, with reaction kinetics being highly dependent on the pH-value of the mixture, and high CO_2 pressures. In addition, heavy metals, such as lead and zinc, were effectively immobilized within agglomerates of calcium carbonates and aluminosilicates. Accelerated carbonation of industrial alkaline residues not only effectively captures CO_2 but also stabilizes harmful leachable elements. This technology represents a versatile approach to complement industrial carbon capture utilization and storage (CCUS) applications. It will foster cross-industry collaboration and mutual synergies, particularly in the context of anticipated carbon pricing. Finally, the resulting carbonated materials have potential applications in the construction sector, in line with circular economy principles.

Sommario

La tecnologia di carbonatazione accelerata (ACT) è una tecnologia promettente per la mitigazione dei cambiamenti climatici nel breve e medio termine, in quanto offre modi sostenibili per sfruttare e ridurre al minimo le emissioni di anidride carbonica (CO_2) nell'atmosfera. Questa tecnologia offre anche enormi opportunità di sfruttare miliardi di tonnellate di residui alcalini industriali provenienti dal settore energetico da tutto il mondo, che finora sono stati smaltiti in discarica come rifiuti pericolosi a causa di percolati nocivi, tra cui sali, sostanze chimiche clorurate e alcaline e metalli pesanti. Questo studio esplora l'utilizzo di questi materiali alcalini, ricchi di calcio e magnesio, per il sequestro di CO_2 tramite ACT. Come processo controllato e accelerato che imita i processi naturali di erosione che durano secoli, l'ACT sottopone gli ossidi metallici, ad esempio provenienti da residui di combustione/cenere, ad un flusso controllato di CO_2 umida, promuovendo una rapida mineralizzazione in $(Ca,Mg)CO_3$—spesso in pochi minuti. Questo studio mira soprattutto a migliorare la fattibilità dell'ACT per le applicazioni industriali, concentrandosi sul tempo di processo, sull'efficienza di sequestro della CO_2 e sulla stabilizzazione dei composti lisciviabili. Miscele di vari residui alcalini industriali—ceneri volanti (MSWI FA) e ceneri pesanti dell'incenerimento dei rifiuti solidi urbani, ceneri volanti di carbone (CFA), residui della desolforazione dei gas di scarico (FGD) e ceneri volanti di sughero (CkFA)—sono state fatte reagire con CO_2 in condizioni variabili di pressione (5-45 bar), temperatura (35-75 °C) e contenuto d'acqua (0.7-1.2 L/kg). Le CkFA sono state incluse come potenziale alternativa alle CFA e alle FGD. L'efficienza della carbonatazione e l'immobilizzazione dei metalli pesanti sono state valutate con tecniche XRD-Rietveld, SEM-EDS e ICP-OES. I risultati hanno dimostrato che le miscele di diversi residui mostrano prestazioni di carbonatazione superiori rispetto ai singoli residui, raggiungendo un sequestro di 199-248 kg CO_2/mt di MSWI FA in meno di 90 minuti. La presenza di acqua è fondamentale per una carbonatazione efficiente, con una cinetica di reazione fortemente dipendente dal valore del pH della miscela e da alte pressioni di CO_2. Inoltre, metalli pesanti come piombo e zinco sono stati efficacemente immobilizzati all'interno di agglomerati di carbonati di calcio e alluminosilicati. La carbonatazione accelerata dei residui alcalini industriali non solo cattura efficacemente la CO_2, ma stabilizza anche gli elementi nocivi lisciviabili. Questa tecnologia rappresenta un approccio versatile per integrare le applicazioni industriali di cattura, utilizzo e stoccaggio del carbonio (CCUS). Favorirà la collaborazione tra industrie e le sinergie reciproche, in particolare

nel contesto della prevista tariffazione del carbonio. Infine, i materiali carbonati che ne derivano hanno potenziali applicazioni nel settore delle costruzioni, in linea con i principi dell'economia circolare.

List of Papers

This dissertation is based on the following four papers:

I. **G. P. Sorrentino**; A. Zanoletti; S. Ducoli; A. Zacco; P. Iora; C. M. Invernizzi; G. Di Marcoberardino; L. E. Depero; E. Bontempi.
Accelerated and Natural Carbonation of a Municipal Solid Waste Incineration (MSWI) Fly Ash Mixture: Basic Strategies for Higher Carbon Dioxide Sequestration and Reliable Mass Quantification
Environ Res 2022, 217, 114805, https://doi.org/10.1016/j.envres.2022.114805

II. **G. P. Sorrentino**; R. Guimarães; B. Valentim; E. Bontempi.
The Influence of Liquid/Solid Ratio and Pressure on the Natural and Accelerated Carbonation of Alkaline Wastes
Minerals 2023, 13(8), 1060, https://doi.org/10.3390/min13081060

III. **G. P. Sorrentino;** R. Guimarães; A. Cornelio; A. Zanoletti; B. Valentim; E. Bontempi.
Mitigating CO_2 Emissions through an Industrial Symbiosis Approach: Leveraging Cork Ash Carbonation
Heliyon 2024, 10(12), e32893, *https://doi.org/10.1016/j.heliyon.2024.e32893*

IV. **G. P. Sorrentino**; T. E. Müller; A. Cornelio; E. Bontempi.
Long-term Carbon Capture through Carbonation and Enhanced Stabilization of Alkaline Incineration Residues
Manuscript in Preparation

Therefore, the main content of this dissertation reproduces sections, including text and graphics, in part verbatim from the aforementioned papers. Each chapter indicates which paper it is based on. The dissertation excludes the following papers:

V. E. Bontempi; **G. P. Sorrentino**; A. Zanoletti; I. Alessandri; L. E. Depero; A. Caneschi.
Sustainable Materials and their Contribution to the Sustainable Development Goals (SDGs): A Critical Review Based on an Italian Example
Molecules 2021, 26(5), 1407, https://doi.org/10.3390/molecules26051407

VI. L. Fiameni; A. Fahimi; C. Marchesi; **G. P. Sorrentino**; A. Zanoletti; K. Moreira; B. Valentim; G. Predeanu; L. E. Depero; E. Bontempi.
Phosphorous and Silica Recovery from Rice Husk Poultry Litter Ash: A Sustainability Analysis Using a Zero-Waste Approach
Materials 2021, 14(21), 6297, https://doi.org/10.3390/ma14216297

VII. G. Biava; A. Zacco; A. Zanoletti; **G. P. Sorrentino**; C. Capone; A. Princigallo; L. E. Depero; E. Bontempi.
Accelerated Direct Carbonation of Steel Slag and Cement Kiln Dust: An Industrial Symbiosis Strategy Applied in the Bergamo–Brescia Area
Materials 2023, 16(11), 4055, https://doi.org/10.3390/ma16114055

List of Figures

List of Tables

List of Nomenclature and Abbreviations

AC	Accelerated Carbonation
ACT	Accelerated Carbonation Technology
APC	Air Pollution Control
ASTM	American Society for Testing and Materials
BET	Brunauer-Emmett-Teller
BET-SA	Brunauer-Emmett-Teller Specific Surface
BF	Blast Furnaces
BOF	Blast Oxygen Furnaces
BSED	Backscattered Electron Detection
C-(A-)S-H	Calcium (Alumino)Silicate Hydrates
CCS	Carbon Capture and Storage
CCU	Carbon Capture and Utilization
CCUS	Carbon Capture Utilization and Storage
CDW	Construction\Demolition Wastes
CFA	Coal Fly Ash
CKD	Cement Kiln Dust
CkFA	Cork Fly Ash
COP21	2015 Paris Climate Change Conference
CSH	Calcium Silicate Hydrates
DAQ/PC	Data Acquisition System/Personal Computer
DS	Dry Sieving
EDS	Energy Dispersive X-ray
EDTA	Ethylenediaminetetraacetic Acid
EPA	Environmental Protection Agency
FA	Fly Ash
FGD	Flue Gas Desulfurization Residues
IC	Ion Chromatography
ICP-OES	Inductively Coupled Plasma Optical Emission Spectroscopy
IPCC	Intergovernmental Panel on Climate Change
L/S	Liquid-to-Solid
LOI	Loss on Ignition
MSW	Municipal Solid Waste
MSWI	Municipal Solid Waste Incineration
MSWI BA	Municipal Solid Waste Incineration Bottom Ash
MSWI FA	Municipal Solid Waste Incineration Fly Ash
NC	Natural Carbonation
OPC	Ordinary Portland Cement
PG	Pressure Gauge
PM	Particulate Matter
PS	Paper Sludge
PT	Pressure Transducer
SC	Sample Cylinder
SED	Secondary Electron Detector
SEM	Scanning Electron Microscopy
SS	Sewage Sludge

TC	Thermocouple
TXRF	Total X-ray Fluorescence
VP	Vacuum Pump
WS	Wet Sieving
WtE	Waste-to-Energy
XRD	X-ray Diffraction
XRF	X-ray Fluorescence

Table of Contents

Introduction of the Dissertation
"Carbon Capture through Accelerated Carbonation and Enhanced Stabilization of Industrial Alkaline Residues"

Modern society's reliance on fossil fuels and overexploitation of resources has come at a huge environmental and socioeconomic price, particularly, stemming from greenhouse gas (GHG) emissions into the atmosphere. Over the past two centuries, atmospheric carbon dioxide (CO_2) concentrations have surged from 280 ppm to 420 ppm, with projections indicating a potential rise to 550 ppm by 2050 [1]. The Intergovernmental Panel on Climate Change (IPCC) identifies anthropogenic CO_2 emissions as the primary driver of climate change [1]. Without decisive mitigation by 2030, the global average temperature could increase by 1.8-4 °C by 2100 [1]. Such an increase, in turn, could trigger severe climate effects, including extreme weather events, rising sea levels, and food scarcity [2]—ultimately, leading to forced migration of people, so-called "climate refugees" [3,4].

Given the dire urgency, a multifaceted approach is crucial to address these problems [5], including the use of alternative fuels, renewable energy sources, improved energy efficiency, and zero-emission technologies [6]. Nevertheless, with the global population expected to exceed 9.9 billion in the next 25 years, leading to an 80 % increase in energy consumption [7], short- to medium-term solutions remain paramount [1]. Thus, carbon capture utilization and storage (CCUS) technologies have emerged as key interim solutions which could reduce CO_2 emissions by 9-50 % in the industrial sector by 2050, thereby mitigating cumulative climate change by 15-55 % by 2100 [8].

Among CCUS technologies, so-called 'accelerated carbonation' strategies, have gained attention as potentially long-term and viable methods of CO_2 sequestration. Inspired by natural weathering processes, these methods help to convert CO_2 into insoluble, chemically- and thermodynamically stable carbonate minerals by carbonation reactions [9]. Alkaline earth metal-rich ores, particularly those containing calcium (Ca) and magnesium (Mg), are central to this process due to their reactivity and abundance [10]. Nevertheless, large-scale mining, itself, poses substantial economic and environmental hurdles [11], and optimizing reaction efficiency often requires physical and/or chemical pretreatments of the minerals [12].

An attractive alternative to conventional mining is utilizing industrial alkaline residues [13,14]. These by-products, readily available in billions of metric tons [15], are cost-effective and highly reactive due to their significant Ca and Mg content [9,13]. Often not requiring any pretreatment, these residues enable less energy-intensive operating conditions, thus overcoming the environmental and economic challenges of CCUS technologies [10,16].

Municipal solid waste incineration (MSWI) fly ash (FA), an alkaline residue from waste-to-energy (WtE) plants, is particularly promising for CO_2 sequestration, containing up to 55 wt.% free calcium oxide (CaO) [9]. Even so, MSWI FA, classified as hazardous waste, is typically dumped in hazardous waste landfills because of its elevated content of harmful leachates including salts, chlorinated and alkaline chemicals, and heavy metals [17,18]. With increasing production of MSWI FA in Europe and because of restrictions on landfilling [19], accelerated carbonation could be a potential way to stabilize these industrial residues, reducing the mobility of leachable elements, and ensuring their safe disposal or reuse [20,21].

While the use of industrial alkaline residues for CO_2 sequestration and stabilization is gaining interest, the combined use of different residues to enhance both processes remains underexplored. Generally, CO_2 sequestration and waste management are considered separate processes. Recent research has shown that a mixture of industrial alkaline residues—MSWI bottom ash (MSWI BA), coal fly ash (CFA), and flue gas desulfurization residues (FGD)—can simultaneously stabilize heavy metals in MSWI FA and capture CO_2 through natural carbonation in at least 1 month [22]. The resulting material is resistant to acidic environments, such as acid rain [23]. Despite its potential, this process is time-consuming because of slow reaction kinetics.

Thus, this current study explores the use of such a mixture of alkaline materials for CO_2 sequestration via accelerated carbonation technology (ACT). The hypothesis involves subjecting metal oxides, found in industrial alkaline residues, to a controlled gas stream of moist CO_2, thereby promoting rapid carbonation within minutes. Foremost, this study aims to enhance the feasibility of ACT for large-scale industrial applications, focusing on substantially reducing operating time, improving CO_2 sequestration efficiency, and stabilizing leachable compounds. It also investigates the potential use of alternative residues, such as cork fly ash (CkFA), as substitutes for CFA and FGD, considering that biomass combustion residues are reputed as carbon-neutral.

Aim of the Dissertation and Paper Contributions

The primary aim of this study is to bolster ACT by using the patented[1] technology developed by the Chem4Tech research group (RENDERING project) as a starting point. The specific objectives are:

1. **Assess the suitability of industrial alkaline residues for ACT:**
   Conduct a comprehensive characterization of residues, including particle-size distribution, immediately soluble content, magnetic and paramagnetic separation, BET analyses, ICP-OES analyses on digested and leaching solutions, IC and XRF analyses, XRD-Rietveld, SEM-EDS analyses, LOI, and Total C determination.
2. **Study the feasibility of ACT using the original patented recipe:**
   Perform trials at an initial CO_2 pressure of 15 bar and room temperature, comparing the carbonation and stabilization results with natural carbonation trials performed according to the RENDERING project.
3. **Evaluate the versatility of the technology:**
   Explore the substitution of CFA and FGD with alternative residues such as cork fly ash (CkFA), considering that biomass combustion residues are reputed as carbon-neutral, and compare the results with those obtained using the original recipe.
4. **Investigate the effects of key factors on CO_2 diffusivity:**
   Study the influence of variables such as liquid-to-solid ratio, CO_2 pressure, and agitation, comparing the results with natural carbonation trials.
5. **Improve CO_2 uptake and stabilization performance**:
   Enhance the overall performance of the AC process, focusing on the efficiency of CO_2 sequestration and the stabilization of leachable compounds, thereby improving environmental and operational outcomes.

The effectiveness of the carbonation was evaluated using XRD-Rietveld, LOI, and Total C determination, while the stabilization was assessed using leaching experiments coupled with TXRF, and ICP-OES analyses, supported by SEM-EDS analyses.

[1] Patent number 102019000006651

This dissertation is structured around four papers referred to using Roman numerals (cf. List of Papers), each contributing to different stages of the research. **Figure 1** provides an overview of the dissertation, linking each paper to its respective focus area.

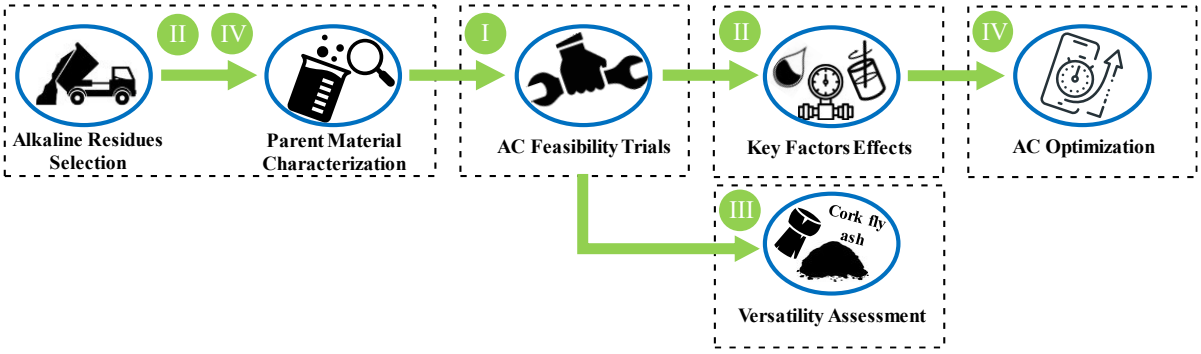

***Figure 1**: Focus areas of the papers (I to IV) contributing to this dissertation.*

Dissertation Outline

Chapter 1: A brief overview of the global challenge posed by CO_2 emissions and the strategies developed to mitigate climate change, with a focus on CCUS technologies.

Chapter 2: Introduction to the theoretical foundation of ACT, focusing on *ex situ* methods, by discussing both direct and indirect carbonation processes, emphasizing the use of industrial alkaline residues in ACT.

Chapter 3: A detailed overview of the nature and properties of the industrial alkaline residues used in this study, i.e., MSWI FA, MSWI BA, CFA, FGD, and CkFA.

Chapter 4: A description of the experimental activities, including sample preparation, carbonation test setups, and analytical techniques employed.

Chapter 5: Presentation of the comprehensive characterization results of the industrial alkaline residues by discussing their suitability for ACT.

Chapter 6: Report on the results from AC feasibility tests, including the use of CkFA as an alternative residue. It also examines the impact of water content, CO_2 pressure, and agitation on CO_2 diffusivity, and presents the results from optimizing AC experiments with a focus on CO_2 uptake and leachable compound mobility.

Chapter 7: A summary of the results, conclusions drawn on the efficacy of carbonation in the context of CCUS technologies, and an outlook on future development possibilities.

Chapter 1: Carbon Capture Utilization and Storage: Methods and Technologies

This chapter provides a brief overview of the global challenges posed by carbon dioxide (CO_2) emissions and various strategies to mitigate their impact on climate change. The central role of CO_2 in driving the climate crisis is discussed, highlighting the urgent need for emission reductions to mitigate further environmental impacts. Attention is given to international efforts to limit the rise in global average temperature, focusing on key agreements such as the Paris Agreement, and the technological innovations needed to meet these ambitious targets.

Regarding technological innovations, carbon capture utilization and storage (CCUS) is introduced as a suite of technologies designed to capture CO_2 emissions from industrial and energy sources, transport them to storage sites, and either permanently sequester or convert the CO_2 into useful products. The aim is to assess the potential of CCUS as a short- to medium-term solution for reducing atmospheric CO_2 emissions while exploring the challenges associated with its deployment, including high energy requirements and economic barriers.

The chapter is structured as follows:

- **Section 1.1**: The role of CO_2 in climate change, focusing on the environmental crisis and the global effort to reduce emissions.
- **Section 1.2**: An overview of CCUS technologies, including the capture, transportation, storage, utilization, and conversion of CO_2.

1.1 Carbon Dioxide and its Role in the Climate Crisis

Anthropogenic CO_2 emissions are the primary driver of climate change [1]. Over the last 250 years, their rise is largely caused by industrial processes, consumption of fossil fuels (i.e., coal, oil, and natural gas), and land-use changes such as deforestation, soil erosion, and animal farms [2,24]. The ongoing economic growth in emerging countries continues to spur global energy consumption which, combined with the slow transition to renewable energy, implies that fossil fuels will dominate the energy mix until at least 2030 [25,26].

The yearly global greenhouse gas (GHG) emissions are estimated in billions of metric tons of CO_2 equivalent (Gt $CO_{2\text{-eq}}$/year). In 2019, GHG emissions reached 59 ± 6.6 Gt $CO_{2\text{-eq}}$ [1], making amounting to a 54 % increase since 1990 (**Figure 2**[2]).

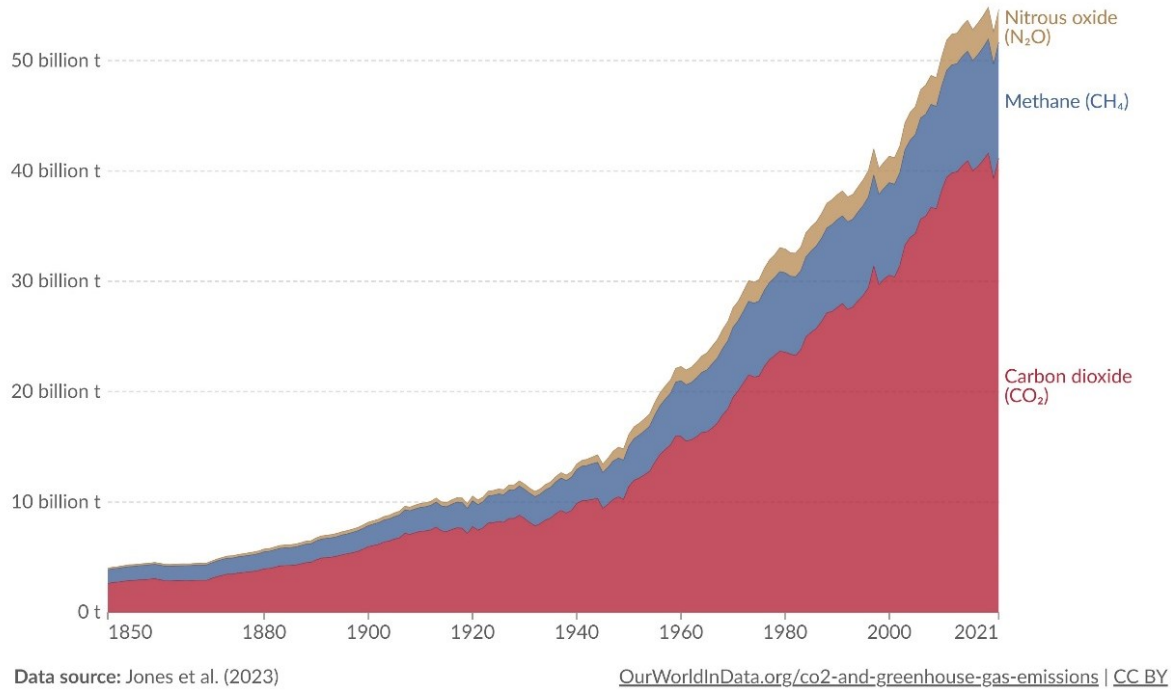

***Figure 2**: Greenhouse gas emissions from all sources from 1850 to 2021, including agriculture and land-use change, measured in mt $CO_{2\text{-eq}}$ over a 100-year timescale.*

This has prompted significant concern from governments, industry, and academia and calls to act. Various measures have been proposed and implemented to address this stark increase in GHG, such as the Kyoto Protocol of 1997, which aimed to reduce emissions by 5 % from 1990 levels in industrialized countries. Nonetheless, the agreement's effectiveness was limited due to non-compliance and withdrawals. Substantial progress was made at the 2015 Paris Climate Change Conference (COP21), where 196 countries committed to limit the annual increase in

[2] [249] – with major processing by Our World in Data

global average temperature to no greater than 1.5 °C above pre-industrial levels by 2050 [27]. This commitment included a 45 % emissions reduction by 2030 [27].

To achieve these goals, countries are also collaborating under the 17 Sustainable Development Goals (SDGs), introduced with the "2030 Agenda for Sustainable Development", focusing on advancing renewable energy and supporting economically disadvantaged countries [28]. In addition to international agreements, several economic and technological measures have been explored to mitigate CO_2 emissions. Carbon pricing mechanisms play a key role in incentivizing emission reductions. Two main types are [29]:

1. Emissions Trading Systems (ETS), which allow low-emission sectors to trade excess allowances with higher-emission sectors, creating a marketplace for emission permits.
2. Carbon taxes, which place a direct tax on the carbon content of fossil fuels or GHG emissions.

These systems encourage industries to adopt cleaner technologies, enhance energy efficiency, and shift toward renewable energy sources [30,31].

1.2 Carbon Capture Utilization and Storage (CCUS) Technologies

Addressing climate change requires multifaceted strategies to reduce CO_2 emissions, including preventive measures and direct extraction from flue gases [5]. Preventive approaches focus on improving energy efficiency by enhancing energy conversion technologies, utilizing alternative fuels such as biomass or renewable energy sources, and adopting zero-emission methods [6]. By contrast, direct CO_2 extraction refers to carbon capture utilization and storage (CCUS) technologies [1]. It is essential to interweave these strategies as a whole to accomplish the goal of reducing emissions.

The development of CCUS typically involves three separate stages [32] (**Figure 3**[3]): (i) separating CO_2 from industrial flue gas; (ii) transporting it to a storage location, and (iii) either storing or utilizing the CO_2.

Separation remains one of the most challenging stages, as current technologies are energy-intensive, and only a few are widely adopted due to their high cost and the large volume of flue gas to be treated [33].

Transporting CO_2 to storage sites usually relies on pipelines or ships [1]. Recent research suggests reusing existing transportation methods to reduce costs [34,35]. Nevertheless, road

[3] made as an adaptation from [250]

and rail transport of CO_2 is only feasible for small-scale operations due to technical requirements, such as maintaining a temperature of -35 °C and a pressure of 22 bar [36], making this option economically unfavorable.

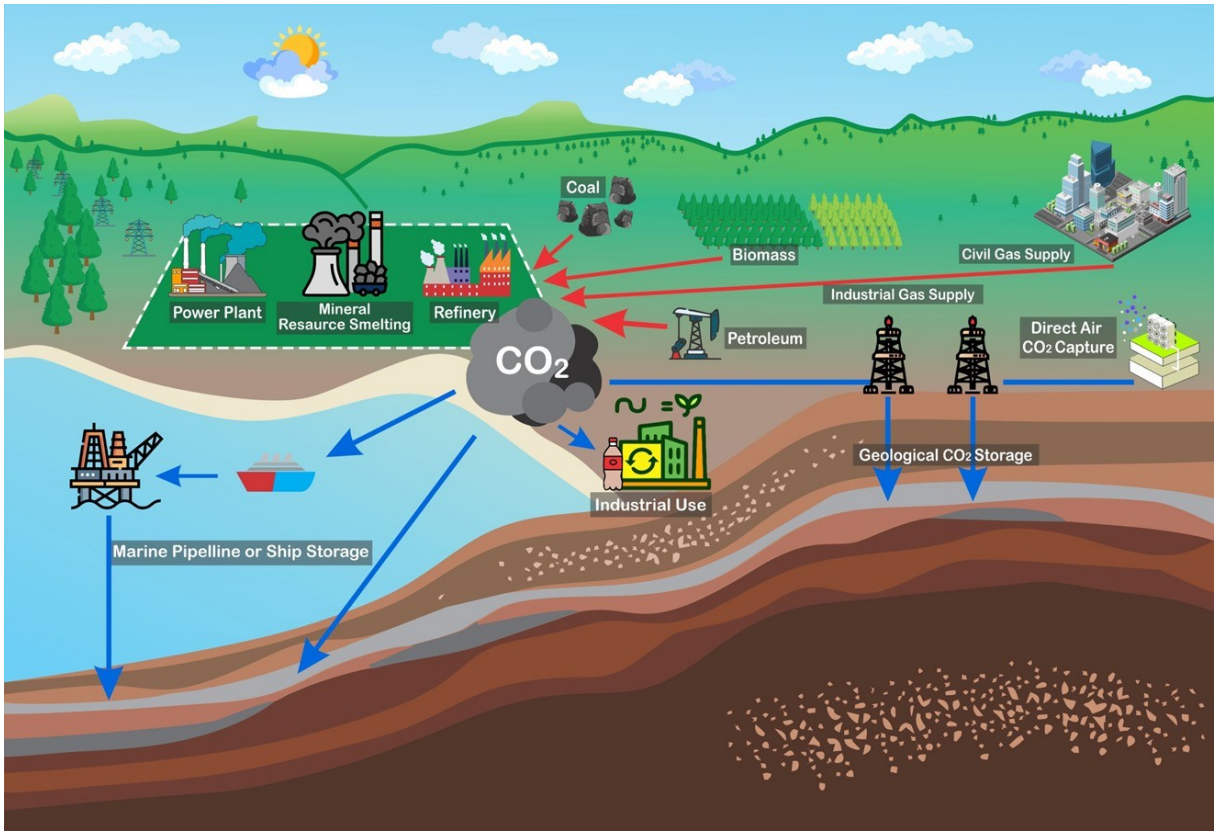

***Figure 3**: Schematic diagram of CCUS systems applied to different emission sources.*

After capture, CO_2 can be either stored (CCS) or used and/or converted (CCU). In CCS, supercritical or liquid CO_2 is injected into subsurface geological formations [37]. The estimated storage capacity is about 1 Tt CO_2, far exceeding the amount required through 2100 to limit average global warming to 1.5 °C [1]. Nevertheless, successful long-term storage requires careful monitoring of site characteristics to avoid risks such as leakages or seismic activities [38]. Ocean storage is another potential solution, where CO_2 is injected into deep oceans, forming carbonic acid (H_2CO_3). Although this method has vast potential, it is still in the nascent development stage, and there are concerns about its environmental impact such as ocean acidification [39,40]. No pilot plants have been developed yet, and the long-term effects remain largely unexplored [1].

Emerging post-combustion methods directly utilize and/or convert CO_2 during the capture process, avoiding the need for separate storage sites. These methods include:

- Biological methods, such as using microalgae and enzyme-based processes [41].

- Accelerated carbonation methods, which use natural ores or industrial alkaline residues to convert CO_2 through exothermic reactions that form stable carbonate minerals [42].

These methods require low energy consumption, making them potentially cost-effective and durable solutions [9,43]. CCUS approaches can be summarized as carbon separation (capture), direct usage (utilization), conversion into chemicals and/or fuels, and sequestration (storage) (**Figure 4**[4]).

On this basis, this research will concentrate on accelerated carbonation technologies using combinations of industrial alkaline residues. This method is considered a promising approach for addressing CO_2 sequestration and waste management. More specific details will be discussed in the upcoming sections.

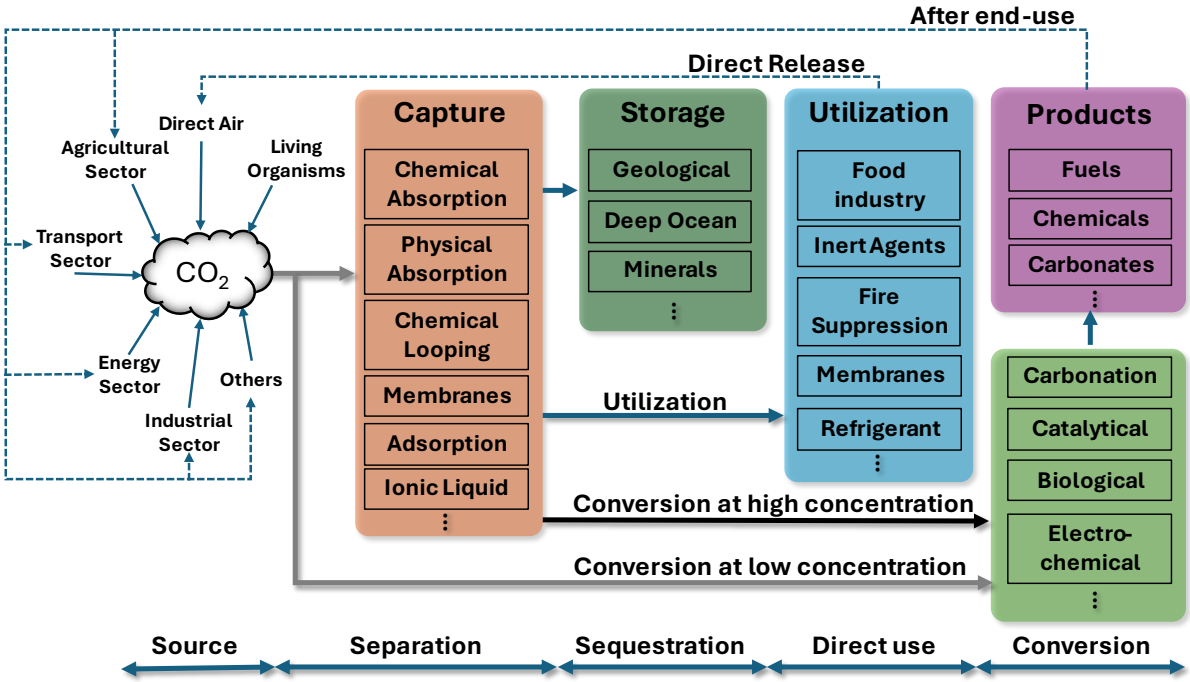

***Figure 4**: Concepts of CCUS methods post-combustion.*

[4] made as an adaptation from [55]

Chapter 2: Theoretical Foundation of Accelerated Carbonation Technology

This chapter provides an in-depth overview of the theoretical foundation of accelerated carbonation technology (ACT), a promising technology for mitigating climate change in the short- to medium-term. ACT is inspired by natural weathering processes, where carbonation reactions occur slowly over millions of years due to low carbon dioxide (CO_2) concentrations in the atmosphere (approx. 0.03-0.06 %) [32,44]. Mimicking these natural weathering reactions, ACT aims to significantly accelerate these reactions under controlled conditions.

This chapter first introduces carbonation mechanisms, followed by a brief description of in situ and ex situ methods, highlighting their respective advantages and limitations. Different pathways for ex situ ACT are discussed, emphasizing the role of direct and indirect carbonation, as well as the key operational parameters—temperature, pressure, particle size, and pH-value—that influence reaction efficiency.

The concept of exploiting industrial alkaline residues, rich in reactive oxides, is introduced as an alternative to natural ores. These residues offer a more sustainable solution by reducing the need for large-scale mining and providing an effective means of CCUS [11]. Additionally, ACT offers the potential to stabilize hazardous residues, further enhancing its environmental benefits [45,46]. The chapter also explores the potential of combining different industrial residues to improve the properties of carbonated materials, facilitating their reuse.

The chapter is structured as follows:

- **Section 2.1**: An exploration of carbonation mechanisms, focusing on the chemical and physical properties that make materials suitable for ACT.
- **Section 2.2**: A comparison of the pros and cons of in situ and ex situ ACT methods.
- **Section 2.3**: A detailed overview of ex situ ACT, differentiating between direct and indirect carbonation processes, key process parameters, and the potential of using industrial alkaline residues instead of natural ores.

2.1 Introduction to Carbonation Mechanisms

The carbonation process can be summarized by the following general chemical reaction [1]:

$$MO + CO_2 \rightarrow MCO_3 + \text{heat} \quad (1)$$

where a metal (M) reacts exothermically with atmospheric CO_2, to form insoluble, chemically- and thermodynamically stable carbonate minerals [9]. The amount of thermal energy released depends on the specific metal and its host ore. The divalent metals hypothetically suitable for carbonation include alkali metals (Na, K), alkaline earth metals (Ca, Mg), as well as elements such as manganese (Mn), zinc (Zn), and lead (Pb) [6]. Nevertheless, the corresponding oxides exhibit varying affinities for carbonation, ranked as follows: alkaline oxides (CaO, MgO) are the most reactive, followed by amphoteric oxides (Al_2O_3, MnO, and Fe-oxides), and lastly acidic oxides (SiO_2). Although alkali metals (K, Na) can form (bi)carbonates, their solubility in water makes them unsuitable for long-term CO_2 mineralization, because they would eventually release it back into the atmosphere [47].

The capacity of these materials to sequester CO_2 is directly influenced by the concentration of the metals, especially alkaline earth (hydr)oxides in the matrix. Indeed, other metals, including Fe, Zn, Ni, Co, Cu, and Mn, are also not ideal for carbonation because of their distinct and valuable properties and difficulties in collection and utilization [48]. Instead, Ca\Mg-rich silicates are ideal for this process due to their abundance in the Earth's crust [20]. Silicates and carbonates are particularly stable and suitable for long-term storage, due to their lowest free energy-formation [32]. They can remain stable over geological timescales or be repurposed as filler materials in construction or mining [32]. Mineral sequestration offers a viable long-term solution without the risks of leakage or the need for continuous monitoring [1], unless the carbonates are exposed to strong acidic environments [48].

Since natural carbonation reactions occur slowly, this current research focuses on accelerating the carbonation process to bolster efficiency for industrial applications [1]. This involves optimizing key operation parameters such as particle size, CO_2 pressure, pH-value, temperature, and liquid-to-solid (L/S) ratio [44,49]. Selfritz (1990) conducted early investigations, exposing Ca-silicates to highly pure CO_2 and moisture, speeding up carbonation reactions that ranged from minutes to hours [50]. Consequently, carbonation is an appealing option, particularly in regions lacking underground reserves or marine storage capacity, being an effective alternative to traditional CCS. On this basis, the next section delves into the theoretical basis behind the ACT approaches.

2.2 In situ and Ex situ Carbonation: Pros and Cons

Accelerated carbonation can be carried out through in situ or ex situ methods [9].

In situ carbonation involves injecting CO_2 into silicate rocks beneath the surface, where it reacts to form carbonates [51]. This method, similar to CCS, can potentially sequester large amounts of CO_2. Despite its potential, in situ carbonation faces several challenges [52] including:

- Identifying suitable locations with favorable geothermal gradients
- Simulating temperature and pressure effects on CO_2 and Ca\Mg solubility
- Optimizing reaction kinetics, and
- Reducing energy consumption.

Due to these challenges, in situ methods may be merely a feasible solution for large-scale applications [51].

By contrast, ex situ carbonation involves reacting CO_2 with metal oxide-rich materials in a controlled environment (e.g., reactors). While ex situ carbonation sequesters a smaller amount of CO_2 compared to in situ carbonation, it is more practical for small- to medium-sized sources of CO_2 emission [51]. Moreover, ex situ processes offer greater flexibility in the choice of materials: not only do they use natural ores, but they also employ industrial alkaline residues (**Figure 5**[5]).

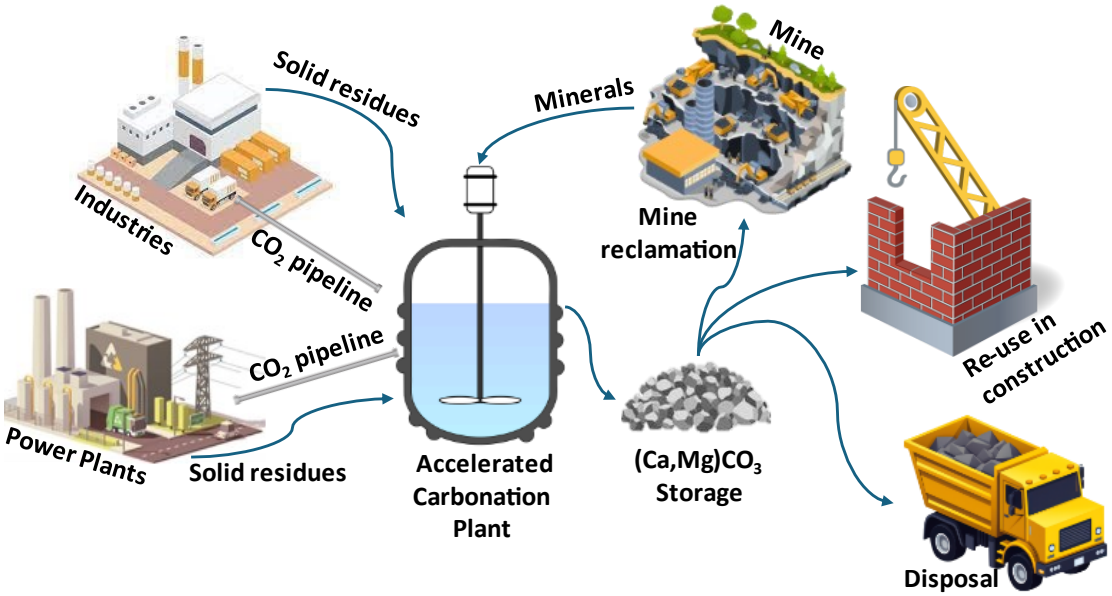

***Figure 5**: Scheme of ex situ ACT using industrial residues.*

[5] made as an adaptation from [251]

These materials can be repurposed in sectors such as construction, supporting a circular economy approach. Given these advantages, ex situ ACT was chosen as the focus of this study. The next sections will explore two commonly used ex situ approaches: direct and indirect accelerated carbonation.

2.3 Ex situ Accelerated Carbonation: Direct and Indirect Approaches

The first step in implementing ACT is selecting appropriate materials. As previously outlined, minerals containing metal oxides, such as Ca and Mg, are ideal for CO_2 sequestration. An example is wollastonite ($CaSiO_3$), which is a readily extractable Ca-rich mineral commonly found in metamorphic limestones, making it particularly suitable for carbonation [6].

To enhance the reaction efficiency, natural ores generally require mineral surface activation [51]. This can be achieved through physical (e.g., reducing particle size, vapor activation, or magnetic separation) and/or chemical pretreatments (e.g., using acids) [9,12]. The particle size is crucial for carbonation kinetics—it was demonstrated that reducing the size of olivine particles from 250 μm to 40 μm increased carbonation efficiency [53]. Once activated, minerals can be carbonated via two primary methods: direct and indirect carbonation [9,54].

2.3.1 Direct Carbonation: Gas-solid and Aqueous Carbonation

Direct mineral carbonation is a one-step process that can be performed either through gas-solid (dry) or aqueous (wet) carbonation, depending on the L/S ratio. The capability of oxides to form carbonates is affected by the following factors [55]:

- Total reactant content.
- Solubility (in aqueous carbonation).
- Number of surface alkaline sites on the gas-solid interface.
- Chemisorption capacity for CO_2.

2.3.1.1 Gas-solid Carbonation

This method, typically performed with a low L/S ratio (< 0.2), was first explored using gaseous or supercritical CO_2 [55,56]. The reaction occurs as follows [55]:

$$(\mathrm{Ca,Mg}) - \mathrm{silicate}_{(s)} + \mathrm{CO_2}_{(g)} \rightarrow (\mathrm{Ca,Mg})\mathrm{CO_3}_{(s)} + \mathrm{SiO_2}_{(s)} \quad (2)$$

While gas-solid carbonation has the advantage of simplicity and low water consumption, the reaction tends to be slow, especially in ambient conditions [56]. For instance, serpentine (100 μm) exposed to CO_2 at 340 bar and 500 °C for 2 h, achieved only about 25 % conversion

[56]. Pretreatments to increase the surface area can improve the process [9], but the energy-intensive conditions required make this method impractical for large-scale industrial applications. Because of the limitations of gas-solid carbonation, research has focused more on aqueous carbonation performance, which enhances reaction kinetics by introducing water [48].

2.3.1.2 Aqueous Carbonation

By adding water to the process, ions can be mobilized by dissolution, favoring the reactivity of alkaline metals with carbonic acids in the liquid phase [48]. The theoretical basis beyond this technique occurs mainly in three phases as shown in **Figure 6**[6].

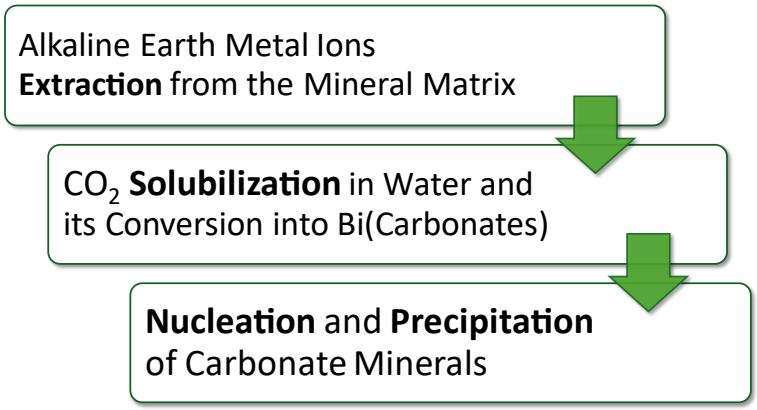

***Figure 6**: Synthesis of the macro-phases of direct aqueous carbonation.*

Since most alkaline minerals are seldom found in their pure state, the chemistry of the reaction may be complex. These materials are often combined with other oxide phases, such as silicates, aluminates, and ferrites [48]. Therefore, many other compounds may also participate in the carbonation process, such as calcium silicate hydrates (CSH), forming various co-precipitates, including calcite, vaterite, and aragonite [57]. The mechanisms related to the process of aqueous carbonation are elucidated as follows:

Extraction of Alkaline Earth Metal Ions from the Matrix

During the leaching process, the dissolution of Ca\Mg-containing compounds such as burnt lime (CaO) and larnite (Ca_2SiO_4), leads to hydroxide ions (OH^-), thereby increasing the pH above 11-12, as shown by the following equations [48]:

$$(Ca, Mg)O_{(s)} + H_2O_{(l)} \rightarrow (Ca, Mg)^{2+}_{(aq)} + 2OH^-_{(aq)} \quad (3)$$

$$(Ca, Mg)_2SiO_{4(s)} + 2H_2O_{(l)} \rightarrow 2(Ca, Mg)^{2+}_{(aq)} + H_2SiO_{4(s)\downarrow} + 2OH^-_{(aq)} \quad (4)$$

[6] [52]

Once the solubility threshold of the solute-solvent system is reached, the pH-value remains constant. In general, higher temperatures and lower pH-values enhance metal ion dissolution [55]. The characteristics of solid materials change significantly during this step. Coarse or granular materials could contain an internal soluble component potentially exploitable for the carbonation process [48]. Indeed, key factors influencing dissolution kinetics include particle size and specific surface area [55]. Studies show that smaller particles (45-75 μm) can dissolve over 90 % of Ca-species within 24 h, while larger particles (150-250 μm) show less than 40 % dissolution [58]. Since grinding solids can be energy-intensive, determining the optimal particle size for carbonation is crucial.

The L/S ratio also affects metal ion leaching, as it controls how much of the metal ions can dissolve and migrate into the solution [48]. Leaching is primarily solubility-controlled, meaning that once equilibrium with certain mineral phases is reached, the concentration remains constant regardless of the L/S ratio [59].

Solubilization and Dissolution of CO_2 into the Solution

CO_2 solubilizes in water (solvent) according to Henry's law, which states that the solubility of a gas is directly proportional to its partial pressure (p_{CO_2}), as described in Eq. (5) [60]:

$$[CO_2]_{(aq)} = H_{CO_2,T} * p_{CO_2} \tag{5}$$

The concentration of CO_2 dissolved in water ($[CO_2]_{(aq)}$) is governed by Henry's constant ($H_{CO_2,T}$), which decreases as temperature (T) increases, reducing the gas's solubility as follows [61]:

$$H_{CO_2,T} = H_{CO_2,298\,K} * \exp\left[C * \left(\frac{1}{T} - \frac{1}{298\,K}\right)\right] \tag{6}$$

where C is a gas-constant depending, for example, 2400 K for CO_2; $H_{CO_2,298K}$ is Henry's constant at 298 K, which is $10^{-1.468}$ M atm^{-1} for CO_2 [61].

As shown below, CO_2 dissolves resulting in the carbonic acid (H_2CO_3) formation:

$$CO_{2(g)} + H_2O_{(l)} \rightarrow H_2CO_{3(aq)} \tag{7}$$

which dissociates into bicarbonate (HCO_3^-) and carbonate (CO_3^{2-}) ions, as shown in Eqs. (8) and (9), depending on the pH-value, respectively:

$$H_2CO_{3(aq)} \rightarrow H^+_{(aq)} + HCO^-_{3\,(aq)} \tag{8}$$

$$HCO^-_{3\,(aq)} \rightarrow H^+_{(aq)} + CO^{2-}_{3\,(aq)} \tag{9}$$

Figure 7 shows the fraction of each carbon species presented as a function of the pH-value [62]. At lower pH (< 6) the generation of H_2CO_3 prevails, while HCO_3^- predominates at mid-pH (~ 8); and CO_3^{2-} predominates at high pH (> 10) [63].

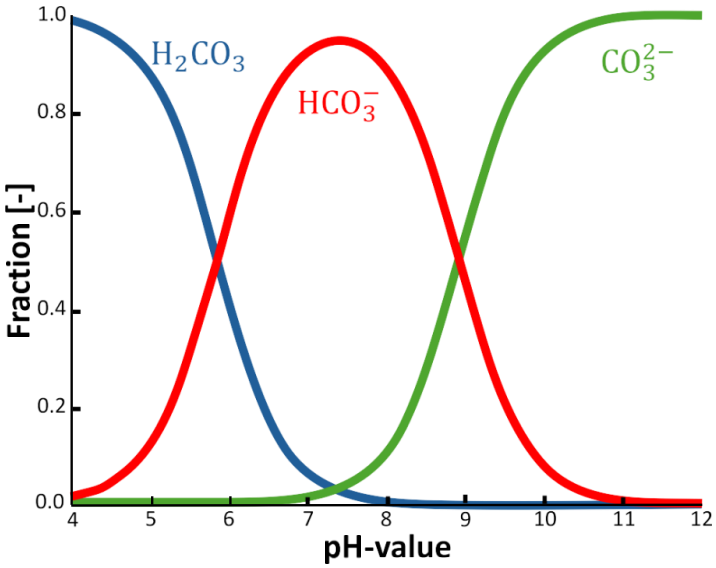

***Figure** 7: Mole fractions of CO_2 (H_2CO_3), HCO_3^- and CO_3^{2-} at different pH-values.*

Nucleation and Precipitation of Carbonate Minerals

As described in Eq. (10), $(Ca,Mg)^{2+}$ ions interact with CO_3^{2-} ions, producing carbonate precipitates, which are highly insoluble in alkaline conditions [64]:

$$(Ca, Mg)^{2+}_{(aq)} + {CO_3^{2-}}_{(aq)} \rightarrow (Ca, Mg)CO_{3\,(nuclei)} \rightarrow (Ca, Mg)CO_{3\,(s)\downarrow} \quad (10)$$

Consequently, carbonation is more likely to occur in alkaline environments, where carbonate ions are abundant. As CO_3^{2-} forms, H^+ ions are released as well, lowering the pH by reacting with OH^- ions to produce water, as shown below:

$$H^+_{(aq)} + OH^-_{(aq)} \rightarrow H_2O_{(l)} \quad (11)$$

On the other hand, if the concentration of alkaline compounds exceeds the solubility threshold, the pH remains constant due to the undissolved deposits that continue generating OH^- and $(Ca,Mg)^{2+}$ ions, readily reacting as just outlined. After consuming the undissolved deposit, the continual solubilization of CO_2 into the solution during carbonation causes a gradual drop in pH to around 8-9, where bicarbonate ions (HCO_3^-) become prominent [48]. In this case, $(Ca,Mg)^{2+}$ ions could combine with the HCO_3^- ions, resulting in the formation of $(Ca,Mg)CO_3$, as described by Eq. (12):

$$(Ca, Mg)^{2+}_{(aq)} + 2{HCO_3^-}_{(aq)} \rightarrow (Ca, Mg)CO_{3\,(s)\downarrow} + {CO_2}_{(g)} + H_2O_{(l)} \quad (12)$$

This process continues until the pH-level reaches acidic-neutral values between 5 and 6, at which point most cations from the alkaline minerals should be fully depleted. Common precipitates include common carbonates found in the Earth's crust, such as dolomite ($CaMg(CO_3)_2$), magnesite ($MgCO_3$), and calcite ($CaCO_3$) [48].

Main Parameters Influencing the Accelerated Carbonation

The aqueous carbonation process is essentially an acid-base reaction, where an alkaline solution is neutralized by carbonic acids. It can be summarized in eight steps, as shown in **Figure 8**[7].

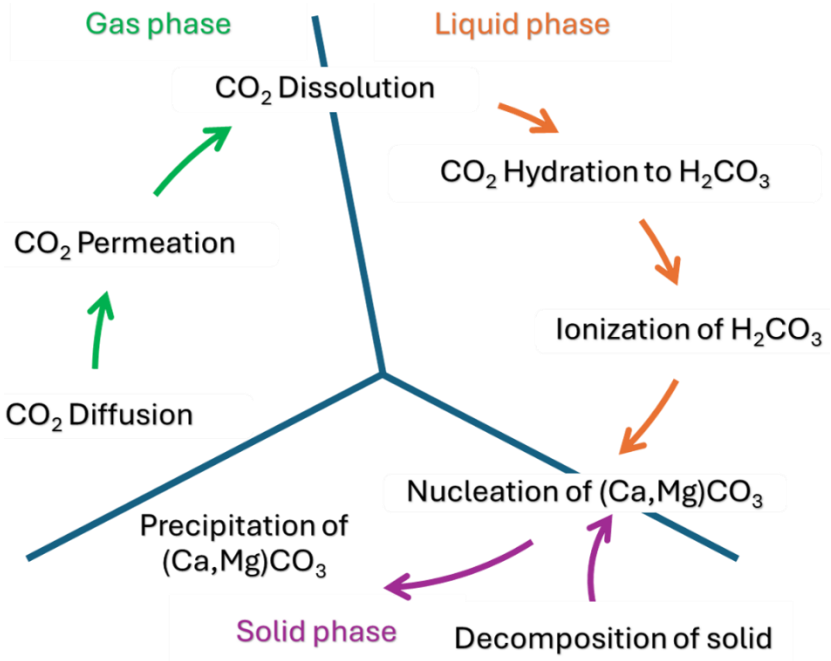

***Figure 8**: Generic aqueous carbonation mechanisms.*

Initially, $(Ca,Mg)^{2+}$ and OH^- from alkaline materials dissolve in the water, raising the pH-value above 11-12. As CO_2 solubilizes and dissolves into the alkaline solution, the high pH ($\sim$ 12) favors the formation of carbonate ions (CO_3^{2-}), which react with $(Ca,Mg)^{2+}$ to form nucleation points for $(Ca,Mg)CO_3$, followed by their precipitation. For instance, the nucleation and precipitation of $CaCO_3$ occur when the pH exceeds 9. CO_3^{2-} is accompanied by H^+ ions generation, decreasing the pH solution by interacting with OH^- ions. **Table 1**[8] summarizes the key factors affecting gas, liquid, and solid phases during carbonation. Their effect on $(Ca,Mg)^{2+}$ leaching, CO_2 solubilization\dissolution, and $(Ca,Mg)CO_3$ nucleation\precipitation can be summarized as follows:

[7] made as an adaptation from [65]
[8] made as an adaptation from [65]

- High temperatures and low pH-values promote metal ions leaching but reduce CO_2 solubilization\dissolution and carbonate nucleation\precipitation. Temperatures between 60-80 °C and a pH-value of around 10 are considered optimal for efficient carbonation [65].
- Lower CO_2 concentrations in the gas phase prolong the carbonation time but do not significantly affect the total amount of carbonates precipitated [66].
- The L/S ratio influences the extent of metal and non-metal ions leaching from solids, though the solubility equilibrium primarily governs their concentration [48].
- Particle size and BET surface area play a crucial role in dissolution kinetics—larger particles may contain valuable reactants, while a higher BET surface area increases reactivity. Therefore, finding the optimal particle size is essential for efficient carbonation, particularly given the energy demands of pretreatments [65].

In summary, the carbonation process is controlled by the balance between CO_2 solubilization\dissolution and carbonate nucleation\precipitation, which depends on the solubility and kinetic reactions of the raw material and resulting products [9].

***Table 1**: Essential operational parameters necessary for efficient carbonation.*

	Phases		
	Gas	**Liquid**	**Solid**
Chemical properties	▪ CO_2 concentration ▪ Organic/Inorganic ▪ Particulate matter contents ▪ Other air pollutants	▪ Organic/Inorganic ▪ Anions/Cations concentration ▪ pH ▪ Permeability	▪ Compositions ▪ Heavy metals ▪ Free water content ▪ Permeability
Physical properties	▪ CO_2 pressure ▪ Flow rate ▪ Relative humidity ▪ Temperature	▪ Temperature ▪ Liquid-to-solid ratio	▪ Particle size ▪ Mineralogy ▪ BET surface area ▪ Porosity/Permeability ▪ Surface activities ▪ Microstructure

2.3.2 Indirect Carbonation

Indirect mineral carbonation is a multi-phase pathway, performed via aqueous carbonation. The theoretical foundation of this technique is distinguished by three phases as shown in **Figure 9**[9]:

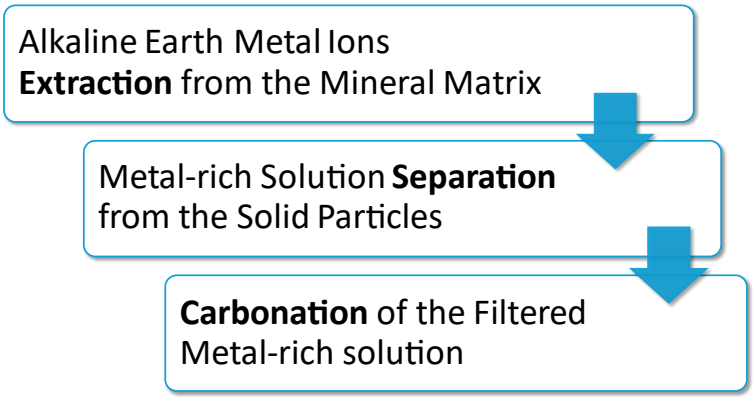

***Figure 9**: Synthesis of the macro-phases of indirect aqueous carbonation.*

Metal ions can be extracted using either acidic or alkaline methods. Early developments in indirect carbonation used acetic vinegar to extract Ca^{2+} from silicates, as shown in Eq. (13) [67]. The Ca^{2+}-rich solution is then separated from the tailings, primarily SiO_2, and CO_2 is added to the solution, resulting in a nearly pure $CaCO_3$ product, suitable for commercial use, and a total acetic acid recovery, as shown in Eq. (14) [67]:

$$CaSiO_{3(s)} + 2CH_3COOH_{(aq)} \rightarrow Ca^{2+}_{(aq)} + 2CH_3COO^-_{(aq)} + SiO_{2(s)\downarrow} + H_2O_{(l)} \quad (13)$$

$$Ca^{2+}_{(aq)} + 2CH_3COO^-_{(aq)} + CO_{2(g)} + H_2O_{(l)} \rightarrow CaCO_{3(s)\downarrow} + 2CH_3COOH_{(aq)} \quad (14)$$

A different approach involves extracting Mg^{2+} from serpentine ($Mg_3Si_2O_4(OH)_4$), using acids such as hydrochloric acid (HCl), acetic acid (CH_3COOH), ethylenediaminetetraacetic acid (EDTA), orthophosphoric acid (H_3PO_4), or oxalic acid ($C_2H_2O_4$) [68]. The best extraction efficiency was achieved using a combination of H_3PO_4, $C_2H_2O_4$, and EDTA [68]. Nevertheless, the limited dissolution of CO_2 in acidic solvents reduces the sequestration output [68].

The pH-swing technique was introduced to address this challenge, where metal extraction occurs in an acidic phase, followed by carbonation in an alkaline phase [69]. A modified version uses a weak base/strong acid solution of ammonium chloride (NH_4Cl) for basic extraction, allowing rapid pH adjustment causing effective metal-ion separation of earth metals (Eq. (15)) and precipitation of the carbonate (Eq. (16)) [70]:

[9] [48]

$$CaSiO_{3(s)} + 2NH_4Cl_{(aq)} \rightarrow CaCl_{2(aq)} + SiO_{2(s)\downarrow} + 2NH_{3(aq)} + H_2O_{(l)} \quad (15)$$

$$2NH_{3(aq)} + CO_{2(g)} + CaCl_{2(aq)} + H_2O_{(l)} \rightarrow CaCO_{3(s)\downarrow} + 2NH_4Cl_{(aq)} \quad (16)$$

As the reaction progresses, the alkalinity increases due to the production of ammonia, which is advantageous for the subsequent absorption of CO_2.

The main drawback of indirect carbonation is the high energy requirement for evaporating the solution, which, along with fluctuations in free energy from intermediate product generation, limit its economic viability without chemical recycling [67].

2.3.3 The Advantages of using Industrial Alkaline Residues in Accelerated Carbonation

While ex situ ACT with natural ores can sequester substantial amounts of CO_2, it poses important economic and environmental hurdles by requiring disruptive and energy-intensive large-scale mining [11]. A more sustainable alternative is the use of industrial alkaline residues—by-products from thermal operations, construction, and demolition activities, such as fly ashes (FA), steel slags, and construction\demolition wastes (CDW). These residues are abundant, inexpensive, and highly reactive, making them ideal candidates for ACT [13,71], offering several engineering, environmental, and economic benefits (**Figure 10**[10]).

These alkaline residues can sequester significant amounts of CO_2, up to 311-373 kg CO_2/mt alkaline residue [72,73], because of their substantial concentrations of highly reactive metal oxides, such as CaO and MgO [9]. Moreover, their availability at industrial sites makes them ideal for on-site carbon capture applications, supporting industrial circularity and synergies, avoiding large-scale mining, thus reducing associated environmental impacts [13].

Additionally, the carbonation process facilitates waste disposal, reduces landfill usage, and helps develop alternative construction materials, decreasing the demand for natural resources [54]. Inter alia, it also stabilizes leachable alkaline compounds and heavy metals (e.g., Cu, Zn, Cd, Cr, Pb) present in alkaline residues, and neutralizes alkaline\acid wastewater, improving environmental safety [45,46], and minimizing transportation costs [10,74]. Finally, many residues, such as FA, do not require mechanical pretreatments, because they already have suitable grain sizes for the carbonation process [16], which along with the exothermic nature of the carbonation reaction, can reduce energy consumption [9], making the process cost-effective.

[10] made as an adaptation from [51]

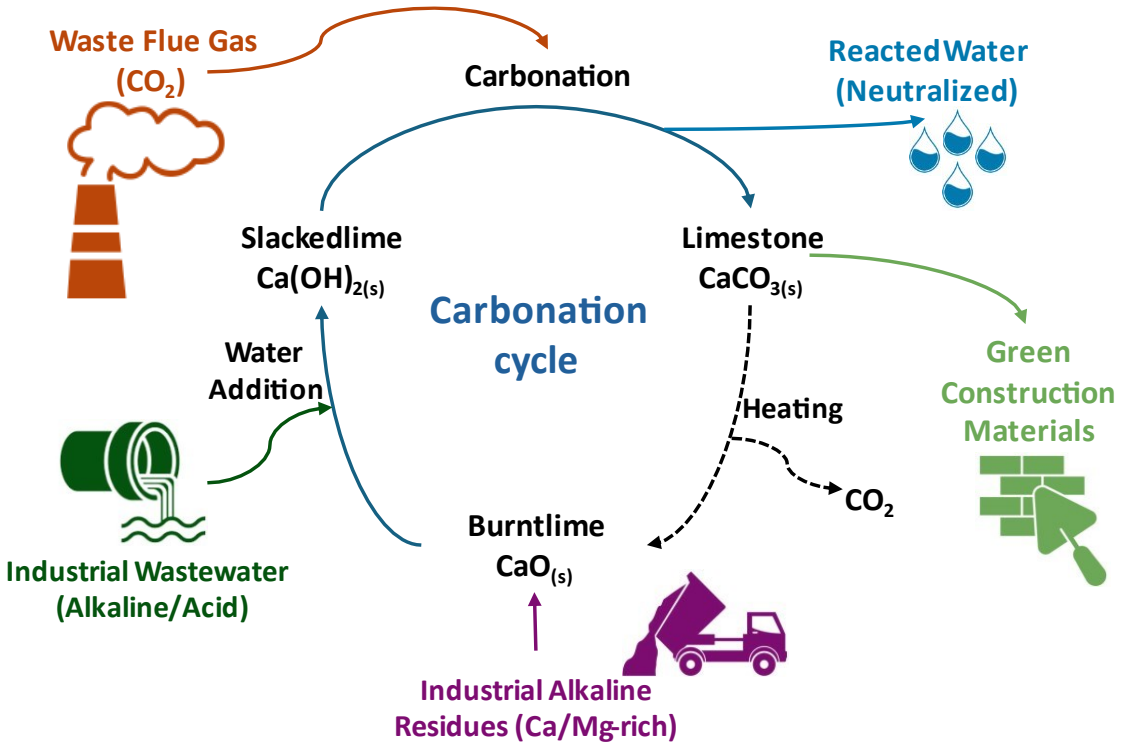

***Figure 10**: Novel method for combining CO_2 mineralization and industrial alkaline residue utilization via ACT.*

For the alkaline residues, the ACT was mainly investigated through direct aqueous carbonation [75,76], and subdivided into:

- Wet process, with a L/S ratio lower than 1.5 [77,78].
- Slurry process, with a L/S ratio higher than 5 L/kg useful when Ca or Mg are bonded to silicates in low-soluble residues [79].

Several materials such as steel slags, CDW, FA, and bottom ash (BA) have been continuously studied. As a result, assessing the efficiency of various residues in the carbonation process is challenging due to their variable qualities. Some residues may offer lower sequestration potential but are produced in large quantities, making them economically viable [6]. Others, with higher reactivity, may be available in smaller amounts but still valuable in industrial applications [6].

Different models have been proposed to better understand the carbonation mechanisms for industrial alkaline residues, such as the *surface coverage model* [80,81], which can be summarized by four primary mechanisms (**Figure 11**[11]) [9]:

1. Conversion of carbonate ions (CO_3^{2-}) within solid particles,

[11] made as an adaptation from [9]

2. Crystallization of new mineral phases on grain surfaces,
3. Leaching of Ca^{2+} ions and their precipitation as $CaCO_3$,
4. Deposition of carbonates on grain surfaces.

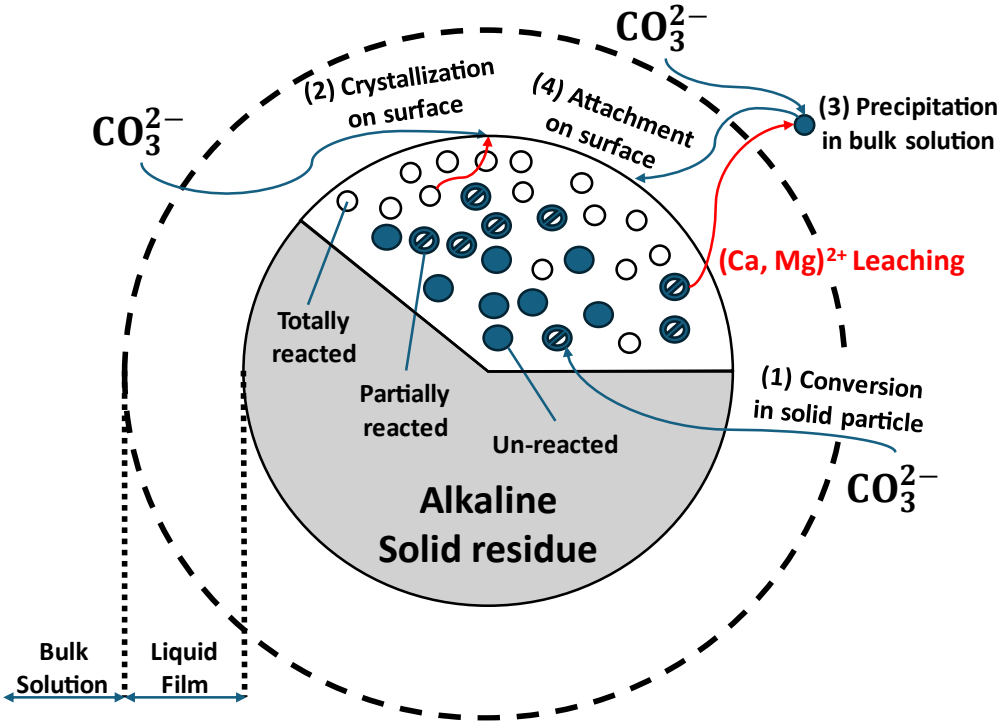

***Figure 11**: Mineral carbonation mechanisms for alkaline mineral particles according to the surface coverage model.*

As highlighted by the model, the suitability of alkaline residues for carbonation depends on their alkaline earth metals concentration and accessibility. Thus, analogous to natural ores, the carbonation efficiency for alkaline residues varies strongly depending on the mineralogical composition and particle size. Residues with small particles (< 106 μm) show more efficient carbonation than larger ones, such as FA (27-139 kg CO_2/mt FA) [9], while those richer in free CaO exhibit high carbonation potential but might require mechanical pretreatments [82,83], such as steel slag and cement kiln dust (CKD) (129-311 kg CO_2/mt residue) [9]. As expected, residues with high Ca and Mg content, particularly those with no pretreatment requirement and produced near the emission sources are optimal [16]. A wider overview is provided in the ternary diagram, depicted in **Figure 12**[12], which is based on major oxides and classifies many industrial alkaline residues based on three key properties [16]:

- **CO_2 capture capability**: Measured by the ability of the material to absorb and/or adsorb CO_2 per unit of mass or volume [9]. Many alkaline residues, such as municipal solid

[12] made as an adaptation from [48]

waste incineration fly ash (MSWI FA), CKD, and ordinary Portland cement (OPC), show high CO_2 capture capability.

- **Hardness properties**: Indicates the resistance of the material to mechanical deformation or abrasion [84]. It relates to grindability, meaning the ease with which the material may be finely ground [85]. Materials originating from blast oxygen furnaces (BOF), for example, are found in this category.
- **Pozzolanic properties**: Refers to siliceous and/or aluminous materials, that, when finely ground (< 150 µm), can chemically react with Ca^{2+} to form compounds with cementitious properties, contributing to the compressive strength of the material [86]. Examples include municipal solid waste incineration bottom ash (MSWI BA) and coal fly ash (CFA).

The diagram highlights that some residues exhibit a balance of these properties, suggesting that combining different alkaline residues could produce final materials with enhanced performance through synergistic effects not only in CO_2 sequestration but also in pozzolanic activities and mechanical properties, which are paramount for potential reuse.

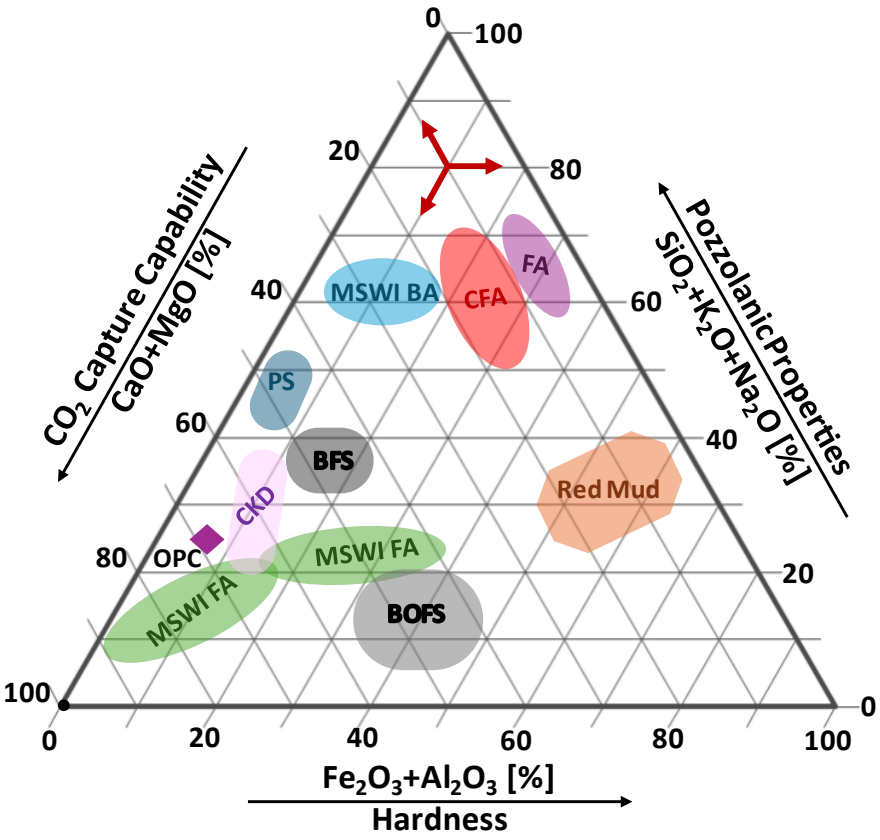

***Figure 12**: Normalized phase ternary diagram (CO_2 Capture Capability – Hardness – Pozzolanic Properties) of several industrial alkaline residues.*

In light of this, the ACT using industrial alkaline residues presents a sustainable alternative to using natural ores. These residues offer significant engineering, environmental, and economic benefits, especially when produced and carbonated on-site. Their flexibility, given by the wide range of selections, combined with their ability to sequester CO_2 and stabilize heavy metals, makes them ideal candidates for ACT. This current research work focuses on the potential of these residues for both carbonation and stabilization mechanisms, particularly in applications where multiple residues are combined to optimize performance. The industrial alkaline residues selected in this study are MSWI FA, MSWI BA, CFA, flue gas desulfurization residues (FGD), and cork fly ash (CkFA), which will be further discussed in the next chapter.

This approach aligns with the EU circular economy policies, which advocate for the use of waste in sustainable applications to close the material loop, orienting towards the Zero Waste strategy, defined by the Zero Waste International Alliance (ZWIA), as [87]:

"*Designing and managing products and processes systematically to eliminate the waste and materials, conserve and recover all resources, without burning or burying them*".

Chapter 3: Overview of the Selected Industrial Alkaline Residues

This chapter examines the state of the art regarding the industrial alkaline residues selected for this study: municipal solid waste incineration fly ash (MSWI FA) and bottom ash (MSWI BA), coal fly ash (CFA), flue gas desulfurization residues (FGD), and cork fly ash (CkFA). The aim is to evaluate their role in accelerated carbonation technology (ACT) and their potential synergistic effects when blended, particularly in enhancing properties of the final material post-carbonation, which is critical for reuse in a circular sustainable economy.

An overview highlights the energy-sector plants responsible for generating these residues as well as their environmental and socioeconomic significance. Each residue is described in terms of its collection process, macroscopic and microscopic characteristics, and potential reuse, with attention to the challenges posed by their inherent properties.

Given the ongoing decline in coal usage for energy production, cork fly ash (CkFA) is included as a potential substitute for CFA and FGD, allowing for an assessment of the versatility of the recipe to the accelerated carbonation process. To the best of the author's knowledge, no previous studies have explored the carbonation of CkFA using ACT.

The chapter is structured as follows:

- **Section 3.1**: An overview of waste incineration, focusing on its by-products, MSWI FA and MSWI BA.
- **Section 3.2**: An overview of coal combustion, focusing on its by-products, CFA and FGD.
- **Section 3.3**: An overview of biomass incineration, especially cork powder incineration, with a focus on its by-product, CkFA.

3.1 Waste-to-Energy Plant Ashes

When recycling is unfeasible, waste-to-energy (WtE) is a widely recognized strategy for waste management, reducing waste mass and volume by approx. 90 % [88]. This process alleviates landfill pressure and is promoted within the circular economy framework. The rise in WtE plants (**Figure 13**[13]) has been largely driven by the growth of the world population and stricter landfill regulations, resulting in a surge in waste incineration from 32-70 Mt (117 %) in Europe between 1995 and 2018 [19]. Despite global waste management regulations, waste generation per capita is expected to increase, leading to more waste incineration, especially in regions such as sub-Saharan Africa and South and East Asia because of improvements in living standards [89]. Prior to Brexit, Germany, France, the Netherlands, Sweden, Italy, and the UK accounted for 75 % of the EU's incineration plant capacity [90]. These plants recover energy in the form of electricity and heat (district heating), contributing approx. 2.4 % of total energy output in Europe in 2018, equivalent to 40 Mt of oil [19].

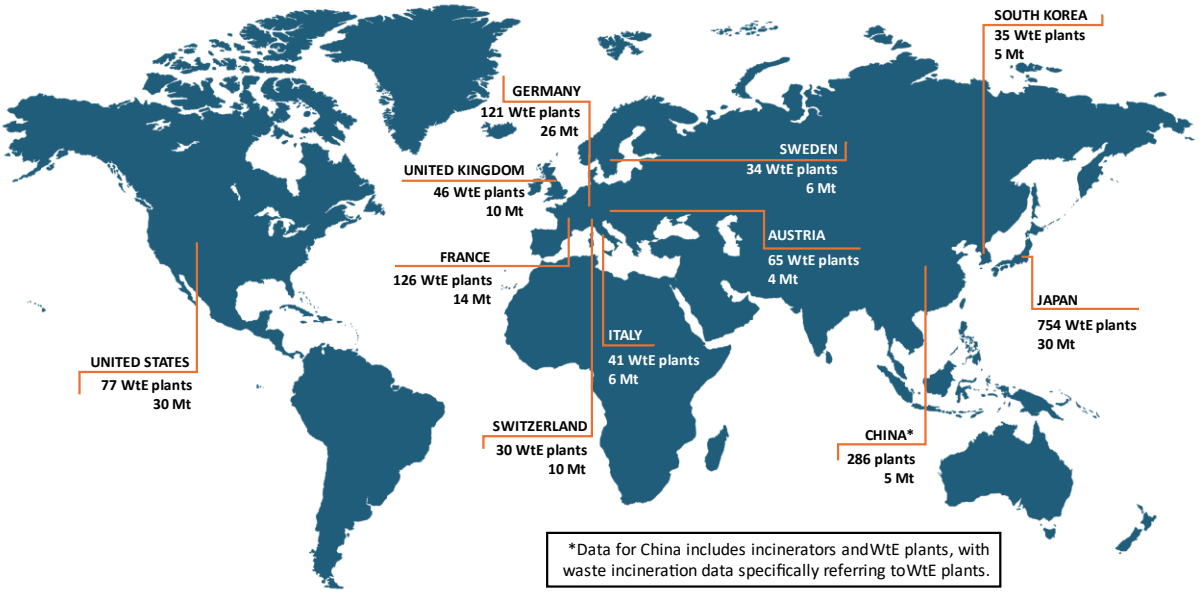

***Figure 13**: First 11 countries with the highest number of WtE plants with the respective amount of waste incinerated in 2019, aimed at energy recovery.*

Waste incineration typically occurs between 850-1400 °C, depending on the waste type, pretreatments, and combustion chamber technology [91]. Despite its benefits, waste incineration also presents environmental challenges; for instance, 52 Mt of CO_2 were emitted in 2019, exceeding the annual GHG emissions of Portugal [90]. Additionally, waste

[13] Data from [252]

incineration produces municipal solid waste incineration (MSWI) ashes, which are classified into two main types: fly ash (MSWI FA) and bottom ash (MSWI BA). The characteristics of these ashes are influenced by the waste type, temperature, and combustion system used [92].

On the one hand, stricter waste management regulations, coupled with enhanced recycling and composting initiatives, have the potential to reduce ash generation in Europe and other industrialized countries. On the other hand, the rising energy demand and more lenient waste disposal regulations in developing countries have led to a proliferation of MSWI plants and a corresponding increase in ash production [93]. In 2021, China incinerated 210 Mt of MSW producing 6.3 Mt of MSWI FA [94].

3.1.1 MSWI Fly Ash from Co-incineration

MSWI FA accounts for 1-3 wt.% of the incinerated waste. It is a fine, hazardous residue collected in silos downstream of the WtE plant until disposal [95]. An air pollution control (APC) system downstream of the combustion chamber, helps to remove pollutants through chemical and/or physical processes. Indeed, during the co-incineration of municipal solid waste (MSW) and sewage sludge (SS), the generated flue gas generally contains heavy metals, ash, particulate matter (PM), organic and inorganic chemicals, residues from incomplete combustion, acid gases, and other harmful contaminants [18,95]. The WtE plant in Brescia, Italy, exemplifies such an approach, consisting of four distinct sequential stages [95]:

- Post-combustion at temperatures exceeding 850 °C to decompose dioxins and volatile organic compounds (VOCs).
- Reduction of nitrogen oxides (NOx) by injecting urea.
- Scrubbing of acid gases with slaked lime and activated carbon.
- Filtration using baghouse filters.

Baghouse filters, widely adopted in many facilities, are made of permeable material, allowing flue gas to pass through while capturing ash particles. As ash accumulates on the filters, it forms a progressively thicker layer known as 'cake', allowing the remaining slaked lime to react with acidic chemicals, activated carbon to adsorb residual dioxins and VOCs, and PM to accumulate on the cake. The ash layer, MSWI FA, is periodically removed, collected by a hopper, and stored in silos for disposal [95].

MSWI FA contains various leachable pollutants and hazardous substances, such as salts, chlorinated and alkaline chemicals, and heavy metals [95]. Consequently, the EU Incineration Directive (2000/76/EC) mandates proper handling and disposal in special, hazardous waste

landfills, with guidelines set by regulatory bodies, such as the Environmental Protection Agency (EPA). Various treatment methods have been proposed, such as washing, chelating, vitrification, and cement solidification [96]. Even so, these methods often face limitations, including the complexity of chemical treatments and high costs [97]. Moreover, while some of these technologies are labeled as "zero-waste" treatments [98], many of them require additional pretreatments, limiting their widespread adoption [18].

MSWI FA disposal not only results in an irreversible loss of materials, contradicting circular economy principles but also incurs significant costs due to stringent regulations and long-term environmental impacts [99]. Recent research has explored innovative uses for MSWI FA, particularly in the construction industry, to enhance the strength and durability of concrete, thus reducing the ecological footprint of cement production [100]. Nevertheless, MSWI FA must be washed to remove salt and soluble compounds, that negatively affect cement quality [101]. Additionally, MSWI FA holds the potential for recovering valuable minerals and metals, such as copper, zinc, and aluminum [102]. These evolving methods underscore the importance of innovative and environmentally friendly waste management approaches in the contest of MSWI, particularly for those countries (e.g., Taiwan) where waste incineration is massively adopted because of the lack of space [103].

Because of its high calcium content and alkalinity, MSWI FA could potentially be utilized for ACT. According to the literature, MSWI FA can sequestrate up to 110-139 kg CO_2/mt MSWI FA [9]. Moreover, accelerated carbonation can stabilize these ashes, thus reducing heavy metal mobility and improving environmental compatibility, to ensure safe disposal in landfills or potential reuse [104]. Nevertheless, these processes are not thoroughly understood, particularly regarding the kinetics of carbonation and the formation of mineral phases that can immobilize pollutants.

3.1.2 MSWI Bottom Ash from Co-incineration

MSWI BA accounts for 25-30 wt.% of the incinerated waste, although it represents only 5-10 % of the total volume. It is a coarse, non-hazardous residue collected at the bottom of the combustion chamber [105]. MSWI BA is extracted using a water-sealed hopper mechanism, which controls combustion, reduces ash particle release, lowers ash temperature, and extinguishes any remaining combustion [95].

MSWI BA is composed of non-combustible components and incompletely burned organic waste [106,107]. Among others, it is composed of permeable, silty, and grey sand along with

pebbles, unburned organic material, silicon and aluminum minerals, glass, ceramics, and metal fragments [108]. It may also contain trace contaminants such as heavy metals and persistent organic pollutants [106,107]. Although MSWI BA is typically considered non-hazardous, the possible presence of leachable heavy metals in the finer fraction [109], requires careful handling to prevent environmental and public health risks. MSWI BA is also characterized by a high concentration of amorphous material formed during combustion and rapid water-cooling [110]. This amorphous phase is typically metastable and may change over time due to variations in its mineralogical and chemical composition [111,112]. Despite extensive research, the behavior of this amorphous phase is not yet fully understood.

Recycling MSWI BA is regularly conducted in several countries, including Spain, Italy, Germany, the Netherlands, China, the USA, and Taiwan [113]. Historically, MSWI BA has been used as filler material in construction applications, such as road building, concrete, bricks, and tiles production [114]. Substituting natural resources, such as clay and sand with MSWI BA in these applications can reduce the environmental impact of the building industry [115,116]. Additionally, MSWI BA is increasingly used in metal recovery adhering to the principle of urban mining [22,107]. Ongoing research has focused on maximizing the recycling potential of MSWI BA, particularly for recovering valuable metals such as copper, zinc, and aluminum [117]. Nonetheless, the lack of standardized testing procedures has resulted in varying restrictions across different countries. For instance, European regulations permit the reuse of MSWI BA, provided that the concentrations of leachable hazardous components remain below specified limits [118].

Thus, accurate characterization of MSWI BA by size fraction is essential to maximize its recycling potential and develop sustainable applications within the circular economy. Pretreatment processes, including screening, separation, and grinding, are typically required to prepare MSWI BA for specific applications [117,119]. The fraction below a diameter of 4 mm is often separated due to the presence of inorganic salts, such as chlorides, sulfates, and leachable heavy metals such as copper, chromium, molybdenum, lead, zinc, and antimony [88,120]. The increasing emphasis on integrating MSWI BA into the circular economy framework is reflected in the growing trend toward sustainable and diverse applications [121,122]. For this reason, MSWI BA has been also studied for the ACT. According to the literature, it can sequestrate up to 32-102 kg CO_2/mt MSWI BA [123,124].

3.2 Coal-Power Plant Residues

Coal-power plants have long been a bulwark of global energy production. These plants generate thermal energy, which is converted into electricity. In 2020, coal accounted for approx. 36 % of the world's electricity generation, with major contributions from China, India, and the USA [125]. Despite increasing emphasis on renewable energy sources, coal remains a significant part of the energy mix, particularly in regions with abundant coal reserves [126]. The widespread use of coal-fired power plants is primarily driven by the availability of coal as a cheap and abundant resource, especially in developing countries with rapidly growing energy demand [127].

Coal combustion typically occurs between 1000-1600 °C, depending on the coal type, pretreatments, and combustion chamber technology [128]. Coal-power plants have a significant environmental impact, responsible for about 28 % of global CO_2 emissions from the energy sector in 2022 [129]. Additionally, coal combustion generates significant amounts of residues, which are classified into three main types: fly ashes, bottom ashes, and flue gas desulfurization residues (FGD). The characteristics of these residues are influenced by the coal type, temperature, and combustion system used [130].

In recent years, stringent environmental regulations and efforts to reduce GHG emissions have led to a decline in coal-power plants in Europe and other industrialized countries [131]. Between 1990 and 2021, coal-fired power capacity in the EU decreased by 79%, propelled by policies aimed at reducing carbon emissions and transitioning to cleaner energy sources [132]. Nevertheless, in countries such as China and India, coal-power capacity continues to grow, fostered by rapid industrialization and economic expansion [133]. As the world shifts towards a more sustainable energy future, the role of coal-power is increasingly being questioned, with many advocating for a transition to low-carbon alternatives such as renewables and natural gas [134].

3.2.1 Coal Fly Ash

Coal Fly Ash (CFA) accounts for 25-30 wt.% of the combusted pulverized coal [135]. It is a fine, residual material collected from the APC system, typically using electrostatic precipitators, cyclone separators, or baghouses [136]. CFA is composed of inorganic crystalline minerals, such as quartz and aluminosilicates, along with small amounts of unburned carbon [137], amorphous aluminosilicates, and magnetic phases of iron oxide [138,139]. CFA may also contain trace elements that could pose environmental and health risks over time [140].

Morphologically, CFA particles range from uneven, rough surfaces to smooth, spherical shapes [141]. The particle size of CFA plays a crucial role in its toxicity, influencing both the chemical and biological reactivity [142].

Several countries, including Italy, France, and Japan, extensively utilize CFA as a raw material, with its use also rising in developing countries such as India. CFA has been employed in various industrial processes, such as cement, bricks, and asphalt filler production [143]. Due to its pozzolanic reactivity, CFA can substitute Portland cement, enhancing the strength and durability of concrete [144,145]. Indeed, growing environmental awareness and the need for sustainable building materials have increased interest in using CFA as a substitute for natural resources, addressing both resource depletion and fly ashes disposal [146]. According to the American Society for Testing and Materials (ASTM), CFA is classified into two groups based on chemical and physical properties [111,140]: Class F, typically derived from anthracite or bituminous coal, has a high calcium content and low loss on ignition, making it suitable for concrete production to improve strength and durability [146]. Class C, usually produced from lignite or sub-bituminous coal, has lower calcium content and higher loss on ignition, and it is used for applications such as flowable fill and soil stabilization [147]. Additionally, CFA is a potential resource for rare earth elements [147,148] and can be employed for water remediation [137,149]. CFA has been also considered for ACT, reporting a relatively low CO_2 sequestration capacity of up to 27-70 kg CO_2/mt CFA (see **Figure 12**) [9], even though a higher performance (132 kg CO_2/mt CFA) has been reported in the literature [13].

Global CFA production exceeds 800 Mt/year [150]. In 2018, China, the largest coal consumer globally, produced over 500 Mt of CFA with a utilization rate of 70-80 % [151], driven by the high electricity demand met by numerous coal-power plants across the country [151]. India produces over 200 Mt, with utilization rates increasing from 10 % to 92 % between 1997 and 2022 [152]. Despite its potential, future CFA production is expected to decline as countries adopt cleaner energy sources and enforce stricter regulations on coal-power plants [153].

3.2.2 Flue Gas Desulfurization Residues

FGD is a fine residual material collected downstream of the APC system, using wet or dry scrubbing systems that inject burnt/slaked lime or limestone to reduce sulfur dioxide (SO_2) emissions from flue gases [154]. SO_2 is a significant contributor to acid rain and poses both environmental and health risks [155]. Consequently, FGD is composed of inorganic minerals,

primarily burnt/slaked lime, calcium sulfates, and sulfites [155]. Additionally, traces of silicon, aluminum, iron oxides, and unburned carbon—possibly originating from CFA—may be present [155,156].

FGD residues exhibit long-term stability in the environment. The solid material is collected and used in various industrial applications, including cement production and agricultural soil enhancement [157,158]. For instance, FGD can be used to produce cement, plaster, and natural gypsum for wallboard manufacturing [159]. Moreover, FGD is widely utilized in agriculture as a soil amendment to improve soil quality and as a source of calcium, an essential plant nutrient [160]. As expected, FGD has been considered for ACT as well (see **Figure 12**), reporting among the highest CO_2 sequestration capacity, up to 373 kg CO_2/mt FGD [72], reaching an efficiency of 96-98 % [72,73].

As elucidated for CFA, FGD utilization is facing a cross-behaved trend. Indeed, in well-established industrialized countries, such as the USA, the utilization rate decreased from 79 % to 57 % in the period 2006-2016 [73], while in China it increased from 5 % to 72 % in the period 2005-2013 [161]. Nevertheless, analogous to CFA, FGD usage is expected to decrease due to the ongoing reduction in coal-based energy production [153].

3.3 Biomass-to-Energy Plant Ashes

Biomass combustion, a well-established method of obtaining energy from organic materials (e.g., wood, agricultural residues, and dedicated energy crops), plays a crucial role in the global transition to sustainable energy [162]. Within this broad field, cork powder combustion represents a unique segment of renewable energy. The cork industry is primarily located in the Mediterranean region, with the Iberian Peninsula accounting for approx. 147 kt/year (79 %) of the cork produced worldwide [163]. Portugal, alone, accounts for almost 85 kt/year, which represents 46 % of the total global cork production [163]. During cork production, over 20-30 % of the material is discarded as waste, primarily as cork powder and other residual substances [164].

Cork powder represents a good source of energy production due to its predominant composition of suberin (45 %), lignin (27 %), polysaccharides (12 %), tannins (6 %), ceroids (5 %), and ash (5 %) [165,166]. The use of cork powder to generate energy not only offers a sustainable solution to managing cork waste but also contributes to local energy security in cork-producing regions. This process involves burning cork powder to produce heat and electricity, whereby the temperature conditions depend on the composition of this biomass and

its moisture content [167]. Additionally, the burning yields cork ashes, which are classified into two main types: cork fly ashes (CkFA) and cork bottom ashes [168].

The advantages of cork powder include its high energy density and the economic and environmental benefits of utilizing waste material from an industry already integral to the region [169]. Even so, like other biomass sources, challenges remain, such as the seasonal availability of cork biomass and the need for efficient combustion technologies to minimize emissions and enhance energy recovery [170,171]. Cork power plants, while niche power sources, are part of the broader push towards biomass energy as a key component of the circular economy and renewable energy frameworks [168]. As the world seeks to reduce its reliance on fossil fuels and cut greenhouse gas emissions, cork combustion offers a promising, albeit specialized, solution within the diverse field of biomass energy.

3.3.1 Cork Fly Ash

CkFA is a fine residual material collected from the APC system downstream of the combustion chamber, typically using electrostatic precipitators, cyclone separators, or baghouses [168]. It is composed of aluminosilicate glassy materials, titanospheres, quartz relics, carbonates, phosphates, and small amounts of unburned carbon [172]. Additionally, CkFA contains various salts, alkaline and chlorinated chemicals, as well as trace amounts of toxic elements, particularly in the smaller fractions [172].

CkFA is commonly disposed of in landfills rather than being repurposed [173]. Although limited literature exists on reusing CkFA, conventional methods for ash reuse are not always suitable for this material. For instance, studies have shown that cork ash does not meet the chemical requirements for use as a pozzolan or filler in cementitious materials [174]. Furthermore, its use as a fertilizer is discouraged for crops intended for human and animal consumption due to the potential presence of heavy metals [172].

Despite these limitations, CkFA remains a viable candidate for recycling. It can be transformed into biochar, which has shown promise as an adsorbent for heavy metals [175]. Additionally, it can be incorporated into lightweight aggregates for sustainable building materials, contributing to reduced density and enhanced thermal properties [176]. Another promising recent approach involves the carbonation of biomass ash [177]. With its significant amounts of alkaline substances, it has a high potential for CO_2 capture [178,179]. Further research is required to explore the CO_2 sequestration capacity of various types of biomass ash

and the carbonation mechanisms of both fresh and stored ash [31]. To the best of the author's knowledge, no previous studies have explored the carbonation of CkFA using ACT.

The increasing emphasis on integrating CkFA into the circular economy aligns with a growing trend toward diverse, sustainable applications [168].

Chapter 4: Experimental Activities

This chapter elucidates the experimental activities and analytical techniques used to thoroughly characterize the industrial alkaline residues studied—municipal solid waste incineration fly ash (MSWI FA) and bottom ash (MSWI BA), coal fly ash (CFA), flue gas desulfurization residues (FGD), and cork fly ash (CkFA). It also describes the sample preparation and experimental setups for performing the accelerated carbonation (AC) and natural carbonation (NC) processes, as well as the analytical techniques used to characterize the carbonated samples.

The chapter is structured as follows:

- **Section 4.1**: The preparation of the bulk residues to obtain representative subsamples is described.
- **Section 4.2**: The procedure for digesting bulk samples to analyze their elemental composition is outlined.
- **Section 4.3**: The leaching tests conducted on each bulk sample to determine the elemental composition of the leachates are detailed.
- **Section 4.4**: The preparation of the polished block for the SEM-EDS analyses is explained.
- **Section 4.5**: The carbonation trials are outlined, including specific sample preparation for various experiments (feasibility studies, liquid-to-solid (L/S) ratio and CO_2 pressure effects evaluation, alternative residues studies with CkFA, and optimization studies) and the experimental setups used.
- **Section 4.6**: The analytical techniques employed are described, including:
    - Physical characterization: particle-size distribution, immediate soluble content, Brunauer-Emmett-Teller (BET) analyses, and magnetic and paramagnetic separation.
    - Chemical characterization: Inductively coupled plasma optical emission spectroscopy (ICP-OES), Ion chromatography (IC), Total X-ray fluorescence (TXRF), X-ray fluorescence (XRF), X-ray diffraction (XRD-Rietveld), Scanning electron microscopy with energy dispersive X-ray spectroscopy (SEM-EDS), moisture content, Loss on ignition (LOI), and Total carbon (C) determination.

Scientific contribution

This chapter is partially based on the following publications, although the format has been adapted to align with the structure of this dissertation. The content reflects my independent work, including data curation, literature review, formal analysis, investigation, methodology, visualization, and writing. This chapter duly credits the original author of any work not authored by me, and cited parts are reproduced by permission from Elsevier BV and MDPI:

I. **G. P. Sorrentino**; A. Zanoletti; S. Ducoli; A. Zacco; P. Iora; C. M. Invernizzi; G. Di Marcoberardino; L. E. Depero; E. Bontempi.
Accelerated and Natural Carbonation of a Municipal Solid Waste Incineration (MSWI) Fly Ash Mixture: Basic Strategies for Higher Carbon Dioxide Sequestration and Reliable Mass Quantification
Environ Res 2022, 217, 114805, https://doi.org/10.1016/j.envres.2022.114805

II. **G. P. Sorrentino**; R. Guimarães; B. Valentim; E. Bontempi.
The Influence of Liquid/Solid Ratio and Pressure on the Natural and Accelerated Carbonation of Alkaline Wastes
Minerals 2023, 13(8), 1060, https://doi.org/10.3390/min13081060

III. **G. P. Sorrentino;** R. Guimarães; A. Cornelio; A. Zanoletti; B. Valentim; E. Bontempi.
Mitigating CO_2 Emissions through an Industrial Symbiosis Approach: Leveraging Cork Ash Carbonation
Heliyon 2024, 10(12), e32893, *https://doi.org/10.1016/j.heliyon.2024.e32893*

IV. **G. P. Sorrentino**; T. E. Müller; A. Cornelio; E. Bontempi.
Long-term Carbon Capture through Carbonation and Enhanced Stabilization of Alkaline Incineration Residues, -Manuscript in Preparation

4.1 Bulk Sample Preparation

The industrial alkaline residues used in this study were provided by the waste-to-energy plant and the coal-power plant located in Brescia (Italy), operated by A2A, and the champagne stopper production plant located in Mozelos (Portugal), operated by RELVAS II.

Due to the inhomogeneity of the residues, a process to obtain representative samples was conducted. All the samples were divided into four equal sections using the cone method. The macroscopically coarse samples (> 150 μm) were cut off at a diameter of 2 mm, and the fraction below a particle diameter of 2 mm was then ground by a Retsch RM 200 mechanical mill (Hann, Germany) until the whole sample passed through a 100 mesh (150 μm) screen. Eventually, a rotating sample divider equipped with a vibrating feeder Retsch PT 100 + DR 100 (Hann, Germany) was used to obtain smaller sub-samples, each weighing approx. 10 g.

4.2 Bulk Sample Digestion

Digestion vessels were charged with approximately 250 mg of bulk sample and 10 mL of concentrated HNO_3, sealed, and left overnight under a hood. The vessels were subjected to microwave irradiation using the Microwave MARSXpress from CEM Corporation (USA). After cooling, the samples were combined with 10 mL of deionized water, mixed, and filtered through a glass microfiber filter. The solutions were transferred to 50 mL polyethylene (PE) bottles. This procedure was performed by the Geographical Institute, Ruhr-Universität Bochum (Bochum, Germany).

4.3 Leaching Tests

Leaching tests were conducted according to the CEN EN 12457-2 guidelines [180], adapted as described by Bontempi et al. (2010) [181]. For each sample, 20 g were mixed with 200 mL of ultrapure water at a 1:10 ratio and stirred at room temperature for 2 h using a magnetic stirrer. The solutions were filtered through 0.45 μm pore size membranes and transferred to polyethylene (PE) bottles. The respective pH-value of the leachates was measured using an inoLab pH 730 (WTW). This procedure was carried out at the Chem4Tech Lab, University of Brescia (Brescia, Italy) and at the Geographical Institute, Ruhr-Universität Bochum (Bochum, Germany).

4.4 Polished Blocks

Polished blocks were prepared according to the ISO-7404-2 standard [182]. For each sample, 5 g were mixed with resin and hardener at a 25:3 ratio, poured into molds, and cured for 24 h at room temperature. Once solidified, the blocks were sectioned perpendicular to their top and bottom faces to avoid any potential bias from particle segregation within the epoxy. Polishing was performed according to the ISO 7404-2 standard [182], using an Ecomet 3 machine from Buehler (Leinfelden-Echterdingen, Germany). Sandpapers with grit sizes of 240, 360, 600, 1200, and 4000 were used sequentially, each for 5 min, to achieve a smooth and even surface. This procedure was carried out at the Faculty of Sciences-DGAOT, University of Porto (Porto, Portugal).

4.5 Carbonation trials

4.5.1 Sample Preparation for Carbonation Processes

In this study, the patented recipe proposed by the Chem4Tech research group (RENDERING project) [22] was adapted for the experimental activities as follows:

MSWI BA was dried at 105 °C for 2 h. Following this, as part of the mechanical pretreatment, magnetic components were removed using a magnet. The sample was then sieved to retain particles smaller than 2 mm in diameter and subsequently ground using a Retsch RM 200 mechanical mill (Hann, Germany) to pass through a 100 mesh (150 μm) screen. This ground fraction will be referred to as "MSWI BA < 2 mm ground". Then, for each residue, subsamples of approx. 50 g were obtained using a rotating sample divider equipped with a vibrating feeder Retsch PT 100 + DR 100 (Hann, Germany).

Two mixtures were prepared for carbonation testing:

- **MIX1**: MSWI FA (59 wt.%), MSWI BA < 2 mm ground (9 wt.%), CFA (14 wt.%), and FGD (18 wt.%) mixed with ultrapure water at liquid-to-solid (L/S) ratios of 0.7, 0.9, and 1.2 L/kg and stirred for 10 minutes to ensure homogeneity.
- **MIX2**: MSWI FA (59 wt.%), MSWI BA < 2 mm ground (9 wt.%), and CkFA (32 wt.%) mixed with ultrapure water at L/S ratio of 0.9 L/kg and stirred for 10 minutes to ensure homogeneity.

4.5.1.1 Carbonation Conditions and Experimental Setup for Feasibility Studies: Assessing CkFA as an Alternative Residue, L/S Ratio, and CO_2 Pressure Effects

MIX1 and MIX2 samples (solid component), weighing 33.5 g each, were mixed with ultrapure water as detailed above, and then subjected to two carbonation conditions:

- **Accelerated Carbonation (AC)**:
  - MIX1 and MIX2 (L/S ratio 0.9) were exposed to 1 g of 99.99 % CO_2 gas at 15 bar in a 75 mL reactor at room temperature for 5, 17, 24, 48, and 72 h.
  - Additional AC trials were performed on MIX1 with L/S ratios of 0.7, 0.9, and 1.2 in a 150 mL reactor. For the L/S ratio of 0.9, one trial had CO_2 pressure kept constant. Trials ran until a pressure plateau was reached.
- **Natural Carbonation (NC)**:
  - MIX1 and MIX2 were stored at room conditions for 1 month, with weekly mild remixing. MIX1 with an L/S ratio of 0.9 was extended to 2 months.

After carbonation, all samples were dried at 105 °C to a constant weight, manually ground, and characterized. Carbonation trials were conducted at the Chem4Tech Lab, University of Brescia (Brescia, Italy). An overview of the AC and NC trials is provided in **Table 2**.

Table 2: *Overview of accelerated (AC) and natural Carbonation (NC) trials for MIX1 and MIX2 with varying time, L/S ratios, reactor volumes, and CO_2 pressures.*

Samples ID	Composition	Carbonation Type	Time	L/S Ratio	Reactor Volume	Initial Total Pressure
MIX1_AC5	MSWI FA, MSWI BA < 2 mm ground, CFA, FGD	Accelerated	5 h	0.9	75 mL	15 bar
MIX1_AC17			17 h	0.9	75 mL	15 bar
MIX1_AC24			24 h	0.9	75 mL	15 bar
MIX1_AC48			48 h	0.9	75 mL	15 bar
MIX1_AC72			72 h	0.9	75 mL	15 bar
MIX1_AC_0.7			17 h	0.7	150 mL	15 bar
MIX1_AC_0.9			72 h	0.9	150 mL	15 bar
MIX1_AC_0.9bis			12 d	0.9	150 mL	15 bar (const.)
MIX1_AC_1.2			51 h	1.2	150 mL	15 bar
MIX1_NC1_0.7		Natural	1 mth	0.7	-	Room Condition
MIX1_NC1_0.9			1 mth	0.9	-	
MIX1_NC2_0.9			2 mths	0.9	-	
MIX1_NC1_1.2			1 mth	1.2	-	
MIX2_AC5	MSWI FA, MSWI BA < 2 mm ground, CkFA	Accelerated	5 h	0.9	75 mL	15 bar
MIX2_AC17			17 h	0.9	75 mL	15 bar
MIX2_AC24			24 h	0.9	75 mL	15 bar
MIX2_AC48			48 h	0.9	75 mL	15 bar
MIX2_AC72			72 h	0.9	75 mL	15 bar
MIX2_NC1_0.9		Natural	1 mth	0.9	-	Room Condition

Experimental Setup for Feasibility Studies

The experimental setup for the AC trials involved two sample cylinders (SC) with volumes of 75 mL and 150 mL, made of stainless-steel (AISI 304 or 316L) from Swagelok. Each SC was equipped with two Swagelok needle valves (V-1 and V-2) for gas supply, venting, and pressure regulation. A pressure transducer (PT) with 0.125 % accuracy and an externally placed thermocouple (TC) with 1.5 °C accuracy were used for data acquisition. A vacuum pump (VP) was used to evacuate air from the SC. CO_2 gas (99.99 % pure) was supplied by SOL Group (Monza, Italy). Data was recorded at 5s intervals using a data acquisition system (DAQ/PC) and processed in a LabVIEW® environment. The setup scheme is shown in **Figure 14**.

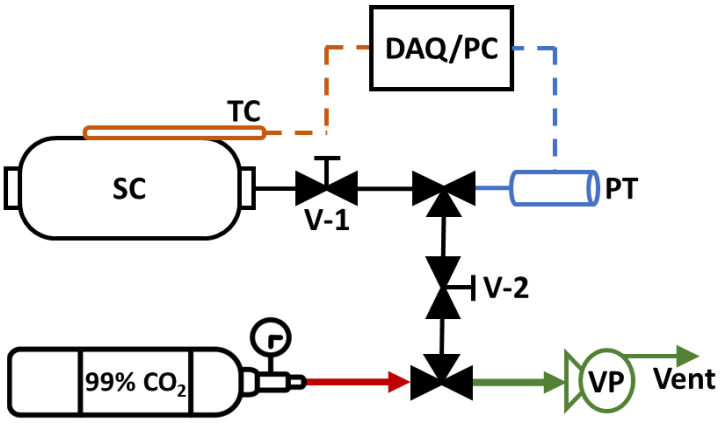

***Figure 14**: Schematic layout of the experimental apparatus:*
Sample Cylinder (SC); Thermocouple (TC); Pressure Transmitter (PT); Needle Valves (V-1 and V-2); Vacuum Pump (VP); 99.99 % CO_2; Data Acquisition System (DAQ/PC).

4.5.1.2 Carbonation Conditions and Experimental Setup for Optimization Studies

MIX1 samples (solid component), weighing 51.6 g each, were mixed with ultrapure water as detailed above, then placed in a 160 mL reactor and exposed to 99.9995 % CO_2 gas.

Two sets of experiments were conducted:

- **Pressure-variation Trials**: MIX1 samples (L/S ratio 1.2) were exposed to a CO_2 pressure of 5, 15, 25, 35, and 45 bar at a constant temperature of 55 °C.
- **Temperature-variation Trials**: MIX1 samples (L/S ratio 1.2) were exposed to a constant CO_2 pressure of 25 bar at 35, 45, 55, 65, and 75 °C.

Each trial was conducted with stirring at 500 rpm for 90 min. Afterward, all the samples were dried overnight at 105 °C, manually ground, and characterized. An additional sample, not subjected to carbonation and labeled as OS, was directly dried, manually ground, and characterized. The respective pH values of the samples were measured before and after the trials using an inoLab pH 730 (WTW). Carbonation trials were conducted in collaboration with the

Carbon Source and Conversion chair, Ruhr-Universität Bochum (Bochum, Germany). A summary of the trials is provided in **Table 3**.

Table 3: *Overview of pressure and temperature-variation trials for optimization of AC process.*

Samples ID	L/S ratio	Total Pressure	Temperature	Time
MIX1_AC_p5	1.2	5 bar	55 °C	90 min
MIX1_AC_p15	1.2	15 bar	55 °C	90 min
MIX1_AC_p25	1.2	25 bar	55 °C	90 min
MIX1_AC_p35	1.2	35 bar	55 °C	90 min
MIX1_AC_p45	1.2	45 bar	55 °C	90 min
MIX1_AC_T35	1.2	25 bar	35 °C	90 min
MIX1_AC_T45	1.2	25 bar	45 °C	90 min
MIX1_AC_T55	1.2	25 bar	55 °C	90 min
MIX1_AC_T65	1.2	25 bar	65 °C	90 min
MIX1_AC_T75	1.2	25 bar	75 °C	90 min
MIX1_OS	1.2	Room Condition	105 °C	Overnight

Experimental Setup for Optimization Studies

The experimental setup for the AC process was provided by Parr Instrument GmbH (Frankfurt, Germany). It consisted of a cylindrical batch reactor (160 mL) and a cylindrical burette (175 mL), both made of stainless-steel. Each was equipped with four Swagelok needle valves for gas supply, venting, pressure regulation, and safety. Pressure gauges (PG), pressure transducers (PT), and thermocouples (TC) were installed for data acquisition. A pressure regulator connected the burette and reactor, and gas management was handled by a Swagelok gas panel. CO_2 gas (99.9995% pure) was supplied by Alphagaz™ (Birmingham, UK). A gas entrainment impeller with holes for suction was used to blow gas into the sample. Temperature control was achieved using a heating mantle, with monitoring provided by internal and external thermocouples. During trials, the burette was used as a control volume to maintain a constant reaction pressure in the batch reactor. Data were recorded at 1s intervals using a data acquisition system (DAQ/PC) and processed in a SpecVIEW® environment. The setup scheme is shown in **Figure 15**.

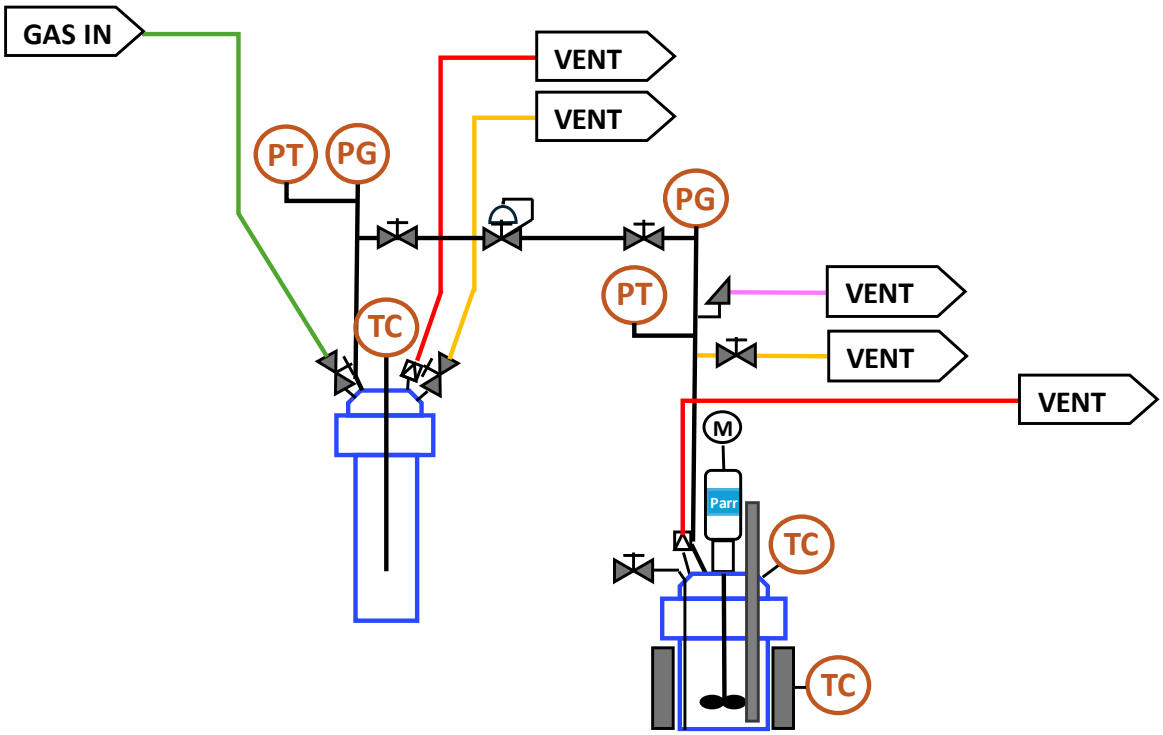

***Figure 15**: Schematic layout of the experimental apparatus: Batch Reactor; Burette; Thermocouples (TC); Pressure Transducers (PT) and Pressure Gauges (PG); Needle Valves; Heating Mantle.*

4.6 Analytical Techniques

4.6.1 Particle-Size Distribution

The particle-size distribution was determined using dry and wet sieving trials. For each bulk sample, 50 g were dried at 50 °C until constant weight. Dry sieving (DS) was performed for 20 min using a Retsch AS200 sieve agitator (Hann, Germany), with a vibration amplitude set at 60 %, as adapted from the EN 15149–2 guidelines [183]. For macroscopically fine samples sieves with a mesh size of 150, 75, 45, and 25 µm were used, while for macroscopically coarse samples sieves with a mesh size of 4, 2, 1, 0.50, 0.25, and 0.15 mm were used.

Wet sieving (WS) was performed using a Fritsch Analysette 3 Spartan sieve agitator (Idar-Oberstein, Germany) equipped with the same set of sieves and a water jet on the top of the sieve column. The sieving continued until the water exiting from the bottom of the column was clear. Each fraction was then filtered and dried at 50 °C until constant weight. DS and WS trials were carried out at the Faculty of Sciences-DGAOT, University of Porto (Porto, Portugal).

4.6.2 Immediate Soluble Content

The immediate soluble content was determined by mixing 10 g of each sample with 300 mL of deionized water at a 1:30 ratio and stirring at room temperature for 15 min using an IKA Microstar 7.5 control (Staufen, Germany), operating at 900 rpm. The solutions were then filtered, and both the water-soluble fractions and non-soluble residues were dried at 50 °C until constant weight. This procedure was carried out at the Faculty of Sciences-DGAOT, University of Porto (Porto, Portugal).

4.6.3 BET Analyses

BET analyses were performed using a Quantachrome instrument (USA). The static volumetric measurement technique was applied, using helium (He) gas 99.9999 % pure for calibrating void volume. Samples were degassed under dynamic high vacuum conditions at 150 °C. Measurements and calculations followed the BET method as outlined in the ISO 9277 standard [184]. Nitrogen (N_2) gas 99.9999 % pure was used for the measurements, with at least 11 data points measured in the range of 0.01 to 0.35 (p/p_0) to estimate the BET surface area (BET-SA). These analyses were carried out by Rubokat GmbH (Bochum, Germany).

4.6.4 Magnetic and Paramagnetic Separation

Magnetic and paramagnetic separation was performed using dry and wet methods. The magnetic fraction was separated using a ferrite magnet, while the paramagnetic fraction was collected with a neodymium magnet. Dry separation was performed by placing the bulk samples in a basin and manually collecting the fraction with the respective magnets. Wet separation was applied by placing the bulk samples in a basin filled with water and continuously agitating using an IKA Microstar 7.5 control system (Staufen, Germany). These procedures were carried out at the Faculty of Sciences-DGAOT, University of Porto (Porto, Portugal).

4.6.5 ICP-OES Analyses

ICP-OES analyses were performed using Spectroblue from Spectro-Ametek (Kleve, Germany) to analyze the elemental composition of the digested and leachate solutions (Sections 4.2 and 4.3). ICP-OES analyses were performed by the Geographical Institute, Ruhr-Universität Bochum (Bochum, Germany).

4.6.6 IC Analysis

IC analyses were performed using IC 881 Compact IC pro from Methrom (Stuttgart, Germany) with conductivity detection and suppressor technique as outlined in the DIN EN ISO 10304-1 standard [185] to analyze the chloride concentration of the leachate solutions (Sections 4.3). IC analyses were performed by the Geographical Institute, Ruhr-Universität Bochum (Bochum, Germany).

4.6.7 TXRF Analyses

TXRF analyses were performed using S2 Picofox from Bruker (Berlin, Germany) to analyze the elemental composition of the leachate solutions (Section 4.3). A Ga-ICP Standard Solution (100 mg/L) from Fluka Sigma Aldrich (Saint Louis, USA) was used as an internal standard. Solutions with a final Ga concentration of 1 mg/L were prepared by mixing 10 mg of Ga-ICP Standard Solution, 100 mg of leachate, and 890 mg of ultrapure water. The solutions were homogenized using a vortex shaker for 1 minute at 2500 rpm. A 10 µL droplet of each solution was placed on a plexiglass slide and dehydrated at 50 °C in a controlled airflow environment.

The TXRF instrument, equipped with a molybdenum (Mo) tube and a silicon drift detector, operated at 50 kV and 750 µA. The X-ray exposition time was 600 seconds. Spectra were analyzed using PICOFOX software (version 2.3.14.0), with routine deconvolution based on mono-element profiles to identify the peak regions. Elements with atomic numbers below 19, such as carbon (C), oxygen (O), and sodium (Na), could not be analyzed due to their low fluorescence yield [186]. The calculation of errors was performed in agreement with Bontempi et al. (2010) [181]. TXRF analyses were carried out at the Chem4Tech Lab, University of Brescia (Brescia, Italy).

4.6.8 XRF Analyses

XRF analyses were performed using RIGAKU Primus IV (Tokyo, Japan), to analyze the major oxide content. The XRF instrument, equipped with a Rh tube, operated at 3 kW. The calibration was conducted using 94 geological standard samples. XRF data for major oxides were obtained and normalized so that the total oxide content sums to 100 %. XRF analyses were performed by the Institute for Geology, Mineralogy and Geophysics, Ruhr-Universität Bochum (Bochum, Germany).

4.6.9 XRD-Rietveld Analyses

XRD analyses were performed using a PANalytical X'Pert PRO diffractometer from Philips (Netherlands). Corundum from Carlo Erba Reagents GmbH (Emmendingen, Germany) was added to the dried samples (25 wt.%) as an internal standard for the Rietveld method [187]. The XRD instrument, equipped with a Cu-K anode, operated at 40 kV and 40 mA. The scan step width (2θ) was 0.017°, and the angle range covered was 10° – 80°. The phases were identified using PANalytical X'Pert HighScore Plus software (version 2.1.0) and the ICDD PDF-2 database 1998. PROFEX software (version 4.3.6) was used to quantify the different crystalline species and the amorphous content by the Rietveld refinement [188] employing the BGMN and the Crystallography Open Databases (COD). XRD-Rietveld analyses were carried out at the Chem4Tech Lab, University of Brescia (Brescia, Italy).

4.6.10 SEM-EDS

Two different SEM-EDS instruments have been employed during this study:

a) SEM-EDS analyses carried out at the Centro de Materiais da Universidade do Porto (CEMUP): A FEI Quanta 400 FEG ESEM/EDAX Genesis X4M was used, operating at 15 kV and in high vacuum mode. Powder and polished block (Section 4.4) samples were carbon sputtered. The backscattered electron detection (BSED) method was used to identify the various phases and provide a detailed structural representation of the particles.

b) SEM-EDS analyses carried out at the Chem4Tech Lab, University of Brescia (Brescia, Italy): A SNE-4500M Plus apparatus from SEC e-beam pioneer (Korea) equipped with EDS detector Xflash® 610 / 630 Mini from Bruker was provided by ABCS srl. The measurements were performed using an acceleration voltage ranging from 1 to 30 kV, and 120 A, under high vacuum conditions. The elemental analysis maps and X-ray spectra were acquired at 20 kV. A secondary electron detector (SED) method was used for the morphological characterization.

4.6.11 Moisture Content

The moisture content was determined according to the ISO 11722 standard [189]. For each sample, 1 g ± 0.1 was placed in Petri dishes and heated at 105 °C for 3 h using a Carbolite Furnace (Sheffield, UK) equipped with N_2 flow. The samples were then cooled at room temperature using a desiccator and re-weighed. This procedure was carried out at the Faculty of Sciences-DGAOT, University of Porto (Porto, Portugal).

4.6.12 LOI Measurements

The LOI was performed according to the ASTM C25-19 standard [190]. For each sample, 1 g ± 0.1 was placed in ceramic crucibles and heated at 1000 °C for 2 h using a 47900-thermolyne muffle from Fisher Scientific GmbH (Schwerte, Germany). The samples were then cooled at room temperature using a desiccator and re-weighed. This procedure was carried out at the Faculty of Sciences-DGAOT, University of Porto (Porto, Portugal).

4.6.13 Total Carbon Content

The total C content was determined using a Vario Max cube from Elementar (Langenselbold, Germany). For each sample, 1 g ± 0.1 was placed into stainless steel crucibles and then incinerated in an oxygen-enriched environment at 900 °C, with He as a carrier gas. The produced gases passed over copper chips at 830 °C, to convert nitrogen oxides to N_2 then through a phosphorus pentoxide absorption tube to remove water. CO_2 and N_2 were separated using an adsorption column and detected. Pure He was used as a reference, while approx. 1.25-2.50 g of the aspartic acid standard was measured as a reference for calibration. The thermal conductivity of the gases and the voltage difference were quantified, and the signal was converted and sent to a PC. The total C determination was performed by the Geographical Institute, Ruhr-Universität Bochum (Bochum, Germany).

Chapter 5: Characterization of the Industrial Alkaline Residues

This chapter explores the different composition of the selected industrial alkaline residues for this study—municipal solid waste incineration fly ash (MSWI FA) and bottom ash (MSWI BA), coal fly ash (CFA), and flue gas desulfurization residues (FGD). These residues were characterized comprehensively to evaluate their role in accelerated carbonation technology (ACT) and their possible synergistic effects when blended, particularly in enhancing CO_2 sequestration, pozzolanic activity, and mechanical properties of the final material post-carbonation, which is crucial for the reuse in construction applications.

Additionally, cork fly ash (CkFA) is also characterized as a potential substitute for CFA and FGD to assess the versatility of this technology, considering that biomass combustion is reputed as carbon-neutral.

The chapter is structured as follows:

- **Section 5.1**: The origin of the industrial residues is presented, with a brief description of their macroscopic characteristics.
- **Section 5.2**: The results of the physical characterization are presented, including particle-size distribution, immediate soluble content, Brunauer-Emmett-Teller (BET) analyses, and magnetic and paramagnetic separation.
- **Section 5.3**: The results of the chemical characterization are presented, including Inductively coupled plasma optical emission spectroscopy (ICP-OES), Ion chromatography (IC), X-ray fluorescence (XRF), X-ray diffraction (XRD-Rietveld), Scanning electron microscopy and energy dispersive X-ray spectroscopy (SEM-EDS), moisture content, Loss on ignition (LOI), and Total carbon (C) determination.

Scientific contribution

This chapter is partially based on the following publications, although the format has been adapted to align with the structure of this dissertation. The content reflects my independent work, including data curation, literature review, formal analysis, investigation, methodology, visualization, and writing. This chapter duly credits the original author of any work not authored by me, and cited parts are reproduced by permission from Elsevier BV and MDPI:

II. **G. P. Sorrentino**; R. Guimarães; B. Valentim; E. Bontempi.
The Influence of Liquid/Solid Ratio and Pressure on the Natural and Accelerated Carbonation of Alkaline Wastes
Minerals 2023, 13(8), 1060, https://doi.org/10.3390/min13081060

III. **G. P. Sorrentino;** R. Guimarães; A. Cornelio; A. Zanoletti; B. Valentim; E. Bontempi.
Mitigating CO_2 Emissions through an Industrial Symbiosis Approach: Leveraging Cork Ash Carbonation
Heliyon 2024, 10(12), e32893, *https://doi.org/10.1016/j.heliyon.2024.e32893*

IV. **G. P. Sorrentino**; T. E. Müller; A. Cornelio; E. Bontempi.
Long-term Carbon Capture through Carbonation and Enhanced Stabilization of Alkaline Incineration Residues, -Manuscript in Preparation

Note: It is important to underscore that a major part of the CkFA characterization was conducted by R. Guimarães, who contributed significantly to our collaborative research paper (III), where the effectiveness of CkFA in ACT was demonstrated. Therefore, while the inclusion of CkFA characterization is essential for the completeness of this study, all credits for this work are attributed to the original researcher, with proper acknowledgment provided throughout the chapter. Further details on the CkFA characterization can be found in the researcher's PhD dissertation [168].

5.1 Origin of the Industrial Alkaline Residues

Five industrial alkaline residues from combustion plants—MSWI FA, MSWI BA, CFA, FGD, and CkFA—were selected as representative residues available worldwide on a billion metric-ton scale [15]. The residues were provided by the waste-to-energy plant and the coal-power plant located in Brescia (Italy), operated by A2A S.p.A., and the stopper-production plant located in Mozelos (Portugal), operated by RELVAS II S.A. Representative images and macroscopic characteristics of the industrial residues are shown in **Table 4**.

Table 4: *Description of the MSWI FA, MSWI BA, CFA, FGD, and CkFA samples.*

Sample Code	Plant Type	Fuel Source	Collection Process Units	Aspect
MSWI FA	Waste-to-Energy Plant	Municipal Solid Waste and Sewage Sludge	Bag Filter	
MSWI BA	Waste-to-Energy Plant	Municipal Solid Waste and Sewage Sludge	Wet Hopper	
CFA	Coal-Power Plant	Hard Coal	Electrostatic Precipitator	
FGD	Coal-Power Plant	Hard Coal	Scrubbing System	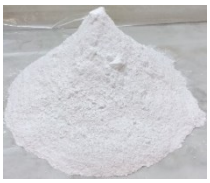
CkFA*	Stopper-Production Plant	Cork Powder	Cyclone	

*[168] picture included

The waste-to-energy (WtE) plant utilizes municipal solid waste (MSW) and sewage sludge (SS) as its energy source in a co-combustion procedure, producing MSWI FA and MSWI BA as a by-product. In the plant, the MSWI FA is collected through an APC system equipped with NO_x abatement using ammonia solution, followed by scrubbing with slaked lime to neutralize hydrochloric acid (HCl) and sulfur oxide (SO_2). The MSWI FA is finally collected with bag

filters and stored. MSWI BA is gathered in wet hoppers beneath the combustion chamber grates, and then passed through a metal recovery before the storage phase.

The coal-power plant employs pulverized hard coal as its energy source, producing CFA and FGD as by-products. In this plant, the APC system downstream of the combustion chamber consists of an electrostatic precipitator responsible for the CFA, followed by a scrubbing phase with slaked lime for the removal of SO_2, responsible for the FGD residues.

The stopper-production plant utilizes cork powder, produced by the plant itself, as its energy source, producing cork fly ash (CkFA) as a by-product. In this plant, the APC system downstream of the combustion chamber consists of a cyclone responsible for the CkFA.

The different origins influence the characteristics of these materials. Indeed, MSWI FA is a fine, grey residue with highly soluble compounds, while MSWI BA is a coarse residue characterized by larger irregular particles of quartz and aggregates. CFA is a fine, black residue composed of aluminosilicates and unburned carbon, while FGD is a fine, white residue consisting mostly of slaked lime, sulfates, and sulfites. CkFA is a fine, dark-white residue composed of burnt and slaked lime and aluminosilicates.

5.2 Physical Characterization

5.2.1 Particle-size Distribution and Immediate Soluble Content

Pretreatment requirements for the selected industrial residues were assessed by particle-size distribution analysis, using dry sieving (DS) and wet sieving (WS) techniques as outlined in Section 4.6.1 (**Table 5**). The results were further correlated with the immediate soluble content, determined as described in Section 4.6.2. For the CkFA sample, only DS data were considered.

Table 5: *Particle-size distribution of the MSWI FA, MSWI BA, CFA, FGD, and CkFA samples.*

Samples	**Process**	**Size Fractions [µm]**				
		> 150	75-150	45-75	25-45	< 25
	Dry sieving (DS)			[wt.%]		
MSWI FA		8.0	9.2	11.8	22.1	48.9
CFA		4.3	8.9	12.6	34.7	39.6
FGD		2.5	8.6	27.2	57.1	4.6
CkFA*		2.9	8.9	21.3	49.5	17.4
	Wet sieving (WS)			[wt.%]		
MSWI FA		6.9	5.7	4.4	4.5	31.5
CFA		3.2	7.3	11.0	16.3	54.4
FGD		0.3	5.1	4.2	4.7	57.2
CkFA		-	-	-	-	-

Dry sieving (DS)	> 4000	2000-4000	1000-2000	500-1000	250-500	150-250	< 150
	[wt.%]						
MSWI BA	41.1	17.8	17.6	9.5	5.1	2.6	6.3

*[168]

Although the MSWI FA and MSWI BA originate from the same combustion plant, significant differences in size were observed. DS experiments revealed that MSWI FA was predominantly composed of fine particles, with over 70 wt.% of the sample passing through a 45 μm sieve. In contrast, MSWI BA consisted mostly of coarse particles, with 58 wt.% exceeding 2 mm in size, though only 6.3 wt.% was smaller than 150 μm. The CFA sample showed a similar profile to MSWI FA, with 74 wt.% passing through a 45 μm sieve, while FGD exhibited slightly coarser particles, with 84 wt.% falling within the 25-75 μm size range. By contrast, the CkFA sample showed a similar profile to FGD, with 71 wt.% in the 25-75 μm size range, and around 17 wt.% passing through a 25 μm sieve [168].

To evaluate the agglomeration influence on DS experiments, WS experiments were also conducted. Due to the coarse nature of MSWI BA, WS was not performed on this sample. WS experiments revealed significant mass reductions, particularly in the MSWI FA, where the mass decreased by up to 47 wt.%. Following WS, the MSWI FA, CFA, and FGD samples were dominated by particles smaller than 25 μm. This reduction suggests the dissolution of salts and sulfates, which may have acted as binding agents. Notably, in the FGD sample, particles smaller than 25 μm increased to 57 wt.%, while those larger than 150 μm were reduced to negligible amounts.

The particle-size distribution analysis indicates that MSWI BA, with its coarser particles, requires mechanical pretreatment to enhance its role in carbonation reactions. Indeed, the smaller particle sizes of the other residues suggest a higher specific surface area, which promotes reactivity and mechanical strength [191]. For this reason, since for MSWI BA the fraction larger than 2 mm is usually employed for metal recovery and building construction, only the fraction with a particle size of < 2 mm was retained and ground as described in Section 4.1. This ground fraction will be referred to as “MSWI BA < 2 mm ground”. It is noteworthy that fine particles may also negatively affect the viscosity and permeability of the slurries used in ACT, which may hinder the mobility of CO_2-rich water, which, in turn, affects the water demand [191]. The WS experiments not only highlighted the strong agglomeration phenomenon affecting the DS experiments, which shifted the particle-size distribution toward smaller dimensions, but also underscored the high solubility of certain residues, particularly MSWI FA and FGD.

On this basis, the determination of the immediate soluble content provides valuable insights into the potential release of compounds relevant to CO_2 sequestration. The MSWI FA sample exhibited the highest soluble content at 45 wt.%, accounting for nearly half of the sample, closely matching the 47 wt.% mass loss observed in the WS experiments. The MSWI BA < 2 mm ground contained 11.5 wt.% of soluble compounds, while CFA had an immediate soluble content of 10 wt.%, consistent with its 8 wt.% WS mass loss. The FGD samples showed a soluble content of 15 wt.% and a WS mass loss of 28 wt.%, likely due to the harsher conditions during WS experiments. CkFA exhibited a soluble content of 11 wt.% [168]. These findings suggest a likely strong contribution in the release of compounds interesting for CO_2 sequestration, such as calcium (Ca) and magnesium (Mg), particularly for MSWI FA.

5.2.2 BET analyses

The reactivity propensity of the selected industrial residues was evaluated through BET analyses to determine the BET surface area (BET-SA) as detailed in Section 4.6.3 (**Table 6**).

Table 6: *BET surface area of the MSWI FA, MSWI BA < 2 mm ground, CFA, and FGD samples.*

	MSWI FA	MSWI BA < 2 mm ground	CFA	FGD	CkFA
			[m²/g]		
BET-SA	7.46	14.29	5.67	7.58	N.A.

N.A.: not analyzed

The results revealed that MSWI FA and FGD exhibited similar BET-SA values, both around 7.5 m^2/g. On the other hand, MSWI BA < 2 mm ground showed a BET-SA value that was twice as high as that of MSWI FA and FGD, while CFA recorded the lowest value, approx. 5.7 m^2/g. Notably, the MSWI FA, CFA, and FGD samples predominantly consist of particles smaller than 75 µm, which typically correlates with higher BET-SA values [191]. Nevertheless, the higher BET-SA of MSWI BA < 2 mm ground suggests that the milling process significantly increased its BET-SA, which is crucial for enhancing both reactivity and mechanical strength.

The BET-SA is influenced by factors such as particle size, structural composition, and material porosity [192]. Based on the BET-SA values, these residues can be classified as small particles with low or non-porosity [192]. As mentioned for the particle-size distribution, BET-SA may also negatively impact the CO_2 diffusivity in the aqueous medium influencing the amount of water required for reactions.

5.2.3 Magnetic and Paramagnetic Separation

The need for magnetic pretreatment for the selected industrial residues was evaluated through magnetic and paramagnetic separation processes as described in Section 4.6.4. This procedure was applied to the bulk MSWI FA and CFA samples, while for MSWI BA, it was conducted on each size faction below 2 mm. Given the origin of FGD, this procedure was not performed on this sample. For the CkFA sample, only magnetic separation data was considered [168].

The magnetic separation of MSWI FA indicated that it predominantly consists of non-magnetic matter, with magnetic and paramagnetic components each accounting for approx. 1.5 wt.% of the total mass. This suggests a minimal presence of magnetically responsive particles in MSWI FA. In contrast, the magnetic separation MSWI BA revealed a distinct correlation between particle size and magnetic content. The results demonstrated that as particle size decreases, the concentration of magnetic material significantly increases, ranging from 8 wt.% to 51 wt.%. The paramagnetic and non-magnetic fractions of MSWI BA exhibited asymmetrical distributions, suggesting a complex mixture of materials within this residue (**Figure 16**).

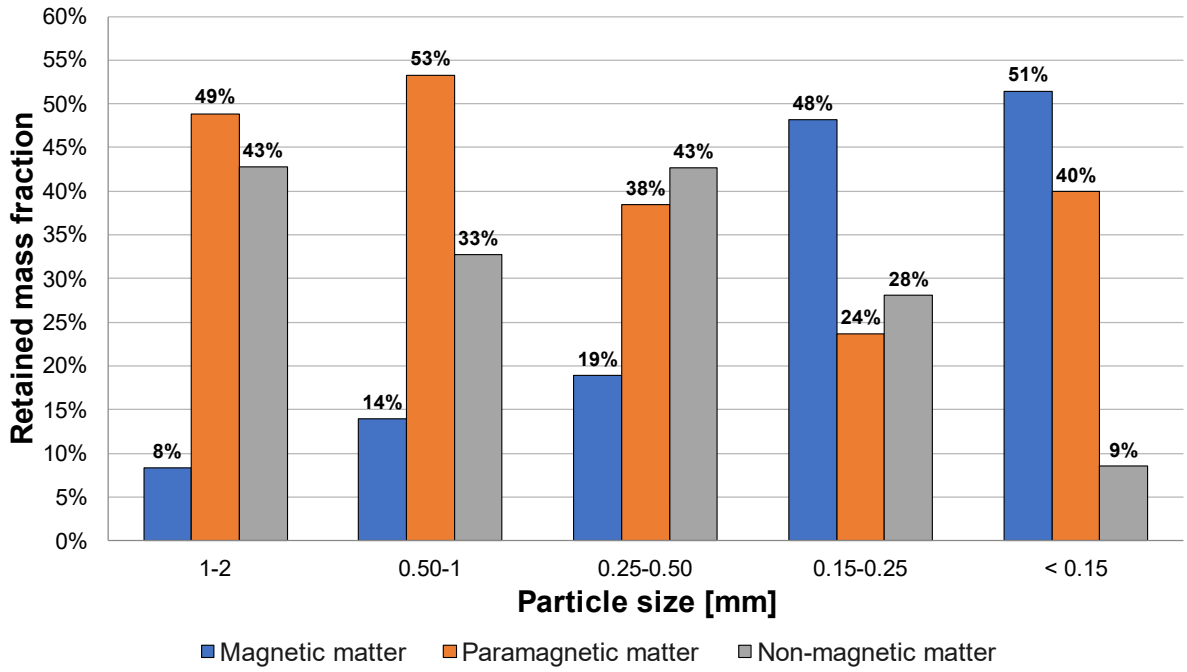

***Figure 16**: Magnetic and Paramagnetic separation for MSWI BA.*

For CFA, the separation results indicated a composition of 45 wt.% of non-magnetic particles, 45 wt.% of paramagnetic particles, and 5 wt.% of magnetic particles. In the case of CkFA, magnetic separation indicated a composition of 97 wt.% non-magnetic particles and 3 wt.% magnetic particles [168].

These findings underscore the distinct characteristics of MSWI BA < 2 mm, particularly its high magnetic content (12 wt.%), which suggests the need for magnetic pretreatment to optimize its role in carbonation reactions. The presence of magnetic material, particularly iron oxides, can adversely affect mineral carbonation processes. Indeed, these magnetic materials can form a passive layer of hematite when exposed to an oxidizing environment, which inhibits the carbonation reaction [193]. Moreover, the observed trend in magnetic content further indicates the importance of considering particle size during magnetic pretreatment. In the case of CFA, the results suggest that selective pretreatment might be necessary, depending on specific process requirements.

5.3 Chemical Characterization

5.3.1 Leaching tests, ICP-OES, and XRF analysis

The potential for CO_2 sequestration and mechanical properties enhancement was evaluated using ICP-OES to analyze the elemental composition of the selected industrial residues, as detailed in Section 4.6.5 (**Table 7**). XRF analyses, outlined in Section 4.6.8 (**Table 8**), were employed to assess the silicon content due to its poor solubility in the digestion acid. Additionally, the leaching propensity of these materials was evaluated by analyzing the elemental composition of the leachates (**Table 7**), complemented with IC analyses to measure the chloride content, as described in Section 4.6.6. For the CkFA sample, ICP-MS and XRF data were considered.

Table 7: *Key data of digested and leachate solutions for the MSWI FA, MSWI BA < 2 mm ground, CFA, FGD, and CkFA samples.*

	MSWI FA		**MSWI BA < 2 mm ground**		**CFA**		**FGD**		**CkFA***	
	Digestion	Leaching	Digestion	Leaching	Digestion	Leaching	Digestion	Leaching	Digestion	Leaching
Elements		pH = 12.5		pH = 12.1		pH = 12.0		pH = 12.7		pH = 12.9
	[mg/kg]	[mg/L]	[mg/kg]	[mg/L]	[mg/kg]	[mg/L]	[mg/kg]	[mg/L]	[mg/kg]	[mg/L]
Ca	306182.3	7761.9	139719.0	357.7	10752.6	220.5	392350.2	1402.0	225000.0	N.A.
Mg	11479.1	< 0.003	14086.9	< 0.003	1643.6	< 0.003	2918.5	< 0.003	26000.0	N.A.
Pb	1770.9	36.4	1018.3	< 0.009	< 0.009	< 0.009	8.7	< 0.009	29.9	< 0.1
Zn	8818.1	4.6	8852.4	0.003	62.6	< 0.001	32.8	< 0.001	187.4	0.3
Mn	263.1	< 0.001	2825.4	< 0.0001	173.9	< 0.001	32.6	< 0.001	2550.0	N.A.
As	12.2	< 0.007	6.2	< 0.007	33.7	< 0.007	< 0.007	0.04	4.2	N.A.
Be	0.5	< 0.001	1.4	< 0.001	3.0	< 0.001	0.2	< 0.001	1.0	N.A.
Cd	93.4	< 0.001	17.3	< 0.001	1.1	< 0.001	< 0.0001	< 0.001	1.3	< 0.032
Co	12.2	< 0.001	66.6	0.002	8.6	< 0.001	0.3	< 0.001	8.1	N.A.
Cr	102.7	0.1	238.6	0.008	36.8	0.2	5.0	0.02	49.0	0.3
Cu	653.8	0.1	3598.3	1.5	42.7	< 0.004	11.0	0.005	224.0	0.04
Mo	9.2	0.1	< 0.002	0.2	29.5	2.1	< 0.002	0.01	1.0	N.A.
Ni	72.4	< 0.002	171.2	0.004	29.6	< 0.002	2.2	< 0.002	27.1	< 0.063
Sb	233.9	< 0.009	< 0.009	0.08	2.7	< 0.009	< 0.009	< 0.009	4000.0	N.A.
Se	< 0.015	0.01	< 0.015	0.01	30.2	1.0	55.7	0.1	N.A.	N.A.

Ti	2168.7	< 0.001	1983.0	< 0.001	444.3	< 0.001	376.5	< 0.001	1000.0	N.A.
V	30.2	< 0.003	42.0	< 0.003	96.4	0.1	4.5	< 0.003	27.0	N.A.
K	21684.6	2214.2	4680.6	111.0	813.8	17.1	172.4	9.8	35000.0	N.A.
Na	23942.1	2361.6	9748.9	383.5	716.5	26.0	419.8	4.3	4000.0	N.A.
Fe	5262.8	< 0.002	44711.3	< 0.002	11276.0	< 0.002	310.7	< 0.002	12000.0	N.A.
Al	13344.1	< 0.001	40372.4	63.5	5984.7	18.9	< 0.001	< 0.001	27000.0	N.A.
P	2880.4	0.3	11327.9	0.2	625.3	0.06	< 0.002	0.05	8000.0	N.A.
Cl	N.A.	16069.6	N.A.	815.1	N.A.	0.3	N.A.	55.0	N.A.	1810.5

N.A.: not analyzed; *[168]

Table 8: *XRF normalized major oxides data of the MSWI FA, MSWI BA < 2 mm ground, CFA, FGD, and CkFA samples.*

Main Oxides	MSWI FA	MSWI BA < 2 mm ground	CFA	FGD	CkFA*
			[%]		
CaO	57.68	27.58	2.53	55.27	37.15
MgO	2.11	4.08	0.96	0.46	5.84
MnO	0.04	0.48	0.05	0.01	0.39
TiO_2	0.51	1.44	1.27	0.05	1.70
K_2O	3.35	1.38	1.40	< LOD	5.85
Na_2O	4.95	2.91	0.56	0.04	0.75
SiO_2	< LOD	32.14	60.05	< LOD	32.97
Fe_2O_3	0.77	8.53	7.30	0.03	2.44
Al_2O_3	0.65	13.57	24.26	< LOD	7.05
P_2O_5	0.37	3.12	0.25	0.02	3.00
SO_3	11.79	3.53	1.36	44.06	2.85
Cl_2O	17.76	1.24	< LOD	0.06	N.A.

LOD: limit of detection; N.A.: not analyzed; *[168]

Despite originating from the same combustion plant, MSWI FA and MSWI BA exhibited significant compositional differences.

In MSWI FA, Ca and Mg, key elements for carbonation, were detected. ICP-OES analysis revealed a particularly high Ca content, confirmed by XRF to constitute nearly half of the residue. This high Ca concentration is consistent with the use of slaked lime in the APC system of the WtE plant used to remove acids (e.g., HCl and HF) and sulfur dioxide (SO_2). Mg was present in much lower concentrations, as corroborated by XRF results. Among heavy metals, lead (Pb), zinc (Zn), and titanium (Ti) were most abundant, likely originating from various municipal waste components such as paints, cosmetics, crystal glass, brass alloy for clothing accessories, batteries, and electronics [194–196]. Elevated concentrations of potassium (K) and sodium (Na) suggest the presence of salts. Iron (Fe) and aluminum (Al), which contribute to material hardness, were found in much lower concentrations compared to Ca. Phosphorous (P) was also detected, consistent with the co-combustion of MSW and SS, which often contain P compounds from sources such as flame retardants, food waste, bones, paper, wood, and textiles [197–199]. SS typically contains 1-3 wt.% of P as well [200,201]. XRF analysis also showed a

consistent presence of chlorine (Cl), likely due to the incineration of plastic materials in MSW [202]. A notable presence of sulfur (S), detected by XRF, can be attributed to the lower boiling temperatures and higher volatility of sulfate phases [203]. The composition of MSWI FA, as plotted in the left corner of the ternary diagram[14] (**Figure 17**), indicates its high potential suitability for CO_2 sequestration.

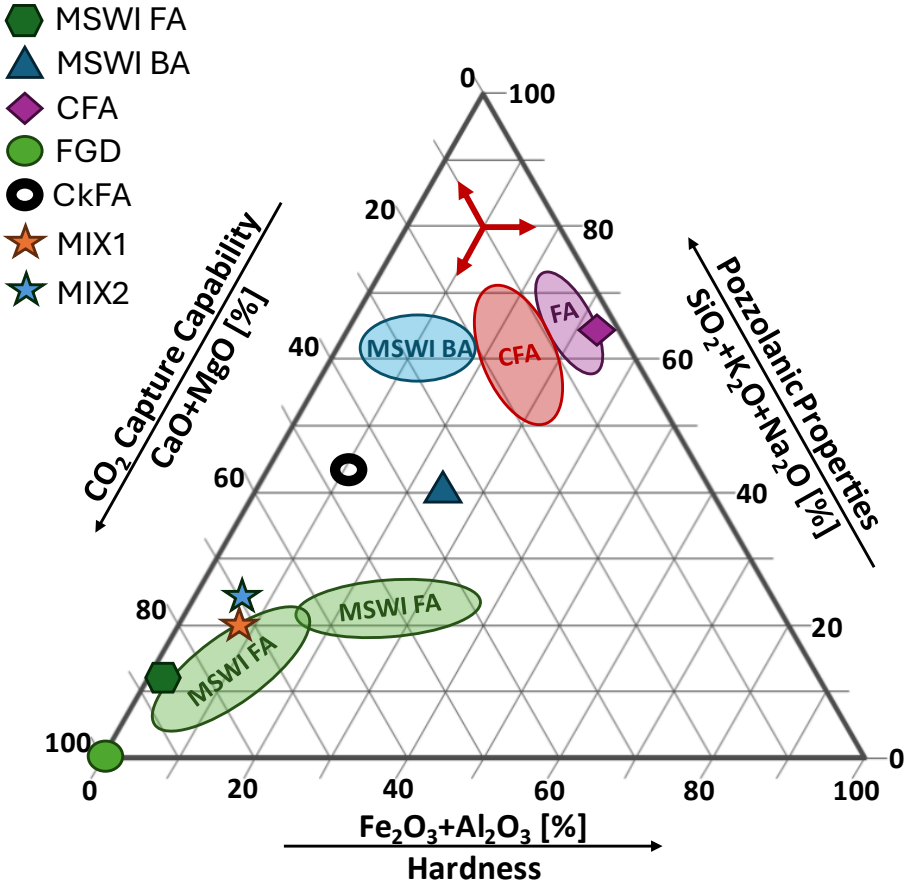

***Figure 17**: Normalized phase ternary diagram (CO_2 Capture Capability – Hardness – Pozzolanic Properties) of the selected industrial alkaline residues contextualized to the residue's areas.*

For MSWI BA, Ca was detected, though at approx. half of the concentration found in MSWI FA, as corroborated by XRF results. The Ca in MSWI BA likely originates from construction debris, certain types of plastics, and biological materials such as paper, waste shells, and bones [204–206]. Mg concentrations were analogous to those in MSWI FA. Heavy metals such as Pb, Zn, manganese (Mn), copper (Cu), and Ti, were prominent in MSWI BA, likely originating from various MSW components, as described for MSWI FA. The similar Pb and Zn concentrations in both MSWI FA and MSWI BA may be attributed to the moderately

[14] The ternary diagram is an adaptation of **Figure 12** according to the literature.

volatile nature of these metals [23]. XRF analyses revealed a high Si content, mainly from glass, amorphous silica, and alumina-silica, consistent with the literature [207,208]. K and Na were found in much lower concentrations than in MSWI FA. In contrast, Fe and Al were found in much higher concentrations in MSWI BA, contributing to the pozzolanic and hardness properties [48], which are important for stabilizing MSWI FA. P was detected at concentrations one order of magnitude higher than in MSWI FA, which is again consistent with the co-combustion of MSW and SS. MSWI BA composition, as plotted near the center of the ternary diagram (**Figure 17**), indicates its potential suitability for CO_2 sequestration while also offering the possibility of obtaining pozzolanic and hardness properties for the final material.

CFA exhibited Ca and Mg concentrations one order of magnitude lower than those in MSWI ashes, making it less suitable for carbonation. Heavy metals were not present in significant concentrations compared to MSWI ashes. XRF analysis indicated the highest silicon content among the residues analyzed, consistent with the literature [139], and lower levels of K and Na compared to MSWI ashes. While Fe and Al were present, their concentrations were lower than in MSWI BA, although XRF showed similar Fe and higher Al content. The composition of CFA, as plotted near the top of the ternary diagram (**Figure 17**), suggests its potential suitability for achieving pozzolanic and hardness properties in the final material. According to the literature, the use of CFA can enhance mechanical properties [209,210].

FGD showed the highest Ca concentration among the residues, consistent with the use of slaked lime in the scrubbing process of the APC system employed in the coal-power plant. Mg concentrations were one order of magnitude lower than those in MSWI ashes. Heavy metals were not detected at significant concentrations. K, Na, and Fe were present in low concentrations, while Al was undetectable by ICP-OES. XRF analyses showed a consistent presence of sulfur, aligning with the purpose of the scrubbing technology. The composition of FGD, as plotted in the left corner of the ternary diagram (**Figure 17**), highlights its high potential suitability for CO_2 sequestration.

For CkFA, Ca was detected in high concentrations, positioning itself between MSWI FA and MSWI BA, as corroborated by XRF results. In contrast, Mg concentrations were the highest among the residues. Heavy metals were not present in significant concentrations except for Ti. XRF analyses revealed a high Si content comparable to that of MSWI BA. K was observed to be the highest among the residues analyzed, while Na was found in low concentrations, comparable to CFA. In contrast, Fe and Al were found in lower concentrations compared to CFA. P was detected in concentrations analogous to those of MSWI BA. The composition of

CkFA, as plotted near the left center of the ternary diagram (**Figure 17**), indicates its potential suitability for CO_2 sequestration while also offering the possibility of obtaining pozzolanic and hardness properties for the final material.

The chemical composition analysis suggests that MSWI FA, MSWI BA, FGD, and CkFA, with their high calcium content, are particularly suitable for CO_2 sequestration. Nevertheless, MSWI FA and BA were also characterized by a high content of heavy metals. By mixing these industrial residues, a final blend (MIX1) with high CO_2 sequestration capability and sufficient pozzolanic and hardness properties can be achieved (**Figure 17**). A similar finding is depicted in **Figure 17** for the blend (MIX2) made by substituting the CFA and FGD with CkFA following the recipe described in Section 4.5.1. Not only could these blends stabilize heavy metals but also render the carbonated material more suitable for various applications, particularly in the construction sector.

To explore the propensity to CO_2 sequestration while minimizing heavy metal leaching, the extent of Ca and heavy metals leaching from the residues was assessed.

Leaching tests, performed at room temperature with ultrapure water, confirmed the high alkalinity of the materials, with leachate pH-values of between 12 and 13. High Ca concentrations in leachates from MSWI FA and FGD were also confirmed, consistent with their bulk compositions. Ca leaching was particularly pronounced in MSWI FA, nearly six times higher than in FGD, reflecting the WS and immediate soluble content results. No data regarding the Ca concentration in the leachates for CkFA were analyzed. Although MSWI BA contained Ca, it did not leach significantly, suggesting it may not contribute substantially to CO_2 sequestration. CFA had a very low calcium content, underscoring its poor suitability for CO_2 sequestration.

Regarding heavy metals, the leachate from MSWI FA contained Pb and Zn at concentrations of 36.4 mg/L and 4.6 mg/L, respectively, which exceed legal limits [211,212]. In MSWI BA, most of the Pb, Zn, and Cu were present in forms not easily dissolved, likely existing in non-silicate minerals such as metallic and spinel inclusions [196]. For CFA, FGD, and CkFA, no detectable amounts of Pb and Zn were present in the leachates.

Additionally, MSWI FA exhibited higher K and Na contents, with the leachate containing a significantly high concentration of Cl, two orders of magnitude higher than the other residues. CkFA also showed a high concentration of Cl, even though it is one order of magnitude lower than MSWI FA.

Overall, MSWI FA and FGD are identified as the most suitable residues for CO_2 sequestration. Nevertheless, the elevated concentrations of Pb and Zn leaching from MSWI FA necessitate a stabilization process to mitigate environmental risks. Regarding CkFA, due to the lack of data on Ca leaching, the verification of its suitability for CO_2 sequestration will be handled in the next section.

5.3.2 Bulk Residues Mineralogy

The carbonation reaction mechanisms and the role of the industrial residues in enhancing the mechanical properties were evaluated through a detailed mineralogical analysis. XRD-Rietveld (**Figure 18**; **Table 9**) and SEM-EDS (**Figure 19**, **Figure 20**, **Figure 21** and **Figure 22**) techniques were employed to identify the mineral phases, as outlined in Section 4.6.9 and 4.6.10a, respectively. Due to the high immediate soluble content in MSWI FA, XRD analysis was also conducted on the washed MSWI FA sample to complement its characterization.

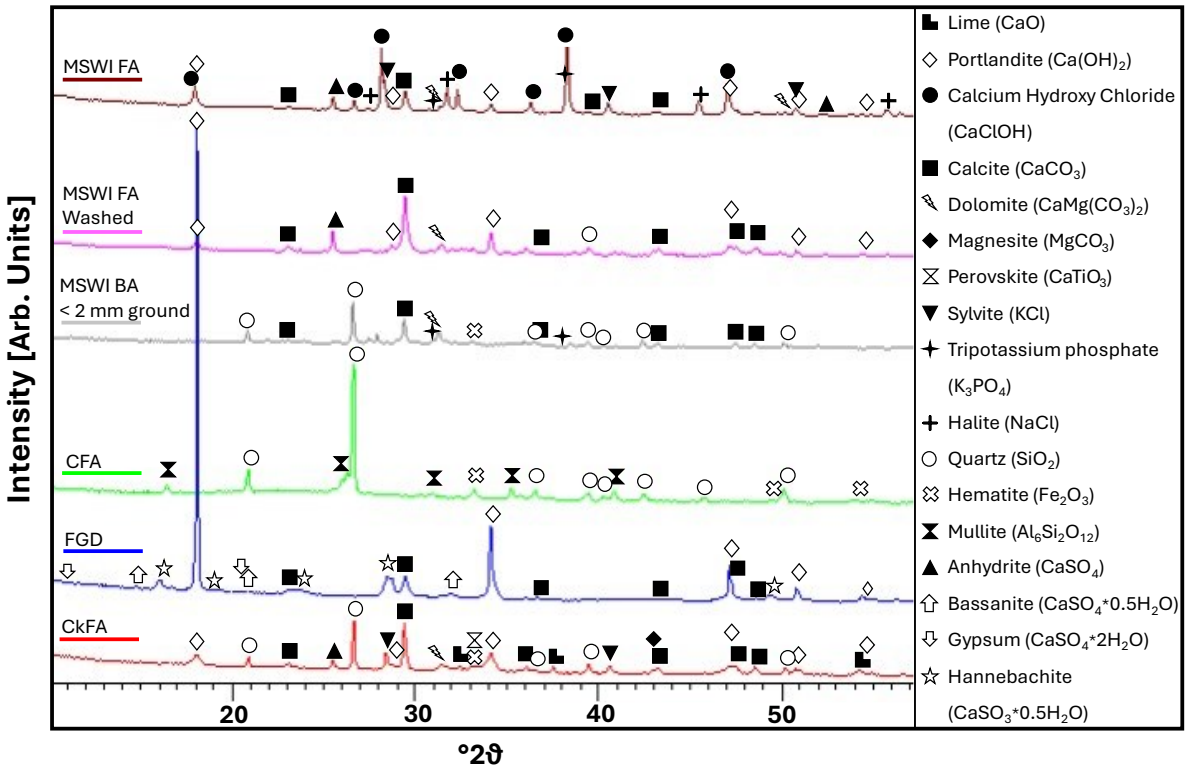

***Figure 18**: XRD patterns of MSWI FA, MSWI FA washed, MSWI BA < 2 mm ground, CFA, FGD, and CkFA.*

Table 9: *XRD-Rietveld analysis of MSWI FA, MSWI BA < 2 mm ground, CFA, FGD, and CkFA samples.*

	MSWI FA	MSWI BA < 2 mm ground	CFA	FGD	CkFA*
		[wt.%]			
Lime (CaO)	-	-	-	-	1
Portlandite ($Ca(OH)_2$)	3	-	-	20	10
Calcium hydroxy chloride (CaClOH)	26	-	-	-	-
Calcite ($CaCO_3$)	11	7	-	11	17
Dolomite ($CaMg(CO_3)_2$)	1	1	-	-	1
Magnesite ($MgCO_3$)	-	-	-	-	3
Perovskite ($CaTiO_3$)	-	-	-	-	3
Sylvite (KCl)	3	-	-	-	3
Tripotassium phosphate (K_3PO_4)	2	7	-	-	3
Halite (NaCl)	5	-	-	-	1
Quartz (SiO_2)	-	8	21	-	12
Hematite (Fe_2O_3)	1	< 1	1	-	2
Mullite ($Al_6Si_2O_{13}$)	-	-	17	-	-
Anhydrite ($CaSO_4$)	4	-	-	-	2
Bassanite ($CaSO_4*0.5H_20$)	-	-	-	5	-
Gypsum ($CaSO_4*2H_20$)	-	-	-	3	-
Hannebachite ($CaSO_3*0.5H_20$)	-	-	-	37	-
Amorphous	44	77	60	24	44

*[213]; The mineral composition of the materials refers to the dry samples.

For MSWI FA, the analyses revealed a variety of Ca-bearing phases, including portlandite, calcium hydroxy chloride (in major amounts), calcite, dolomite, and anhydrite (**Figure 18**, **Table 9**, **Figure 19A-D**), which is consistent with the use of slaked lime in the APC system. Calcium hydroxy chloride and anhydrite likely formed due to reactions of slaked lime with HCl and SO_2, respectively [155,214], while calcite suggests natural carbonation with CO_2 during storage [22]. The high Ca content suggests that it is also present in the amorphous fraction. Apart from dolomite, no crystalline Mg phases were detected, indicating that Mg is predominantly present in the amorphous phase. Heavy metals were not detected in crystalline form, likely due to their relatively low concentration or presence in the amorphous fraction. The sample also contained salts such as sylvite and halite, along with tripotassium phosphate likely derived from biomass and SS combustion condensates. Fe was present as minor amounts of hematite, while Al appeared mainly as amorphous alumina spheres, as revealed by SEM-EDS (**Figure 19A-B**).

The amorphous fraction included partially degraded calcite, amorphous mineral counterparts, either as discrete particles or condensed on the particles' surface, and unburned carbon (**Figure 19A-D**). XRD analysis of the washed MSWI FA confirmed substantial amounts

of soluble crystalline phases, particularly chlorides (**Figure 18**, **Table 9**, **Figure 19A-D**), correlating with the immediate soluble content and the high Cl leaching observed in IC analyses. Salts, particularly chlorides, pose hurdles for reusing these residues, especially in construction, due to their contribution to the rapid corrosion of reinforced concrete [215].

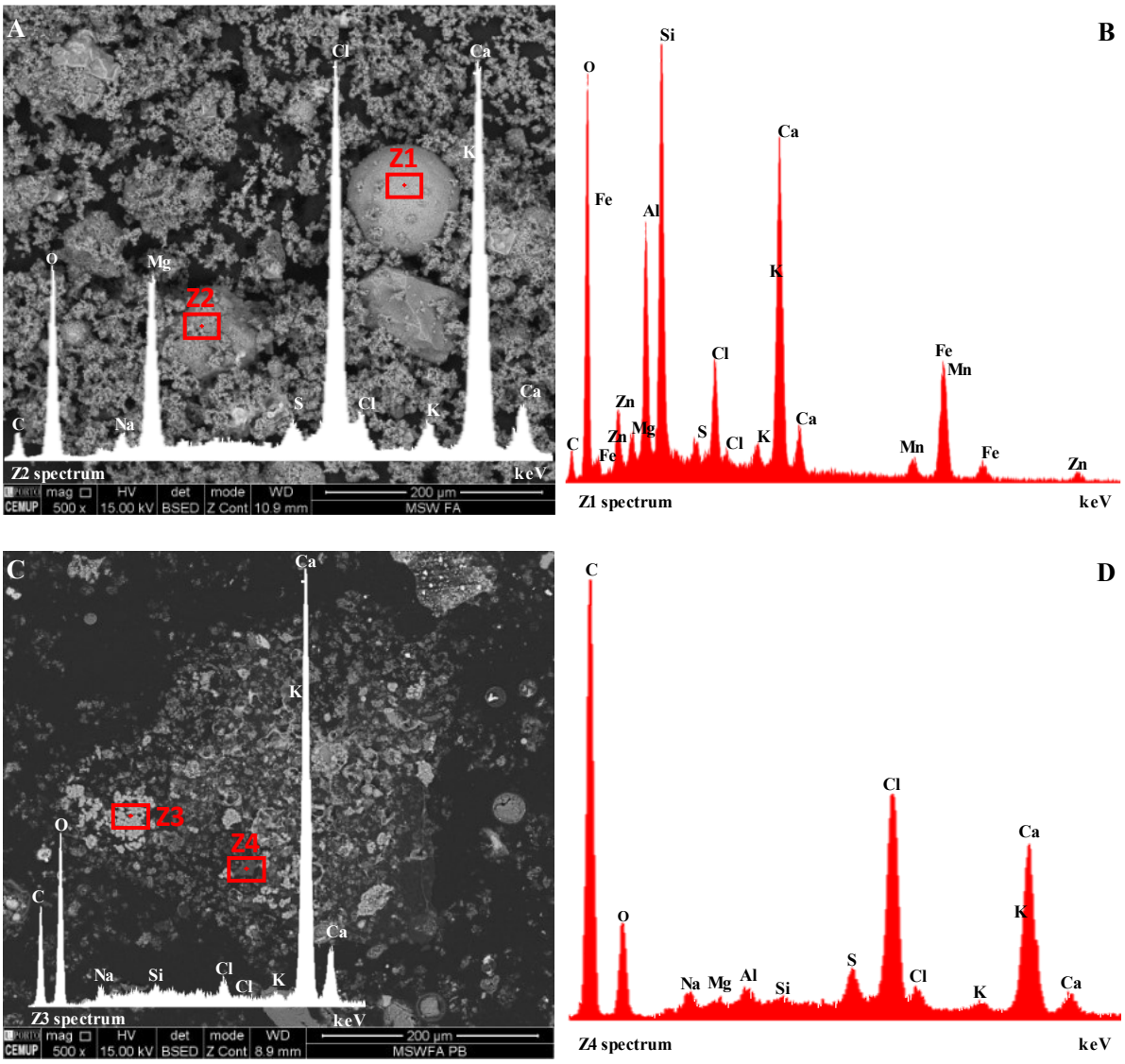

***Figure 19**: SEM Micrographs with EDS spectra of the powder (A, B) and the polished block (C, D) of MSWI FA (Intensity [Arb. Units]).*

In MSWI BA, mineralogical analysis revealed the presence of less reactive Ca phases, mainly carbonates, and silicates such as calcite, and dolomite (**Figure 18**, **Table 9**, **Figure 20A-D**). Minor amounts of calcite relics were also identified. The high Ca content, revealed by the ICP-OES measurements, suggests a substantial portion is present in the amorphous fraction, as observed with SEM-EDS analyses (**Figure 20A-D**). Analogous to MSWI FA, Mg was identified only as dolomite, implying its main presence in the amorphous phase. Heavy metals

were embedded in agglomerates of aluminosilicate glassy spheres, fragments, and other relics (**Figure 20A-D**). The crystalline phases of MSWI BA also included tripotassium phosphate, resulting from SS incineration, and a substantial amount of quartz.

SEM-EDS analysis further revealed that MSWI BA commonly consists of silicates of Fe and Al. The residue is highly heterogeneous, comprising amorphous silica, aluminosilicate slag, amorphous metallic grains of iron, zinc, and various condensed chlorides, phosphates, and sulfates (**Figure 20A-D**). The heterogeneity is attributed to the co-incineration of various wastes, resulting in particles of different sizes and compositions.

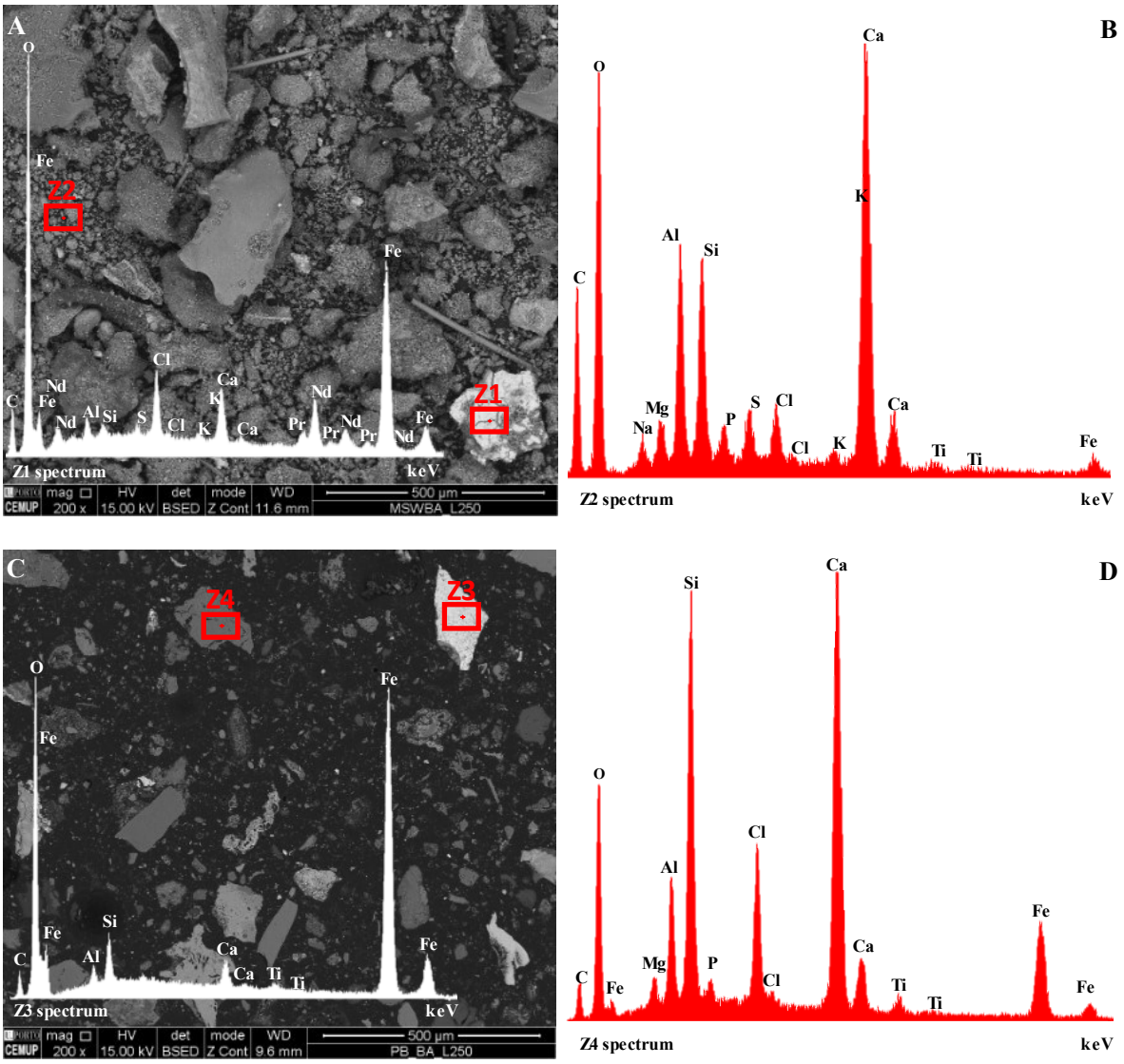

***Figure 20**: SEM Micrographs with EDS spectra of the powder (A, B) and the polished block (C, D) of MSWI BA (Intensity [Arb. Units]).*

The analysis of CFA primarily identified quartz, mullite, and an amorphous aluminosilicate fraction, often in the form of spheres, (**Figure 18**, **Table 9**, **Figure 21A-D**). Unburned carbon was also present as char (**Figure 21A**). No crystalline Ca and Mg compounds were identified, underscoring the different composition compared to MSWI resides.

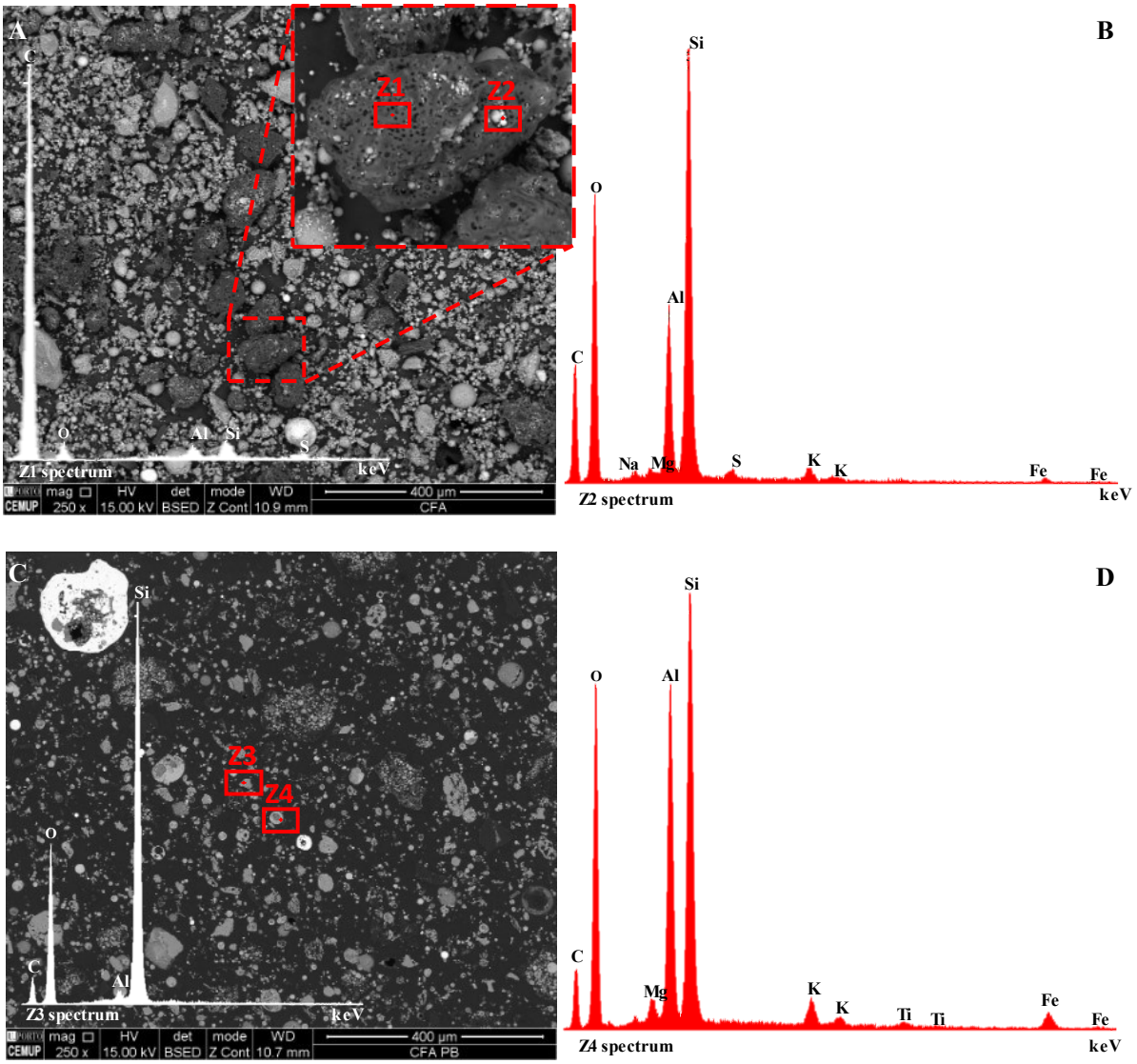

***Figure 21**: SEM Micrographs with EDS spectra of the powder (A, B) and the polished block (C, D) of CFA (Intensity [Arb. Units]).*

FGD residues were predominantly composed of Ca phases, such as hexagonal portlandite[15], calcite, bassanite, gypsum, and hannebachite (**Figure 18**, **Table 9**, **Figure 22A-D**). The high Ca content indicates a significant presence in the amorphous fraction, with no crystalline Mg compounds identified. The high amounts of sulfur-bearing phases (i.e., bassanite, gypsum, and

[15] Based on the literature references [253,254]

hannebachite) reflect the use of slaked lime as a scrubbing agent for sulfur removal from flue gases. The calcite detected might be a result of natural carbonation with CO_2 during storage [22].

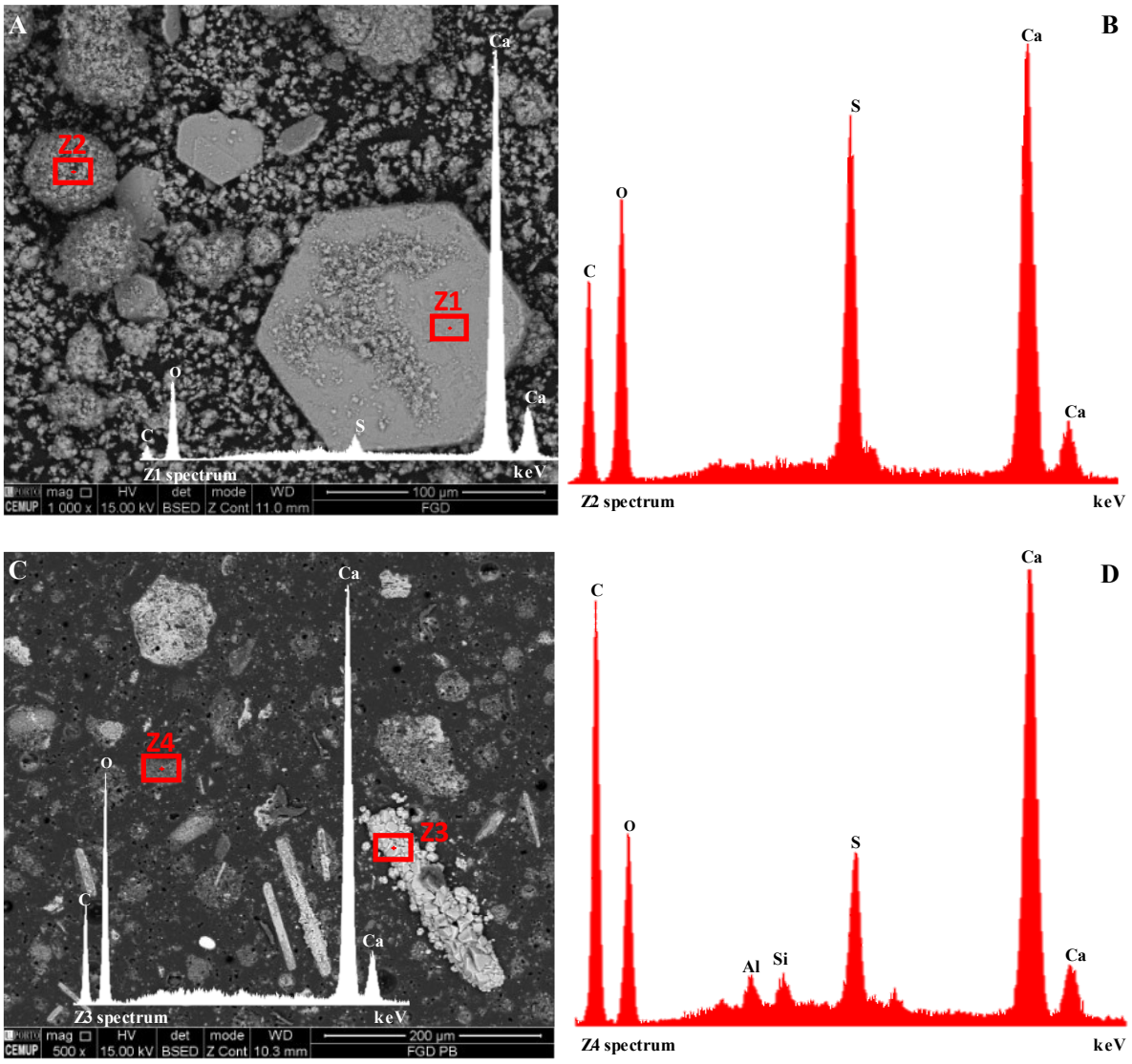

***Figure 22**: SEM Micrographs with EDS spectra of the powder (A, B) and the polished block (C, D) of FGD (Intensity [Arb. Units]).*

For CkFA, the analysis identified a variety of Ca phases, including lime, portlandite, calcite, dolomite, perovskite, and anhydrite (**Figure 18**, **Table 9**). The high abundance of Ca suggests its presence in the amorphous fraction as well. Mg was found as carbonate phases, specifically dolomite and magnesite. Perovskite was the only detected phase containing heavy metals. The sample also included salts such as sylvite, halite, and tripotassium phosphate derived from biomass combustion. Quartz was detected in high concentrations, corroborated by SEM-EDS analyses [168]. Fe was detected in low amounts as hematite, while Al was found as an

amorphous aluminosilicate fraction, also in spherical forms [168]. The amorphous fraction of the CkFA included partially degraded calcite, amorphous discrete particles, and biochar [168].

The mineralogical analysis confirmed that MSWI FA, MSWI BA, FGD, and CkFA contain substantial Ca compounds, corroborating the previous analyses. Nevertheless, only MSWI FA, FGD, and CkFA are particularly rich in reactive crystalline compounds, specifically, lime, portlandite, and calcium hydroxy chloride, making them highly suitable for CO_2 sequestration. In contrast, MSWI BA and CFA are more abundant in silicate and aluminosilicate phases, which contribute towards stabilizing the heavy metals and enhancing the mechanical properties of the final material. Since CkFa also contains substantial quantities of silicates and aluminosilicates, these constituents may also contribute towards such stabilization and enhancement properties. Consequently, these findings highlight the relevance of understanding the mineralogical composition when assessing the potential reuse of industrial residues, particularly in AC technologies and in the development of sustainable construction materials.

5.3.3 Loss on Ignition and Total Carbon Determination

To gain insight into the composition of industrial residues, thermally decomposable compounds and carbon content were assessed through LOI coupled with the total C determination, as elucidated in Section 4.6.12 and 4.6.13, respectively (**Table 10**). The moisture content, measured as per Section 4.6.11, was accounted for in the LOI calculation to ensure accurate results.

Table 10: *Moisture, LOI, and total C content of MSWI FA, MSWI BA < 2 mm ground, CFA, FGD, and CkFA samples.*

	MSWI FA	MSWI BA < 2 mm ground	CFA	FGD	CkFA*
			[wt.%]		
Moisture	1.9	2.9	0.8	1.6	-
LOI (1000 °C)	20.0	10.0	12.1	16.2	15.1
Total C	3.3	3.4	11.0	2.7	3.7

*[168]

The total C analysis for MSWI FA, FGD, and CkFA revealed significantly lower values than the corresponding LOI. This discrepancy suggests that other thermally decomposable compounds are present in addition to unburned carbon. Literature indicates that portlandite decomposes from 400-600 °C [216], while calcium carbonate decomposes from 600-840 °C [217]. The decomposition processes explain the higher LOI observed in these residues. Moreover, calcium hydroxy chloride in MSWI FA, which thermally decomposes within a similar temperature range as portlandite, further contributes to the higher LOI value [216].

Despite having a similar total C-content to MSWI FA and FGD, MSWI BA exhibited a lower LOI. This is likely due to its lower quantity of Ca-based compounds in MSWI BA, as supported by the XRD-Rietveld analyses (Section 5.3.2).

The total C-content of CFA was the highest among the residues and closely matched the LOI value. This high C-content is likely attributed to the presence of unburned carbon, as supported by SEM-EDS analyses (Section 5.3.2). The high temperature of coal combustion leads to the breakdown of carbonates and sulfates, leaving behind a coarse carbonaceous solid residue, known as char (usually > 75 μm). Consequently, CFA size fractions greater than > 75 μm could exhibit high LOI values due to the presence of this unburned carbon.

The comparison of LOI and total C content reveals key insights into the composition of the residues. For MSWI FA, FGD, and CkFA, the higher LOI relative to total C content indicates the presence of thermally decomposable Ca compounds (i.e., lime, portlandite, calcium hydroxy chloride, and calcium carbonate). This presence highlights the potential reactivity of these residues, which is relevant for CO_2 sequestration. In contrast, the findings for MSWI BA, with its lower Ca content, corroborate previous findings and appear unsuitable for CO_2 sequestration.

5.4 Summary and Conclusions

Understanding the composition of industrial alkaline residues is crucial for assessing their potential for CO_2 sequestration, stabilization, and reuse. The residues studied—MSWI FA, MSWI BA, CFA, FGD, and CkFA—show significant variability in their physical and chemical characteristics. A comprehensive characterization, including particle-size distribution, immediate soluble content, BET analysis, magnetic separation, and chemical and mineralogical analyses using ICP-OES, ICP-MS, XRF, IC, XRD-Rietveld, and SEM-EDS, was conducted to assess their suitability for these applications. The LOI and total C content were also determined.

The findings support the selection of these materials for CO_2 sequestration and potential reuse in construction. MSWI FA, CFA, FGD, and CkFA demonstrate particle sizes and BET-SA conducive to high reactivity. In contrast, MSWI BA requires milling to achieve sufficient reactivity by reducing particle size below 150 μm and removing magnetic materials, which could otherwise hinder carbonation efficiency. Although small particle sizes and high BET-SA enhance reactivity, they may limit CO_2 diffusivity by increasing viscosity and lowering permeability in aqueous media. Thus, balancing these parameters with CO_2 mobility and water demand is crucial during the carbonation process.

The high pH-values (12-13) of the leachates confirm the strong alkalinity of these residues, essential for effective carbonation. The presence of soluble Ca compounds in MSWI FA, FGD, and CkFA, was further corroborated by XRD-Rietveld and SEM-EDS analyses, which identified highly reactive compounds such as CaO, $Ca(OH)_2$, and CaClOH. Nevertheless, the presence of leachable Pb and Zn in MSWI FA, exceeding legal limits, accentuates its hazardous nature and thus the need for stabilization.

MSWI BA and CFA, rich in amorphous aluminosilicates and Fe, are likely to enhance the pozzolanic and mechanical properties of the final material post-carbonation. Their role in CO_2 sequestration may be indirect, helping maintain an alkaline environment conducive to $CaCO_3$ precipitation, while stabilizing heavy metals in MSWI FA.

CkFA, with characteristics intermediate to CFA and FGD, may be a potential substitute for both CFA and FGD in ACT.

These findings highlight the potential synergistic benefits of combining these industrial alkaline residues in the proportion proposed in Section 4.5. The resulting material offers better characteristics than the individual residues, balancing CO_2 capture capability, pozzolanic activity, and mechanical properties, thereby enhancing its potential use in ACT and reuse in a circular, environmentally sustainable economy.

Chapter 6: Accelerated Carbonation for Advancing Sustainable Waste Management

This chapter delves into the accelerated carbonation technology (ACT) applied to the selected mixture (MIX1) of industrial alkaline residues—municipal solid waste incineration fly ash (MSWI FA) and bottom ash (MSWI BA), coal fly ash (CFA), and flue gas desulfurization residues (FGD). The study explores the potential for carbon dioxide (CO_2) sequestration and the role of carbonation in stabilizing MSWI FA. Additionally, an alternative mixture (MIX2), where cork fly ash (CkFA) replaces CFA and FGD, was tested to evaluate the versatility of ACT. The main goal here is to substantially reduce the operating time to minutes, as opposed to the months required for natural carbonation (NC). X-ray diffraction (XRD-Rietveld), loss on ignition (LOI), total carbon (C), scanning electron microscopy and energy dispersive x-ray spectroscopy (SEM-EDS), and inductively coupled plasma optical emission spectroscopy (ICP-OES) were used to analyze the carbonated samples.

The chapter is structured as follows:

- **Section 6.1**: An overview of carbonation reactions, focusing on the reactive crystalline compounds in the selected residues.
- **Section 6.2**: Feasibility studies of ACT on MIX1 and MIX2 at an initial CO_2 pressure of 15 bar, comparing these results with NC. The samples were characterized using XRD-Rietveld, SEM-EDS, and TXRF analyses.
- **Section 6.3**: Examination of how variables such as liquid-to-solid (L/S) ratio, CO_2 pressure, and agitation affect CO_2 uptake and operating time. The samples were analyzed using XRD-Rietveld, LOI, and SEM-EDS.
- **Section 6.4**: Optimization results of ACT, demonstrating high CO_2 sequestration in under 60 min, as well as its effectiveness in stabilizing alkaline compounds and heavy metals such as lead (Pb) and (Zn). The study includes pressure- and temperature-variation trials in a batch reactor. The carbonated materials were analyzed via XRD-Rietveld, Total C, SEM-EDS, and ICP-OES, followed by a brief discussion on potential reuse.

Scientific contribution

This chapter is partially based on the following publications, although the format has been adapted to align with the structure of this dissertation. The content reflects my independent work, including data curation, literature review, formal analysis, investigation, methodology, visualization, and writing. This chapter duly credits the original author of any work not authored by me, and cited parts are reproduced by permission from Elsevier BV and MDPI:

I. **G. P. Sorrentino**; A. Zanoletti; S. Ducoli; A. Zacco; P. Iora; C. M. Invernizzi; G. Di Marcoberardino; L. E. Depero; E. Bontempi.
Accelerated and Natural Carbonation of a Municipal Solid Waste Incineration (MSWI) Fly Ash Mixture: Basic Strategies for Higher Carbon Dioxide Sequestration and Reliable Mass Quantification
Environ Res 2022, 217, 114805, https://doi.org/10.1016/j.envres.2022.114805

II. **G. P. Sorrentino**; R. Guimarães; B. Valentim; E. Bontempi.
The Influence of Liquid/Solid Ratio and Pressure on the Natural and Accelerated Carbonation of Alkaline Wastes
Minerals 2023, 13(8), 1060, https://doi.org/10.3390/min13081060

III. **G. P. Sorrentino;** R. Guimarães; A. Cornelio; A. Zanoletti; B. Valentim; E. Bontempi.
Mitigating CO_2 Emissions through an Industrial Symbiosis Approach: Leveraging Cork Ash Carbonation
Heliyon 2024, 10(12), e32893, *https://doi.org/10.1016/j.heliyon.2024.e32893*

IV. **G. P. Sorrentino**; T. E. Müller; A. Cornelio; E. Bontempi.
Long-term Carbon Capture through Carbonation and Enhanced Stabilization of Alkaline Incineration Residues, -Manuscript in Preparation

6.1 Carbonation Reaction Mechanisms

Before the results of carbonation trials are presented, it is important to outline the key reactions that govern the carbonation process for the industrial alkaline residues selected in this study, based on the theoretical framework established in Section 2.3.1.2. Specifically, according to the characterization presented in Section 5.3, the residues contained portlandite ($Ca(OH)_2$) from MSWI FA, FGD, and CkFA, lime (CaO) from CkFA, and calcium hydroxy chloride (CaClOH) from MSWI FA. Considering the aqueous carbonation, the reactions can be summarized as follows [22,52]:

$$CaO_{(s)} + H_2O_{(l)} \rightarrow Ca(OH)_{2(s)} \quad (17)$$

$$Ca(OH)_{2(s)} + CO_{2(g)} \rightarrow CaCO_{3(s)\downarrow} + H_2O_{(l)} \quad (18)$$

$$2CaClOH_{(s)} + CO_{2(g)} \rightarrow CaCO_{3(s)\downarrow} + CaCl_{2(s)} + H_2O_{(l)} \quad (19)$$

These equations encapsulate the essential chemical transformations that occur during the carbonation process.

6.2 Feasibility of Accelerated Carbonation using Industrial Alkaline Residues: Evaluating Original and CkFA-Substituted Mixtures

This section investigates the feasibility of the proposed recipe (MIX1) for accelerated CO_2 sequestration and evaluates the performance of MIX2, where CkFA was used as an alternative to CFA and FGD. The trials were conducted following the sample configuration outlined in **Table 2** and the experimental setup described in **Figure 14** (Section 4.5.1.1).

Five AC trials were performed at 5, 17, 24, 48, and 72 h, along with a blank trial using ultrapure water to monitor the CO_2 sequestration kinetics. The sample IDs for the trials were: MIX1_AC5, MIX1_AC17, MIX1_AC24, MIX1_AC48, MIX1_AC72, MIX2_AC5, MIX2_AC17, MIX2_AC24, MIX2_AC48, and MIX2_AC72. Additionally, NC trials were conducted with MIX1_NC1_0.9 and MIX2_NC1_0.9 over 1 month and compared to AC trials.

6.2.1 CO_2 Pressure Trends during Accelerated Carbonation Trials

The pressure trends (**Figure 23**) showed a rapid logarithmic decrease in CO_2 pressure from 15 bar to approx.—5.8 bar within the first 5 h for both mixtures. Thereafter, the trend declined gradually at different rates: MIX1 reached a plateau at around 2 bar after 24-48 h, while MIX2 stabilized at around 1.9 bar within 17-24 h. In the blank trial, CO_2 solubilization reached only

7.7 bar, indicating that carbonation reactions contributed significantly to pressure reduction in both mixtures already in the first hours. The observed pressure trends approximate first-order reaction kinetics (cf. Eq (10)) [218]. Therefore, it is reasonable to assume a fast reaction-activation to produce calcium carbonate ($CaCO_3$) and subsequent nucleation of $CaCO_3$. These results suggest that both MIX1 and MIX2 are effective in CO_2 sequestration, with MIX2 demonstrating an apparently faster carbonation rate.

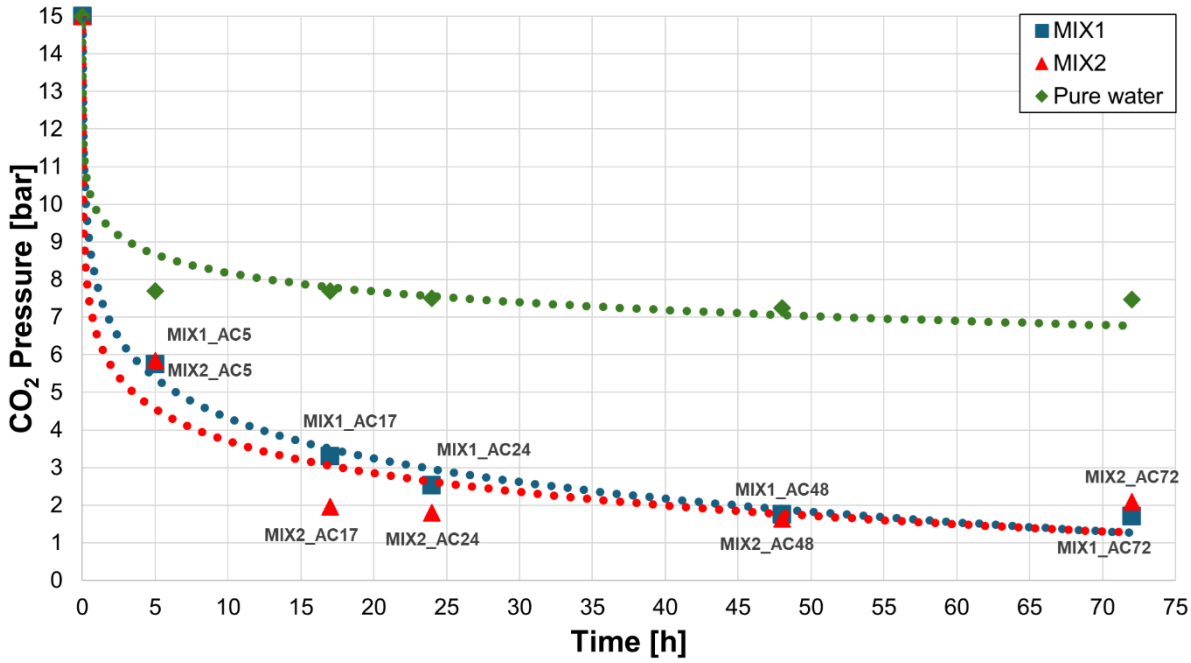

***Figure 23**: CO_2 pressure trends for MIX1 and MIX2 AC trials.*

6.2.2 Characterization of the Carbonated Samples

Mineralogical changes in the carbonated samples were analyzed using XRD-Rietveld (**Figure 24**; **Table 11**), and SEM-EDS analyses (**Figure 25**; **Table 12**), as elucidated in Sections 4.6.9 and 4.6.10b.

The XRD-Rietveld analyses revealed a substantial reduction in $Ca(OH)_2$ and CaClOH content during AC trials, from 5 wt.% and 15 wt.% to 1 wt.% and 10 wt.% for MIX1, and to < 1 wt.% and 7 wt.% for MIX2, respectively. The $CaCO_3$ (specifically, calcite) content increased in both mixtures by 78 % for MIX1 and 46 % for MIX2 after 72 h, indicating effective carbonation. In NC trials, $Ca(OH)_2$ and CaClOH were fully depleted in MIX1, while MIX2 retained 3 wt.% of CaClOH. The total $CaCO_3$ content increased to 28 wt.% and 33 wt.%, for MIX1 and MIX2, respectively. Both NC samples contained calcite and vaterite, with MIX1 having higher vaterite content (5 wt.%).

The formation of calcite and vaterite along with the consumption of the Ca-bearing reactant, confirms successful CO_2 sequestration as described in Eqs. (18) and (19). Calcite is the most stable polymorph of $CaCO_3$, while vaterite, being metastable, converts into calcite over time [22,219]. Its presence may be related to the carbonation of amorphous calcium silicate hydrates (CSH) when the Ca/Si ratio exceeds 0.75 [219] and is favored by lower $[Ca^{2+}]/[CO_3^{2-}]$ ratios [220].

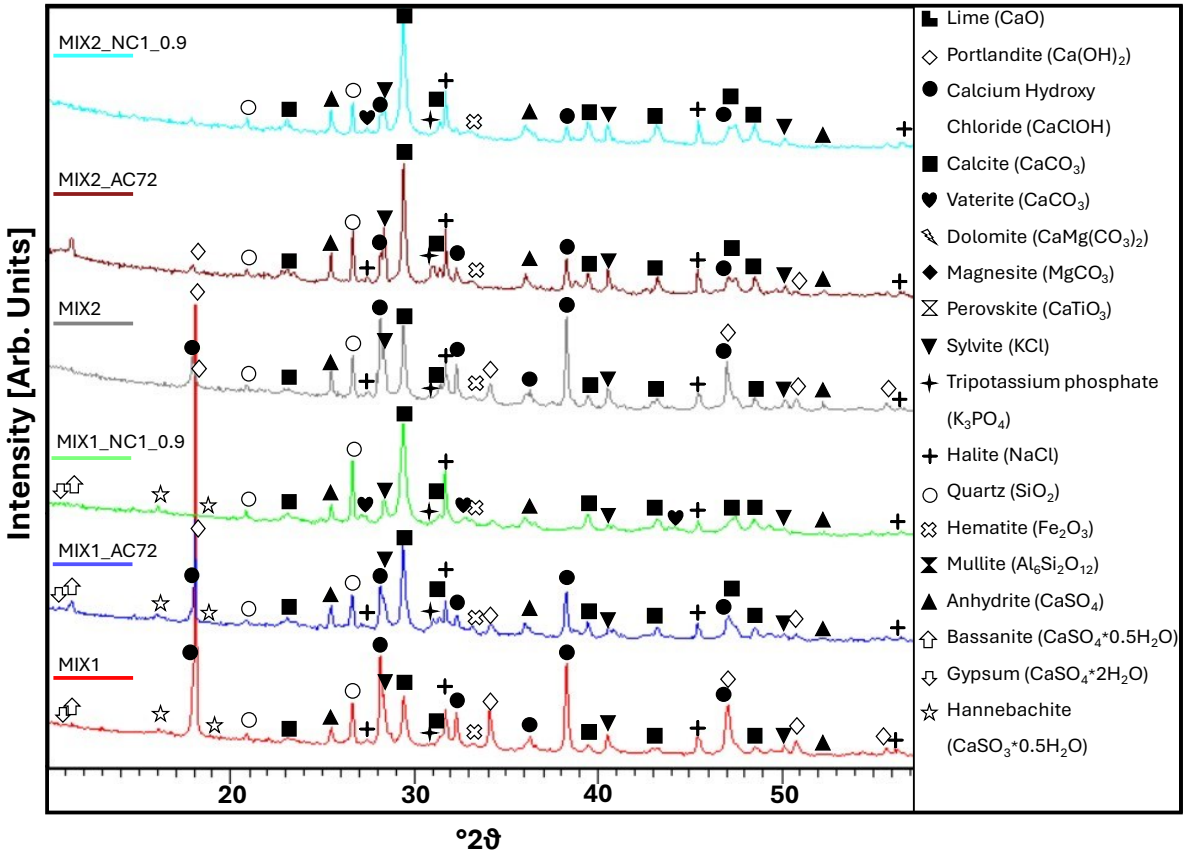

***Figure 24**: XRD patterns of MIX1 and MIX2 with their corresponding AC samples (AC72) and NC samples (NC1_0.9).*

Calcium chloride ($CaCl_2$), a reaction product in Eq. (19), was not detected by XRD-Rietveld refinement, likely due to its possible reaction with CO_2 as shown in Eq. (16), which could produce an acidic environment [221]. Nevertheless, the alkaline environment provided by all the industrial alkaline residues selected, including MSWI BA and CFA, likely buffered this acidic environment, supporting ongoing carbonation reactions [222,223]. Therefore, MSWI BA and CFA indirectly contribute to the carbonation reaction. A slight decrease in KCl for MIX1, after 72 h and during the NC trial, suggests a possible recombination into the amorphous phase. In a prior study involving comparable samples that underwent NC for 3 months, a link between carbonation and a decrease in the amorphous content was observed [22]. Nevertheless, this behavior was not systematically observed, showing no clear trend of the amorphous content.

***Table 11**: XRD-Rietveld analyses of MIX1 and MIX2 with their corresponding AC samples (AC5 to AC72) and NC samples (NC1_0.9).*

	Sample MIX1						
	MIX1	**AC5**	**AC17**	**AC24**	**AC48**	**AC72**	**NC1_0.9**
				[wt.%]			
Portlandite ($Ca(OH)_2$)	5	1	1	1	1	1	< 1
Calcium hydroxy chloride (CaClOH)	15	10	13	9	10	10	< 1
Calcite ($CaCO_3$)	9	14	15	15	15	16	23
Vaterite ($CaCO_3$)	-	< 1	< 1	< 1	< 1	< 1	5
Dolomite ($CaMg(CO_3)_2$)	1	2	2	2	2	2	< 1
Sylvite (KCl)	2	2	2	2	2	1	1
Tripotassium phosphate (K_3PO_4)	2	2	3	3	3	3	1
Halite (NaCl)	3	3	3	3	2	3	3
Quartz (SiO_2)	4	4	4	5	4	5	4
Hematite (Fe_2O_3)	1	1	1	1	1	1	< 1
Mullite ($Al_6Si_2O_{13}$)	2	2	2	2	2	2	1
Anhydrite ($CaSO_4$)	2	3	2	3	3	3	2
Bassanite ($CaSO_4*0.5H_20$)	1	4	6	4	4	4	7
Gypsum ($CaSO_4*2H_20$)	1	1	2	1	2	2	2
Hannebachite ($CaSO_3*0.5H_20$)	7	8	7	4	6	6	4
Amorphous	45	43	38	45	45	43	46
	Sample MIX2						
	MIX2	**AC5**	**AC17**	**AC24**	**AC48**	**AC72**	**NC1_0.9**
Lime (CaO)	< 1	< 1	< 1	< 1	< 1	< 1	< 1
Portlandite ($Ca(OH)_2$)	5	< 1	3	< 1	< 1	< 1	< 1
Calcium hydroxy chloride (CaClOH)	15	9	10	7	9	7	3
Calcite ($CaCO_3$)	13	17	18	19	19	19	31
Vaterite ($CaCO_3$)	-	< 1	< 1	< 1	< 1	< 1	2
Dolomite ($CaMg(CO_3)_2$)	1	2	1	2	2	3	< 1
Magnesite ($MgCO_3$)	1	3	3	3	3	3	1
Perovskite ($CaTiO_3$)	1	2	2	2	2	2	1
Sylvite (KCl)	3	3	3	3	3	3	2
Tripotassium phosphate (K_3PO_4)	3	4	4	5	4	4	3
Halite (NaCl)	3	4	3	4	3	4	3
Quartz (SiO_2)	5	3	5	7	4	4	5
Hematite (Fe_2O_3)	1	1	1	1	1	< 1	1
Anhydrite ($CaSO_4$)	3	5	4	4	4	3	2
Amorphous	47	48	43	45	48	48	48

The mineral composition of the materials refers to dry samples.

SEM-EDS analyses of MIX1_AC5 and MIX1_NC1_0.9 (**Figure 25**, **Table 12**) showed aggregated particles with heterogeneous elemental distribution, consistent with documented carbonated sample morphologies [224]. For instance, MIX1_AC5 showed regions rich in Ca, Na, and Cl (likely CaClOH and NaCl), as well as areas containing Ca, Si, and Al (likely calcium silicate hydrates and calcium aluminate hydrates). Hexagonal $Ca(OH)_2$ crystals were also observed, suggesting incomplete carbonation in MIX1_AC5, corroborated by XRD results.

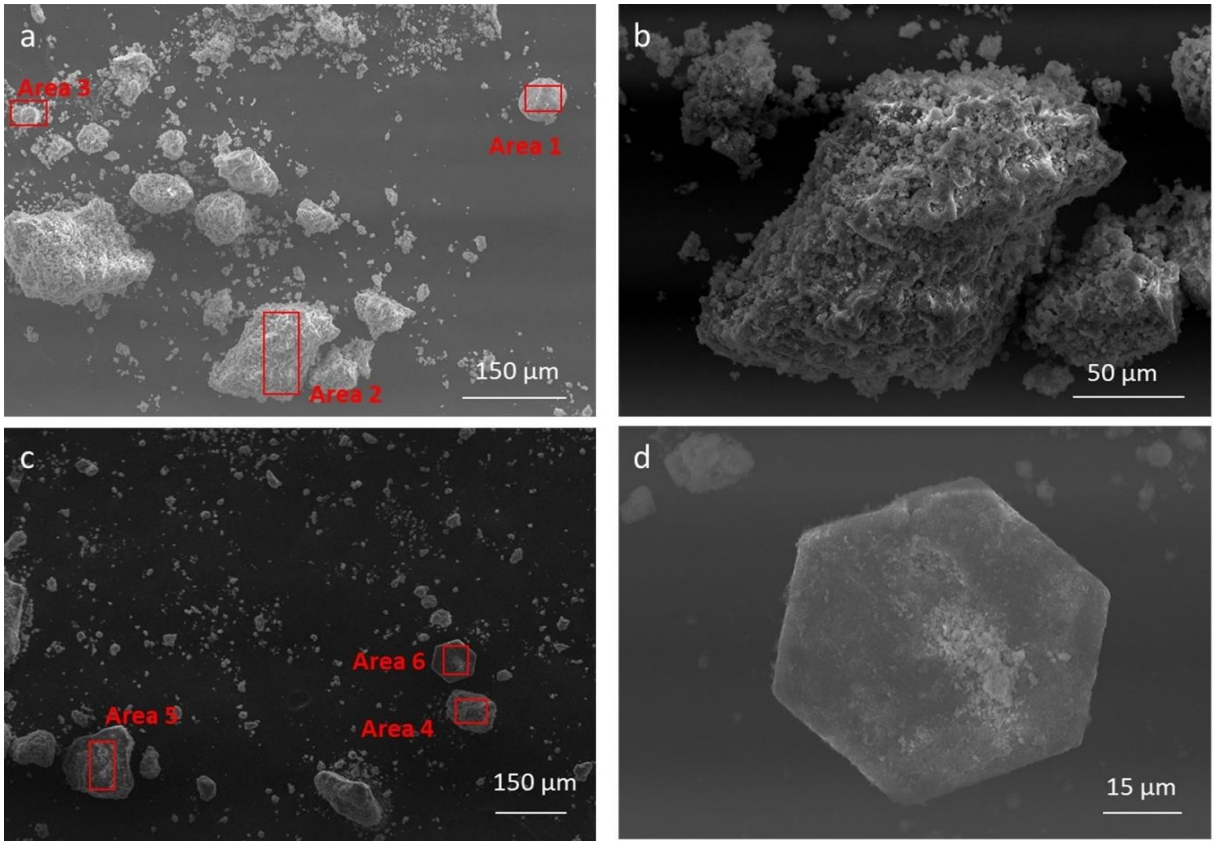

***Figure 25**: SEM Micrographs of samples MIX1_NC1_0.9 (a, b) and MIX1_AC5 (c, d).*

***Table 12**: EDS analysis of samples MIX1_NC1_0.9 (Areas 1, 2, and 3) and MIX1_AC5 (Areas 4, 5, and 6).*

Samples	Areas	Elements												
		Ca	Mg	Zn	Na	K	Si	Fe	Al	P	S	Cl	C	O
		[%]												
MIX1_ NC1_0.9	1	13.3	0.2	-	0.1	0.1	0.1	-	0.1	-	0.6	2.5	51.5	31.6
	2	20.2	0.2	-	6.9	0.3	1.0	-	0.9	0.1	3.5	13.4	24.3	29.3
	3	15.4	1.4	1.7	0.6	0.2	1.9	8.6	1.9	-	3.3	3.5	25.0	36.6
MIX1_ AC5	4	22.6	2.7	-	4.5	5.3	1.5	0.5	1.3	-	3.4	14.2	-	44.1
	5	10.0	0.4	-	4.2	0.2	23.5	-	11.5	-	1.1	1.8	16.8	30.6
	6	38.9	-	-	-	-	-	-	-	-	0.5	0.9	29.0	30.8

6.2.3 CO_2 Uptake Quantification

The amount of CO_2 sequestered during the AC trials was quantified using three methods: (i) mass change before and after the trials (Lavoisier's law), (ii) pressure difference (ideal gas model), and (iii) XRD-Rietveld refinement using the total $CaCO_3$ content. For NC trials, only XRD-Rietveld was applied. The results are shown in **Figure 26**.

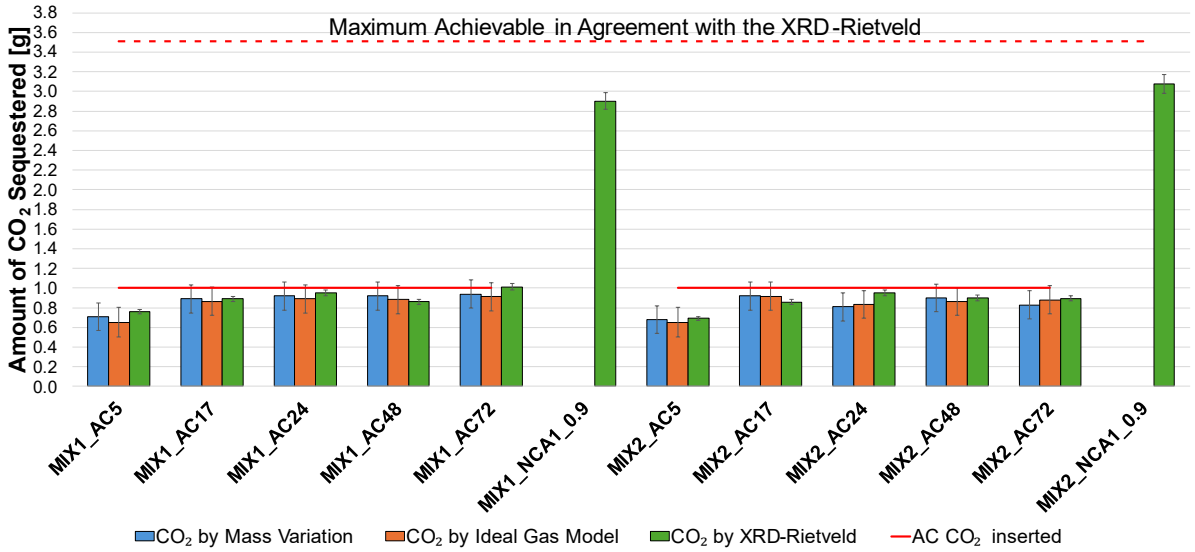

***Figure 26**: Amount of CO_2 sequestrated for MIX1 and MIX2, with their corresponding AC samples (AC5 to AC72) and NC samples (NC1_0.9), evaluated by mass variation, ideal gas law, and XRD-Rietveld refinement methods. AC CO_2 inserted represents the amount of CO_2 inserted in the sample cylinder for AC trials.*

The results from all three methods were consistent, confirming the reliability of these methods for quantifying CO_2 sequestered during AC.

XRD-Rietveld refinement showed that CO_2 uptake increased over time, reaching a yield of 95 wt.% for MIX1 and MIX2 already after 24 h, reflecting fast initial reaction kinetics. Stoichiometric calculations, assuming that the reactions were entirely reliant on crystalline reagents (**Table 11**), indicated a maximum possible CO_2 uptake of 3.5 g for both mixtures (red dashed line in **Figure 26**), confirming that CO_2 was the limiting reactant in AC trials, as shown by residual $Ca(OH)_2$ and CaClOH after 72 h.

In NC trials, MIX1 sequestered 2.9 g of CO_2 and MIX2 sequestered 3.1 g after 1 month, neither in this case reaching the stoichiometric limit that would suggest a potential higher CO_2 sequestration. This points to possible effects, such as temperature, air moisture, or $CaCO_3$ coating layer, which can inhibit the NC process.

Normalized to MSWI FA content, CO_2 uptake in the AC process was 51 kg CO_2/mt MSWI FA for MIX1 and 48 kg CO_2/mt MSWI FA for MIX2. In NC trials, it reached 146 kg CO_2/mt MSWI FA for MIX1 and 155 kg CO_2/mt MSWI FA for MIX2.

These values do not include CO_2 naturally sequestered during storage at incineration plants before the residue sampling. These results demonstrate the feasibility of using industrial alkaline residues for CO_2 sequestration via ACT. The process could sequestrate more CO_2 by optimizing conditions, such as CO_2 pressure or L/S ratios. The substitution of CFA and FGD with CkFA further highlights the versatility of this technology, as CO_2 uptake was similar in both AC and NC trials across mixtures.

6.2.4 Stabilization Results

The role of carbonation in stabilizing MSWI FA, alongside pozzolanic reactions [22], was evaluated using TXRF analyses of the leachates from carbonated samples (Section 4.6.7). To ensure data comparability, leachates from MSWI FA were also analyzed using TXRF (Section 4.6.7). The results are shown in **Table 13** and **Figure 27**.

***Table 13**: TXRF analyses of MIX1 and MIX2 with their corresponding AC samples (AC5 to AC72) and NC samples (NC1_0.9). Data for MSWI FA is also reported.*

		pH	Pb			Zn		
			[mg/L]			[mg/L]		
	MSWI FA	12.3	42.17	±	2.09	9.72	±	1.53
MIX1	**AC5**	12.3	10.69	±	0.66	1.98	±	0.21
	AC17	12.4	8.94	±	1.43	1.33	±	0.73
	AC24	12.2	9.83	±	2.95	1.42	±	0.49
	AC48	12.3	7.31	±	1.22	1.19	±	0.04
	AC72	12.3	7.33	±	2.40	1.50	±	0.47
	NC1_0.9	9.8		< LOD		0.44	±	0.11
MIX2	**AC5**	12.2	5.74	±	0.30	1.31	±	0.27
	AC17	12.3	6.79	±	2.09	1.49	±	0.76
	AC24	12.2		N.A.			N.A.	
	AC48	12.5		N.A.			N.A.	
	AC72	12.2	6.19	±	1.63	1.44	±	0.27
	NC1_0.9	12.2	0.28	±	0.03	0.18	±	0.08

LOD: limit of detection; N.A.: not analyzed

The AC tests maintained a high pH-level (average 12.2), indicating ongoing OH^- and Ca^{2+} ions generation from residual undissolved deposits (e.g., $Ca(OH)_2$ and CaClOH). In contrast, MIX1_NC1_0.9 showed a reduced pH of 9.8 and complete consumption of Ca-reactants, while MIX2_NC1_0.9 retained 3 wt.% of CaClOH, resulting in unchanged pH-values.

Initial Pb and Zn concentrations in MSWI FA leachates were approx. 42 mg/L and 10 mg/L, respectively. The dilution of MSWI FA, caused by the addition of the other industrial residues, reduced these concentrations by roughly 41 %. In AC trials, Pb and Zn concentrations in leachates dropped significantly by 83-85% for both mixtures, potentially due to the stabilizing

effect of drying at 105 °C before characterization, as noted in the literature [17,23]. Nevertheless, Pb and Zn concentrations in MIX1 showed a slight decrease trend over time, likely due to a stabilization effect of the carbonation reactions.

In contrast, NC trials showed Pb concentrations below detection limits for MIX1 (0.0011 mg/L) and 0.28 mg/L for MIX2, while Zn concentrations dropped by an order of magnitude to 0.44 mg/L and 0.18 mg/L for MIX1 and MIX2, respectively. This stabilization is attributed to both pozzolanic and carbonation reactions, forming carbonaceous agglomerates and calcium silicate hydrates (CSH) and calcium (alumino)silicate hydrates (C-(A-)S-H) [22].

These results highlight the potential role of carbonation in enhancing the stabilization of heavy metals, complementing the pozzolanic effect. The use of CkFA as an alternative to CFA and FGD further highlights the versatility of the process, as both mixtures showed comparable performance in stabilizing heavy metals.

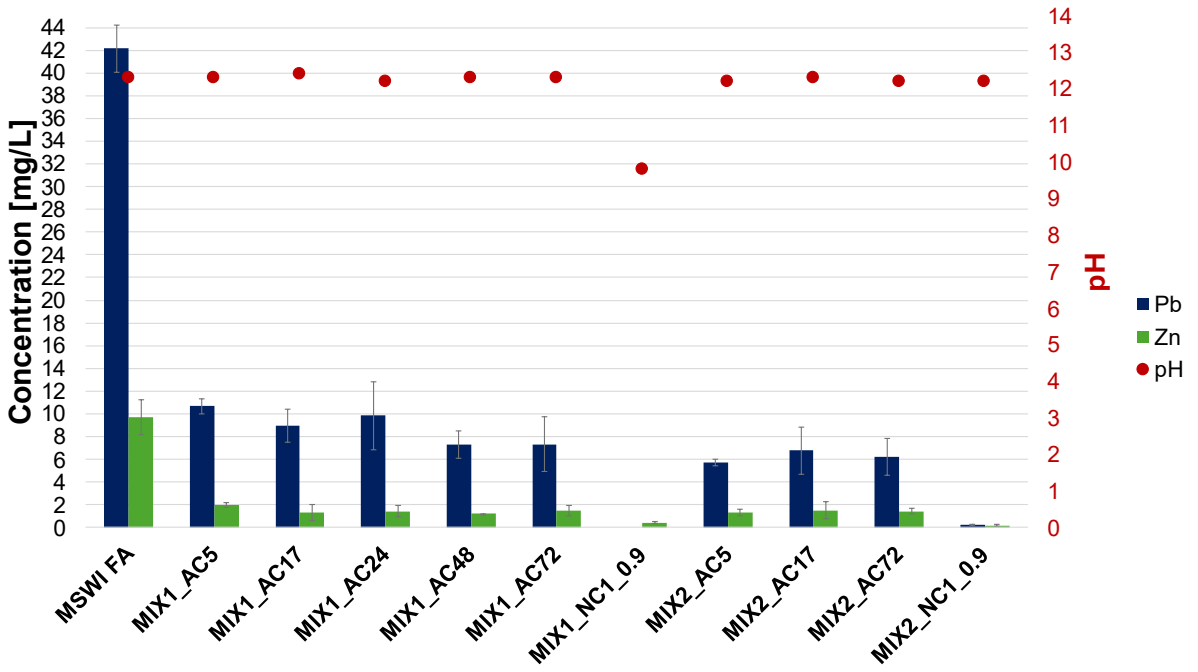

***Figure 27**: Pb and Zn concentrations and pH values of the leachates for MIX1 and MIX2, with their corresponding AC samples (AC5 to AC72) and NC samples (NC1_0.9). Data for MSWI FA is also reported.*

6.2.5 Summary and Conclusions

This study investigated the CO_2 sequestration potential of a mixture of industrial alkaline residues (i.e., MSWI FA, MSWI BA, CFA, and FGD) while also focusing on stabilizing leachable heavy metals. To assess its versatility, CkFA was evaluated as an alternative to CFA and FGD under the same conditions, considering that biomass combustion is reputed as carbon-neutral. The technology was tested using AC with 1 g of CO_2 gas at 15 bar and compared with NC conditions, via sample characterization using XRD-Rietveld, SEM-EDS, and TXRF analyses.

Both mixtures performed similarly. During AC trials, rapid $CaCO_3$ formation occurred, with both MIX1 (with CFA and FGD) and MIX2 (with CkFA) sequestering 95 wt.% CO_2 in 24 h. CO_2 uptake was 51 and 48 kg CO_2/mt MSWI FA, respectively. In NC trials, CO_2 sequestration reached approx. 146 and 155 kg CO_2/mt MSWI FA, due to reactions with both crystalline and amorphous Ca-phases. These results suggest that AC could potentially offer higher CO_2 sequestration, as CO_2 was the limiting reactant in the AC trials.

Regarding heavy metal stabilization, AC trials showed significant reductions in Pb and Zn leaching, likely enhanced by sample drying. NC trials also achieved substantial decreases in Pb and Zn leaching, meeting or nearly meeting regulatory standards for reuse or landfilling. This stabilization is attributed to pozzolanic reactions, which formed C–S–H and C–A(–S)–H phases that can also react with CO_2 to produce $CaCO_3$ phases.

These findings highlight the potential of combining industrial residues for accelerated CO_2 sequestration. The versatility of using alternative residues such as CkFA further supports the potential of this approach. Future investigations, shown in the next section, will explore varying water content, exposure time, and pressure to optimize ACT for MIX1. Potentially expanding the use of similar residues.

This study demonstrates the potential synergistic benefits of these mixtures, offering enhanced CO_2 sequestration, pozzolanic activity, and mechanical properties, contributing to a circular economy, while helping to mitigate harmful environmental effects.

6.3 Enhanced Mass Transfer in Accelerated Carbonation: Influence of Liquid/Solid Ratio and Pressure Adjustments

This section examines the effect of the liquid-to-solid (L/S) ratio and CO_2 pressure on the accelerated CO_2 sequestration process applied to the previously studied MIX1 recipe. Here, only CO_2 uptake was evaluated, which followed the sample configuration outlined in **Table 2** and the experimental setup shown in **Figure 14** (Section 4.5.1.1).

Three AC trials were conducted with L/S ratios of 0.7, 0.9, and 1.2 using a larger sample cylinder (150 mL). For the L/S ratio of 0.9, an additional AC trial was carried out at a constant CO_2 pressure of 15 bar. The sample IDs for the trials were: MIX1_AC_0.7, MIX1_AC_0.9, MIX1_AC_0.9bis, and MIX1_AC_1.2. Additionally, NC trials were conducted over 1 month and compared to AC trials: MIX1_NC1_0.7, MIX1_NC1_0.9, and MIX1_NC1_1.2. A further NC trial for the L/S ratio of 0.9 was extended to 2 months (MIX1_NC2_0.9) only for SEM-EDS analyses.

6.3.1 CO_2 Pressure Trends during Accelerated Carbonation Trials

As in the previous section, the pressure trends (**Figure 28**) showed a rapid logarithmic decrease within the first 2 h, indicating a strong initial carbonation reaction.

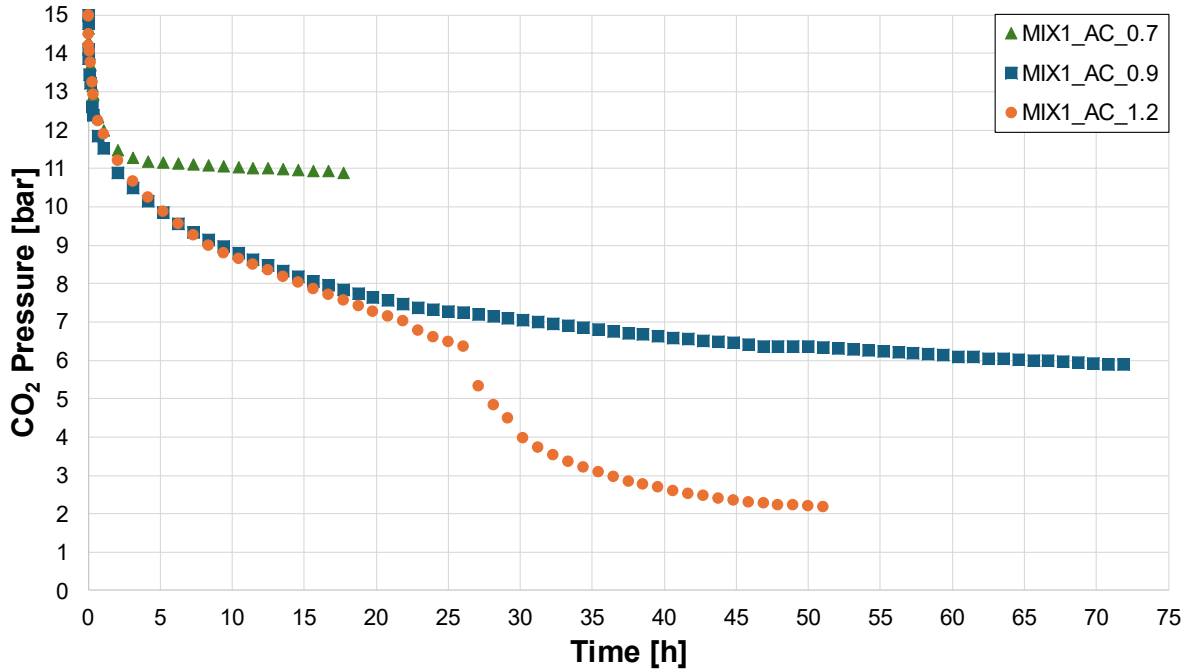

***Figure 28**: CO_2 pressure trends for MIX1 AC trials at different L/S ratios (0.7, 0.9, and 1.2).*

Beyond this initial behavior, the trends showed varying rates of decline based on the L/S ratio. In the MIX1_AC_0.7 trial, the CO_2 pressure decreased within 4 h, stabilizing at around 11 bar until the end of the trial (17 h). The MIX1_AC_0.9 trial, in contrast, experienced a

continuous, gradual pressure decrease after the first 5 h, nearly plateauing at around 6 bar over 72 h. Similarly, the MIX1_AC_1.2 trial showed a smooth pressure decline between 5-26 h, also stabilizing at around 6 bar, comparable to MIX1_AC_0.9. The asymptotic pressure drop suggests a possible conclusion of the carbonation reaction. Afterward, the mixture/CO_2 system was agitated by rotating the sample cylinder, thus reactivating the pressure decrease, which plateaued at around 2 bar after 52 h.

These varying pressure trends highlight the significant role of the L/S ratio in CO_2 diffusivity in the mixture. The behavior observed in MIX1_AC_1.2 implies a reduced mixture permeability, limiting the carbonation reactions. As discussed in Section 5.2.1, all residues except for MSWI BA have an average particle size < 150 µm, with MSWI BA reaching this size post-grinding. Particle-size distribution and specific surface area play an essential role in carbonation efficiency (as mentioned in Section 2.3.1.2), but can also negatively influence viscosity and permeability, thus hindering CO_2 diffusion in the aqueous phase. Consequently, mild agitation of the sample exposed fresh surfaces, reviving the carbonation process. If a different CO_2 supply method had been employed during the test, the reaction could have continued, further emphasizing the importance of mass transfer in enhancing CO_2 sequestration [225]. Potential improvements include the use of an insufflation system or a mechanical stirring system, such as a rotating drum. The positive impact of simply adjusting the setup's position in the MIX1_AC_1.2 test underscores the potential for optimizing carbonation efficiency through enhanced gas-liquid-solid mass transfer.

6.3.2 Characterization of the Carbonated Samples

Mineralogical changes in the carbonated samples were analyzed using XRD-Rietveld and LOI analyses (**Table 14**), as detailed in Sections 4.6.9 and 4.6.12. The samples MIX1_AC_0.9bis and MIX1_NC2_0.9, selected for their expected higher carbonation content, were further studied using SEM-EDS analyses (Section 4.6.10a).

In the AC trials, XRD-Rietveld analyses revealed a substantial reduction in $Ca(OH)_2$ and CaClOH content, which decreased from 5 wt.% and 15 wt.% (MIX1), to < 1-1 wt.% and 7-9 wt.%. Meanwhile, $CaCO_3$ content, specifically calcite and vaterite, increased from 9 wt.% (MIX1) to a maximum of 29 wt.% (MIX1_AC_1.2), indicating effective carbonation. The results also suggest that the L/S ratio influenced the AC reaction, indeed, a lower vaterite content was observed with an increase in the L/S ratio. LOI values increased from 24.2 wt.% (MIX1) to a maximum of 29.5 wt.% (MIX1_AC_1.2), suggesting the presence of carbon-based

substances (carbonates) thus corroborating the XRD-Rietveld results. These findings indicate a direct correlation between L/S ratios and the formation of various carbonates, demonstrating that vaterite formation is also possible under AC conditions. which differs from Section 6.2.2, where CO_2 was the limiting reagent.

***Table 14**: XRD-Rietveld and LOI analyses of MIX1 with the corresponding AC samples (AC_0.7 to AC_1.2, and AC_0.9bis) and NC samples (NC1_0.7 to NC1_1.2).*

	MIX1	AC				NC1		
		0.7	0.9	0.9bis	1.2	0.7	0.9	1.2
				[wt.%]				
Portlandite ($Ca(OH)_2$)	5	1	< 1	< 1	< 1	1	< 1	< 1
Calcium hydroxy chloride (CaClOH)	15	9	9	4	7	< 1	< 1	< 1
Calcite ($CaCO_3$)	9	12	20	24	27	28	32	28
Vaterite ($CaCO_3$)	-	5	4	6	2	5	3	3
Dolomite ($CaMg(CO_3)_2$)	1	1	1	< 1	< 1	< 1	< 1	< 1
Sylvite (KCl)	2	2	2	2	2	1	2	1
Tripotassium phosphate (K_3PO_4)	2	3	2	2	2	2	2	1
Halite (NaCl)	3	2	2	2	3	3	3	2
Quartz (SiO_2)	4	3	5	3	4	5	3	4
Hematite (Fe_2O_3)	1	1	1	1	1	1	1	1
Mullite ($Al_6Si_2O_{13}$)	2	2	2	1	1	1	1	2
Anhydrite ($CaSO_4$)	2	5	2	1	2	2	2	2
Bassanite ($CaSO_4*0.5H_20$)	1	2	2	4	4	5	2	5
Gypsum ($CaSO_4*2H_20$)	1	1	2	1	< 1	1	1	1
Hannebachite ($CaSO_3*0.5H_20$)	7	6	4	4	4	3	3	4
Amorphous	45	46	42	45	40	43	44	46
LOI (1000 °C)	24.2	26.9	27.8	29.0	29.5	30.5	29.2	31.0

The mineral composition of the materials refers to dry samples.

In the MIX1_AC_0.9bis trial, despite having the same L/S ratio as MIX1_AC_0.9, the $Ca(OH)_2$ and CaClOH content dropped to < 1 wt.% and 4 wt.%, respectively. Meanwhile, total $CaCO_3$ content increased to 30 wt.%, with a LOI value of 29 wt.% and a higher vaterite content (6 wt.%). These results indicate that CO_2 pressure also plays an essential role in the carbonation process, as maintaining constant pressure improved CO_2 dissolution and enhanced carbonation efficiency.

For the NC trials, $Ca(OH)_2$ and CaClOH were either fully or nearly depleted. At the same time, total $CaCO_3$ content (sum of calcite and vaterite content) reached a maximum of 35 wt.% in MIX1_NC1_0.9, which is higher than the content obtained under the same conditions in Section 6.2.2. This suggests that the uncontrolled room conditions of the NC trials influenced the results. In contrast to the AC trials, the L/S ratio had a minimal effect on the NC reaction. LOI values in the NC trials increased to a maximum of 31 wt.% (MIX1_NC_1.2),

further supporting the correlation between CO_2 sequestration and the formation of various carbonates, such as calcite, vaterite, or amorphous carbonates, which thermally decompose in a range of 415-990 °C [226] as shown in Section 5.3.3. Eventually, these results apparently do not reveal a direct correlation between L/S ratios and the formation of various carbonates.

Moreover, also for these trials, $CaCl_2$ was not detected by XRD-Rietveld, and KCl showed a slight decrease in concentration. The amorphous content generally increased across all the samples, though it decreased with higher L/S ratios in the AC trials and increased in the NC trials. Moreover, in the NC trials, as the L/S ratio decreased, manual milling of the samples for analysis became more difficult. This could be related to the occurrence of pozzolanic and cementitious reactions because higher L/S ratios in cement are typically associated with lower strength [227].

Figure 29 depicts the internal composition of particles from MIX1_AC_0.9bis and MIX_NC2_0.9 obtained via SEM-EDS analyses.

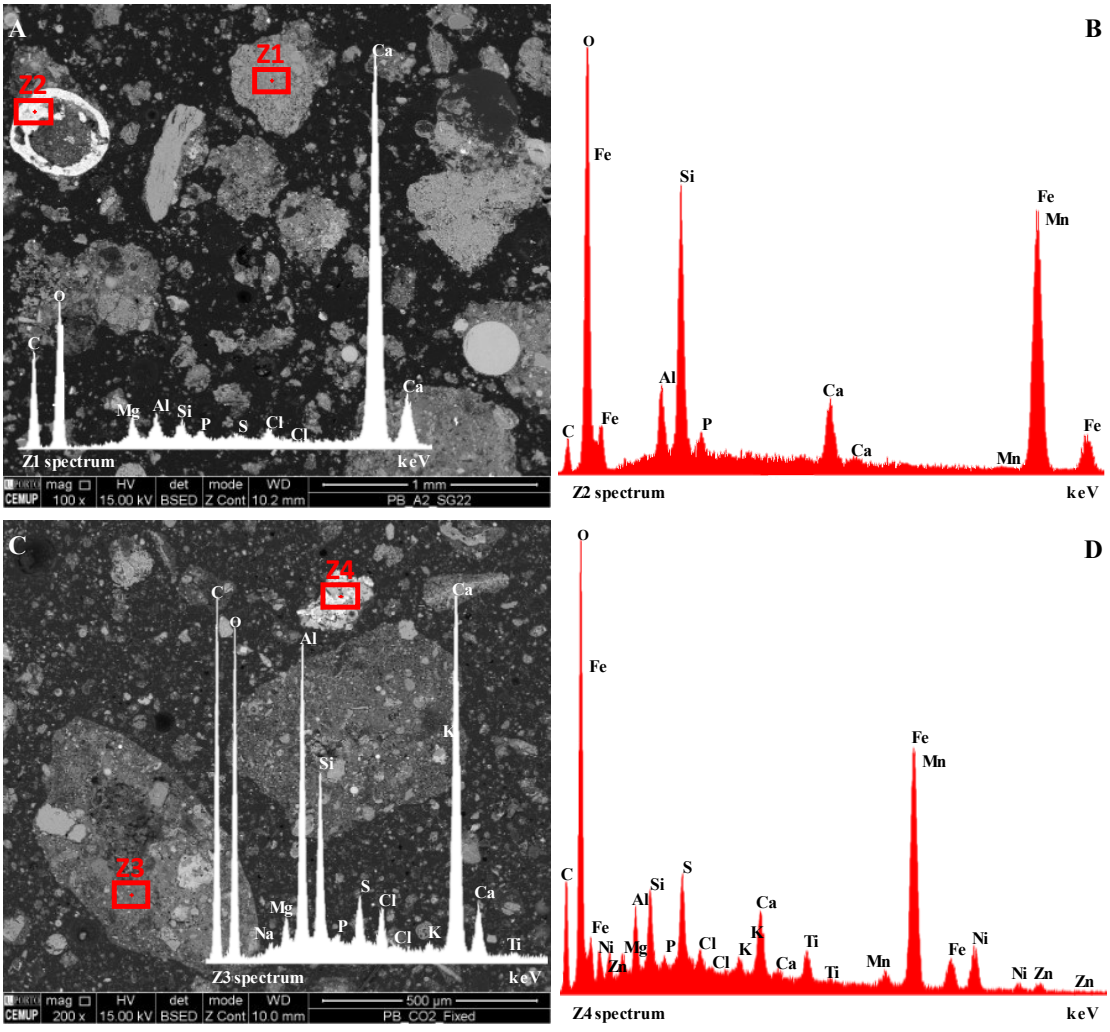

***Figure 29**: SEM Micrographs (polished blocks) and EDS spectra (Intensity [Arb. Units]) of MIX1_AC_0.9bis (A, B), and MIX2_NC2_0.9 (C, D).*

Both samples contain newly formed agglomerations composed of aluminosilicate glassy spheres, fragments, and other relics, all bound together by crystalline and amorphous $CaCO_3$. Additionally, iron-rich particles (**Figure 29A_Z2**) are surrounded by carbonaceous agglomerations resulting from the carbonation process. This discovery offers promising opportunities for further research on the role of carbonation in stabilizing heavy metals using fine industrial alkaline residues, aligning with the outcomes discussed in Section 6.2.4.

6.3.3 CO_2 Uptake Quantification

CO_2 uptake during the AC and NC trials was quantified using the XRD-Rietveld refinement method as explained in Section 6.2.3 and normalized to MSWI FA content. These values exclude CO_2 naturally sequestered during storage at incineration plants prior to residue sampling. The results are presented in **Figure 30**.

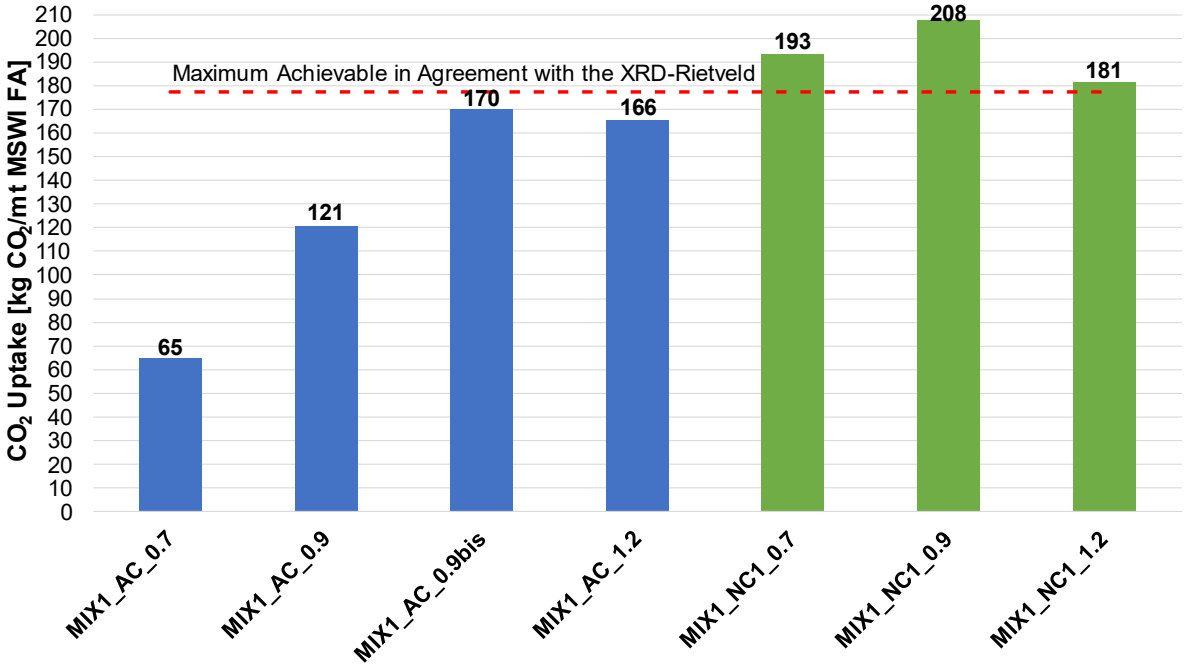

***Figure 30**: CO_2 uptake of AC samples (AC_0.7 to AC_1.2, and AC_0.9bis) and NC samples (NC1_0.7 to NC1_1.2).*

The reduction in the concentrations of the two main reactive species, $Ca(OH)_2$ and CaClOH, and the corresponding increase in $CaCO_3$ confirm that the carbonation occurred in both AC and NC trials as outlined in Eqs. (18) and (19). In particular, XRD-Rietveld analyses showed that CO_2 uptake increased in the AC trials across varying L/S ratios, underscoring the critical role of the L/S ratio. Specifically, CO_2 uptake reached 166 kg CO_2/mt MSWI FA for MIX1_AC_1.2, reflecting the CO_2 pressure trend. For MIX1_AC_0.9bis, where pressure remained constant over time, CO_2 uptake reached 170 kg CO_2/mt MSWI FA, surpassing the uptake in MIX1_AC_0.9, highlighting the significant impact of pressure.

Overall, the NC trials demonstrated a higher CO_2 sequestration in comparison to the AC trials, achieving between 181-208 kg CO_2/mt MSWI FA, as shown in **Figure 30**. As previously noted, the NC trials showed minimal variation, aside from a peak trend observed in MIX1_NC_09. Nevertheless, the L/S ratios might have influenced the rate of CO_2 sequestered within the test period.

In **Figure 30**, The dashed red line represents the stoichiometric amount of CO_2 that would be sequestered on the proviso that the reaction depended solely on crystalline reagents, as explained in Section 6.2.3. The maximum attainable CO_2 uptake in this case would be 177 kg CO_2/mt MSWI FA. Although the AC trials demonstrated higher CO_2 uptakes, showing the influence of L/S ratios and CO_2 pressure, none reached the stoichiometric maximum. Even in MIX1_AC_0.9bis, where CO_2 was not a limiting reactant, the maximum potential uptake was not achieved. This could be attributed to residual $Ca(OH)_2$ and CaClOH in all the AC trials, as well as the absence of an agitation system, which may have limited CO_2 diffusivity, as highlighted in Section 6.3.1.

In contrast, all NC trials surpassed the theoretical limit suggesting an involvement of the amorphous phase in the carbonation process. This phase likely contains Ca bound with silicates or other compounds, such as CSH and C-(A-)S-H, which can react with CO_2 to form crystalline and amorphous carbonates [228,229]. This points to a complex aqueous carbonation nature, involving both crystalline and amorphous phases. Therefore, the XRD-Rietveld analysis does not account for the amorphous phases, thereby possibly underestimating the maximum amount of total CO_2 uptake. This implies that alternative methods could yield different results.

These findings reveal a clear correlation between the total amount of $CaCO_3$ and the L/S ratio. This emphasizes the crucial role of the different L/S ratios in the AC process, as higher L/S ratios can increase the amount of CO_2 dissolved, while also affecting the mixture's permeability. Thus, a lower L/S ratio resulted in a more viscous mixture, reducing both CO_2 solubility and diffusivity within the mixture. Moreover, the results showed also higher CO_2 uptake than the yield reported in the literature by using only MSWI FA [9] (see Section 3.1.1), highlighting the effect of the mixture used.

6.3.4 Summary and Conclusions

This study examined the effect of the L/S ratio and pressure on CO_2 sequestration in the MIX1 (Section 4.5.1), using both AC and NC conditions with L/S ratios of 0.7, 0.9, and 1.2. A separate AC trial with constant CO_2 pressure was also conducted to understand the influence of the pressure. The samples were characterized using XRD-Rietveld, LOI, and SEM-EDS analyses.

A direct correlation was observed between CO_2 uptake and both the L/S ratio and CO_2 pressure in the AC trials. As the L/S ratio increases, the uptake also increases, with MIX1_AC_1.2 reaching 166 kg CO_2/mt MSWI FA. In contrast, NC trials did not follow this trend, sequestering 193, 208, and 181 kg CO_2/mt MSWI FA for L/S ratios of 0.7, 0.9, and 1.2, respectively. These results underscore the importance of the water content in AC processes, where higher ratios enhance CO_2 dissolution by affecting the mixture's permeability. Implementing a stirring system could further improve CO_2 sequestration by enhancing gas-liquid-solid mass transfer. The constant pressure trial demonstrated that maintaining a steady pressure of 15 bar led to the highest CO_2 uptake in the AC trials, with 170 kg CO_2/mt MSWI FA. These results also highlight the positive effect of mixing different alkaline residues, sequestrating higher quantities of CO_2 than the data reported in the literature by using only MSWI FA.

SEM-EDS analysis of the carbonated samples revealed newly formed agglomerates of calcium carbonates and calcium aluminosilicate incorporating other particles, suggesting potential stabilization of heavy metals, supporting the findings in Section 6.2.

In conclusion, the AC process shows promise for increased CO_2 sequestration with optimization. Future studies on MIX1 with an L/S ratio of 1.2 under AC conditions, shown in the next section, will explore the use of stirring mechanisms, varied pressures, and temperatures to enhance CO_2 uptake and further investigate the effects on MSWI FA stabilization.

6.4 Optimizing CO_2 Sequestration and Heavy Metals Stabilization through Accelerated Carbonation

This section focuses on optimizing the accelerated CO_2 sequestration applied to MIX1 by analyzing the effects of pressure and temperature variations. The impact of carbonation on heavy metal stabilization was evaluated, excluding pozzolanic and cement reactions. The trials followed the configuration outlined in **Table 3** and the experimental setup shown in **Figure 15** (Section 4.5.1.2).

Ten AC trials[16] were conducted at a L/S ratio of 1.2 with mechanical agitation, varying pressure (5-45 bar with 10 bar increments), and temperature (35-75 °C with 10 °C increments). The sample IDs[17] for the pressure-variation trials are AC_p5, AC_p15, AC_p25, AC_p35, AC_p45, while for the temperature-variation trials are AC_T35, AC_T45, AC_T55, AC_T65, AC_T75. A control sample, labeled OS, not subjected to carbonation was directly dried and characterized.

6.4.1 CO_2 Pressure Trends during Accelerated Carbonation Trials

The pressure trends for the pressure-variation and temperature-variation trials are shown in **Figure 31**.

For the pressure-variation trials, the carbonation process exhibited three distinct phases: (i) an initial linear pressure decrease, (ii) a rapid non-linear pressure decrease, and (iii) a final plateau. The duration of the first phase decreased with increasing pressure, lasting approx. 20, 15, 14, and 11 min for AC_p15, AC_p25, AC_p35, and AC_p45, respectively. AC_p45 also showed a small rapid drop within the first minute. The slope of the trend steepened with increasing pressure. An exponential drop was observed in the second phase, likely due to the carbonation reaction and subsequent nucleation of $CaCO_3$, which involves CO_2 solubilization and $CaCO_3$ formation. The final phase, resulting in a plateau, was reached after 40, 32, 30, and 25 min for AC_p15, AC_p25, AC_p35, and AC_p45, respectively, indicating a direct correlation between an increase in pressure and an accelerated reaction rate. During this phase, most trials exhibited a plateau, except for AC_p45, which continued to decrease linearly at a much lower rate than the first phase. Interestingly, the AC_p5 trial deviated from this pattern, with a prolonged linear trend of 71 min before shifting to a slower rate and eventually

[16] When extracted, the mixture was separated into a liquid phase and an inert/carbonated sedimented solid phase.
[17] In this section, the code "MIX1" in front of the respective sample IDs will often be omitted and understated.

stabilizing. According to the literature, the crystallization or dissolution of precipitates does not occur immediately, and a characteristic time, often longer than the overall reaction time, is needed to reach equilibrium [230].

In the temperature-variation trials (**Figure 31 bottom**), the behavior was generally analogous to the pressure-variation trials. Identifying a consistent trend was more challenging, however, because of the complex interplay of temperature effects. Higher temperatures can enhance the carbonation reactions [9] but also reduce CO_2 solubility, as described by Henry's law (Eqs. (5) and (6)). The behavior of solid reactants adds another layer of complexity. For instance, **Table 9** shows the presence of CaClOH, which should increase solubility with rising temperatures [231]. On the other hand, $Ca(OH)_2$ is slightly soluble in water (1.85 g/L at 0 ˚C), and its solubility decreases as the temperature increases [232]. This is counter to the usual trend of increasing solid solubility with temperature [65].

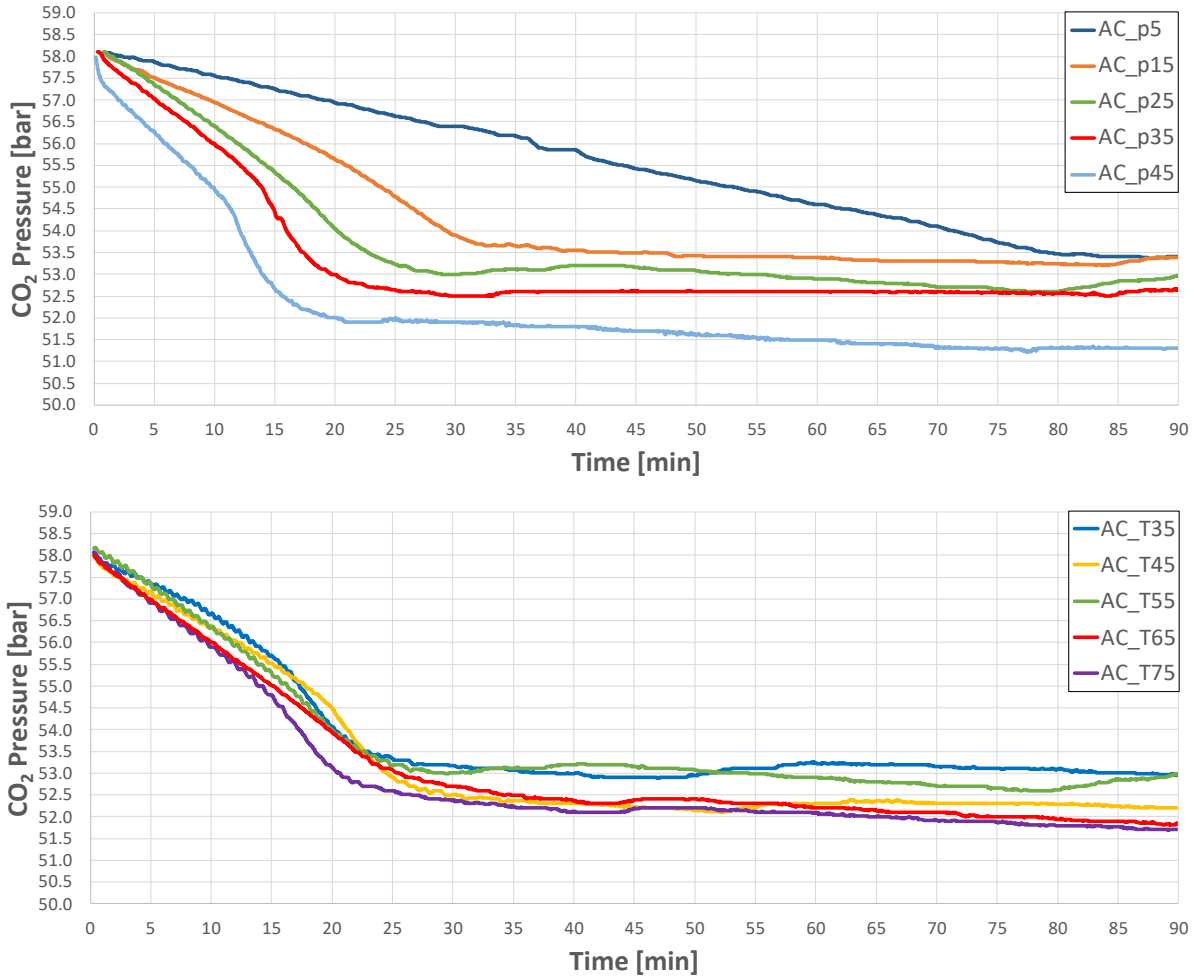

***Figure 31**: CO_2 pressure trend of the pressure-variation (top) and temperature-variation trials (bottom).*

Overall, pressure exerts a strong influence on the reaction rate, while temperature has both positive and negative effects on the carbonation process. Moreover, the pressure dynamics observed in **Figure 31** differ significantly from those discussed in Sections 6.2.1 and 6.3.1. Literature suggests that at 25 °C, calcite growth rates can vary from first- to higher-order reactions (n = 3-3.9), which can be attributed to a combination of adsorption, surface diffusion, and polynucleation [233]. Furthermore, the occlusion of pore structures in industrial alkaline residues by $CaCO_3$ during carbonation has been reported to reduce porosity, tortuosity, and pore area [75]. Nevertheless, since the residues used in this study consist of small, low or nonporous particles (Section 5.2.2), this last phenomenon can likely be ruled out.

6.4.2 Characterization of the Carbonated Samples

Mineralogical changes in the carbonated samples were analyzed using XRD-Rietveld (**Figure 32**, **Table 15**), as outlined in Sections 4.6.9. Additionally, pH-values and total C (**Table 15**) were measured before and after carbonation, as outlined in Sections 4.5.1.2 and 4.6.13.

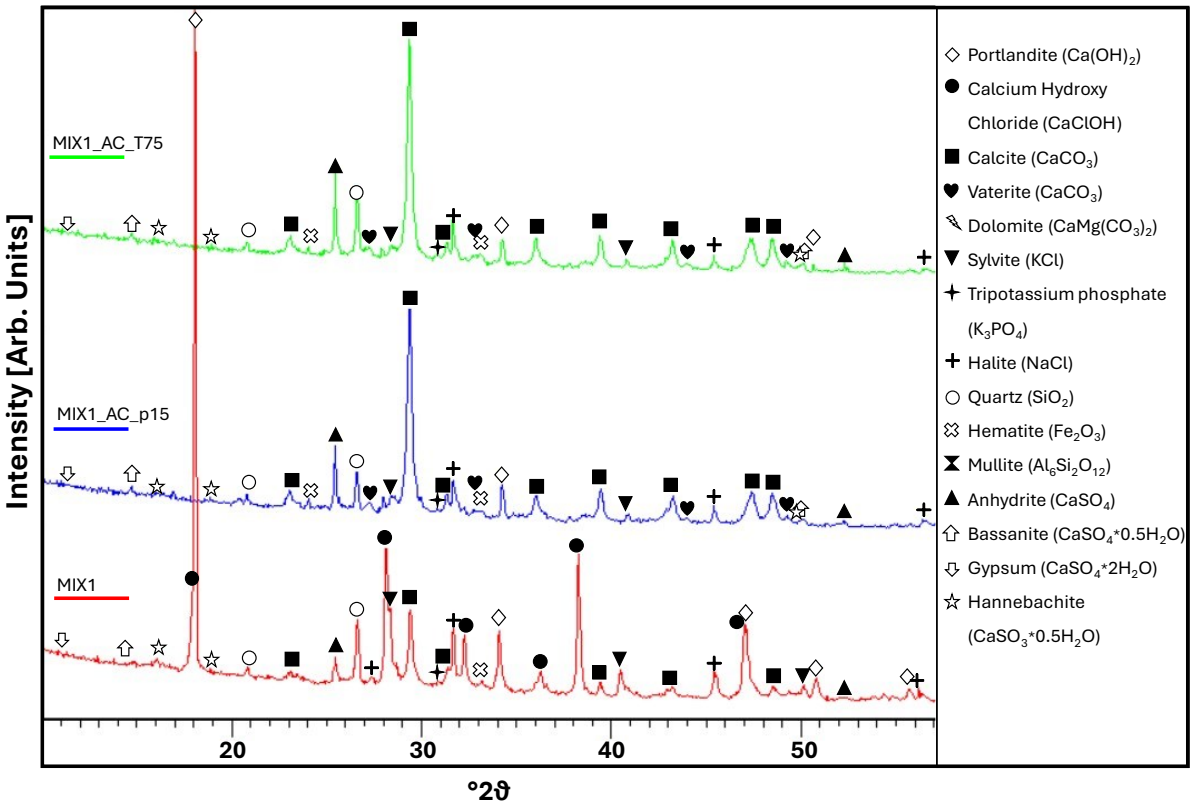

***Figure 32**: XRD patterns of MIX1 and corresponding AC samples from pressure-variation (AC_p15) and temperature variation trials (AC_T75).*

***Table 15**: pH-values of the slurries, XRD-Rietveld, and Total C analyses of MIX1 with the corresponding AC samples for the pressure-variation (AC_p5 to AC_p45) and temperature variation trials (AC_T35 to AC_T75).*

		Pressure-variation Trials				
	MIX1	**AC_p5**	**AC_p15**	**AC_p25**	**AC_p35**	**AC_p45**
	pH=12.1	**pH=5.8**	**pH=5.7**	**pH=5.7**	**pH=5.6**	**pH=5.6**
				[wt.%]		
Portlandite ($Ca(OH)_2$)	5	1	1	1	1	1
Calcium hydroxy chloride (CaClOH)	15	< 1	1	< 1	< 1	< 1
Calcite ($CaCO_3$)	9	37	35	37	33	32
Vaterite ($CaCO_3$)	-	2	3	4	5	6
Dolomite ($CaMg(CO_3)_2$)	1	< 1	< 1	< 1	< 1	< 1
Sylvite (KCl)	2	1	1	< 1	< 1	< 1
Tripotassium phosphate (K_3PO_4)	2	1	1	2	1	1
Halite (NaCl)	3	2	3	2	2	2
Hematite (Fe_2O_3)	4	< 1	< 1	1	< 1	< 1
Mullite ($Al_6Si_2O_{13}$)	1	1	1	1	1	< 1
Quartz (SiO_2)	2	4	4	5	4	4
Anhydrite ($CaSO_4$)	2	3	3	2	3	3
Bassanite ($CaSO_4*0.5H_20$)	1	2	5	5	8	6
Gypsum ($CaSO_4*2H_20$)	1	1	1	< 1	1	1
Hannebachite ($CaSO_3*0.5H_20$)	7	5	5	3	3	4
Amorphous	45	40	37	37	39	37
Total C	3.8	6.8	6.7	7.2	6.8	7.0
		Temperature-variation Trials				
	MIX1	**AC_T35**	**AC_T45**	**AC_T55**	**AC_T65**	**AC_T75**
	pH=12.1	**pH=5.7**	**pH=5.7**	**pH=5.7**	**pH=5.7**	**pH=5.8**
				[wt.%]		
Portlandite ($Ca(OH)_2$)	5	1	< 1	1	1	1
Calcium hydroxy chloride (CaClOH)	15	< 1	< 1	< 1	< 1	< 1
Calcite ($CaCO_3$)	9	33	33	37	32	34
Vaterite ($CaCO_3$)	< 1	3	3	4	5	5
Dolomite ($CaMg(CO_3)_2$)	1	< 1	< 1	< 1	< 1	< 1
Sylvite (KCl)	2	< 1	1	< 1	< 1	< 1
Tripotassium phosphate (K_3PO_4)	2	2	1	2	1	1
Halite (NaCl)	3	2	3	2	2	2
Hematite (Fe_2O_3)	4	< 1	1	1	< 1	< 1
Mullite ($Al_6Si_2O_{13}$)	1	1	1	1	1	1
Quartz (SiO_2)	2	4	5	5	4	3
Anhydrite ($CaSO_4$)	2	2	3	2	2	3
Bassanite ($CaSO_4*0.5H_20$)	1	8	7	5	7	5
Gypsum ($CaSO_4*2H_20$)	1	< 1	1	< 1	1	< 1
Hannebachite ($CaSO_3*0.5H_20$)	7	4	3	3	4	4
Amorphous	45	40	40	37	39	39
Total C	3.8	6.9	6.8	7.2	6.7	6.9

The mineral composition of the materials refers to dry samples.

Across all trials, both $Ca(OH)_2$ and CaClOH were either fully depleted or significantly reduced, while the total $CaCO_3$ content (sum of calcite and vaterite) increased substantially from an initial 9 wt.% to a range of 36-41 wt.%. The highest increases were observed in the AC_p25/AC_T55 samples, which showed about 355 % increase.

In the pressure-variation trials, a crossbreeding behavior was observed: with increasing pressure, the calcite content decreased except for AC_p25, whereas the vaterite content increased. In contrast, during the temperature-variation trials, the calcite content remained stable (32-34 wt.%) across all temperatures except for AC_T55, with the vaterite content increasing at temperatures of ≥ 55 °C. This trend is in concurrence with the literature which suggests vaterite forms at around 60 °C, while aragonite appears above 85 °C [234]. This explains the presence of vaterite and the absence of aragonite (another $CaCO_3$ polymorph) in these trials.

Furthermore, $CaCl_2$ was not detected by XRD-Rietveld analyses, indicating its reaction with CO_2, as previously discussed (Section 6.2.2 and 6.3.2) and highlighted by Eq. (16). The KCl content also decreased, likely recombining into the amorphous phase. Interestingly, the amorphous content showed a reduction of 11-18 % across all trials, suggesting a potential contribution of this phase under the conditions studied.

Total C values doubled, reaching values between 6.7-7.2 wt.%, without a clear trend relative to pressure and temperature variations. Similar trends have been reported in the literature for AC applied to MSWI FA [104]. According to the SEM and LOI data (Section 5.3.2 and 5.3.3), the initial total C content in the mixture stems from unburned carbon from the combustion processes and pre-existing carbonates, in both crystalline and amorphous forms, due to natural weathering during the storage process in the respective plants. Since CO_2 was the only reagent used, the increase in $CaCO_3$ and total C content can be attributed to the carbonation reaction.

The pH-value dropped significantly from an initial value of 12.1 to 5.6-5.8 (**Figure 33**), indicating complete acidification of the slurries. A slight decrease in pH-values was observed as the pressure increased from 5 bar to 45 bar. Meanwhile, a slight peak trend was noted during the temperature-variation trials, with the lowest pH-value recorded at AC_T45. Given the consumption of most reactive crystalline phases, the initial carbonation phase appears governed by compounds providing OH^- ions, which influence the presence of carbonate ions (CO_3^{2-}), predominant at pH > 12, as described in Section 2.3.1.2. The literature also highlights an initial buffering capacity, possibly due to an undissolved deposit [104], which could continuously

generate OH^- and Ca^{2+} ions. This was also demonstrated in Section 6.2, where CO_2 was the limiting reagent and pH-values remained stable at around 12 despite $CaCO_3$ formation.

As the reaction progresses and OH^- ions are consumed, bicarbonate ions (HCO_3^-) which are predominant at pH 8, could be involved, with Ca^{2+} ions likely supplied by the amorphous phase. This would support the continued carbonation reaction, initially via Eq (10), so long as an undissolved deposit persists, and then via Eq. (12). The complex interaction between pH-level and ion availability may explain the variable rates of the pressure drop observed in **Figure 31 (above)**. According to the literature, an optimal pH of around 10 balances the rapid leaching of Ca^{2+} ions with the formation of carbonate ions [48]. Thus, the decrease in pH-value may have accelerated the remaining Ca^{2+} ions leaching while simultaneously slowing CO_2 solubilization.

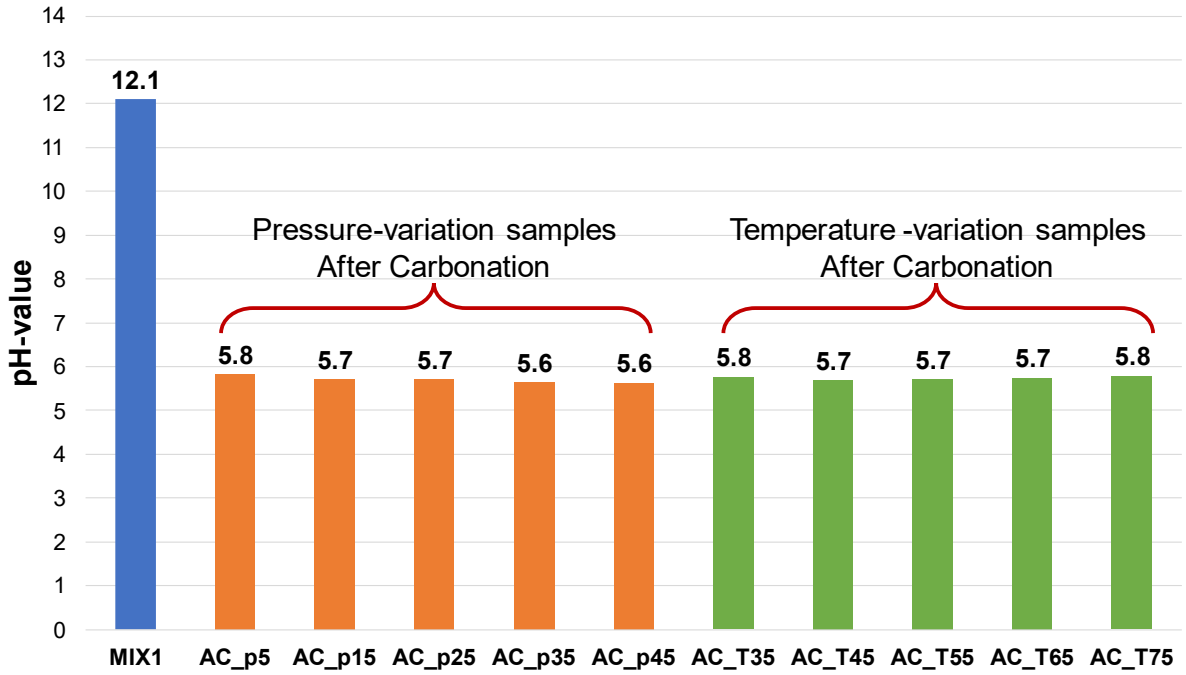

***Figure 33**: pH-values of the slurries before (MIX1) and after the AC trials (AC_p5 to AC_p45 and AC_T35 to AC_T75).*

6.4.3 CO_2 Uptake Quantification

CO_2 uptake during the AC trials was quantified using both the XRD-Rietveld refinement method (Section 6.2.3) and total C measurements, normalized to the MSWI FA content. These values exclude any CO_2 naturally sequestered during storage at incineration plants prior to residue sampling. The results are presented in **Figure 34**.

Both methods yielded similar sequestration capacities, ranging from 199-248 kg CO_2/mt MSWI FA, which is comparable to, or higher than previously reported values for NC trials (Section 6.3.3) and higher than literature data (110-139 kg CO_2/mt MSWI FA) [9].

According to the XRD-Rietveld data, both the pressure-variation and temperature-variation trails exhibited a peak CO_2 uptake of 248 kg CO_2/mt MSWI FA at 25 bar and 55 °C (AC_p25 and AC_T55). In the pressure-variation trials, CO_2 sequestration was highest at moderate pressures, particularly in the 5-25 bar range. In the temperature-variation trials (conducted at a constant pressure of 25 bar), CO_2 sequestration increased progressively with rising temperature. The higher uptakes were sustained within the temperature range of 55-75 °C, consistent with literature reports suggesting 60-80 °C as the optimal range for carbonation processes [9]. Conversely, the total C estimates did not exhibit a consistent trend across the tested conditions, although they did reflect the same peak behavior at 25 bar and 55 °C.

The formation of $CaCO_3$ phases exceeds what could be attributed solely to the carbonation of reactive crystalline phases. As discussed previously (Section 6.3.3), stoichiometric calculations indicate that up to 177 kg CO_2/mt MSWI FA could be sequestered by the carbonation of $Ca(OH)_2$ and CaClOH. Nevertheless, the observed sequestration surpassed this value, suggesting that $CaCO_3$ formation is not limited to these crystalline phases. This supports the hypothesis that the amorphous phase contributes to carbonation under the AC conditions studied, albeit through slower kinetics. The pressure data further suggests that crystalline Ca-bearing species may be responsible for the initial pressure drop before the plateau is reached, as shown in **Figure 31**.

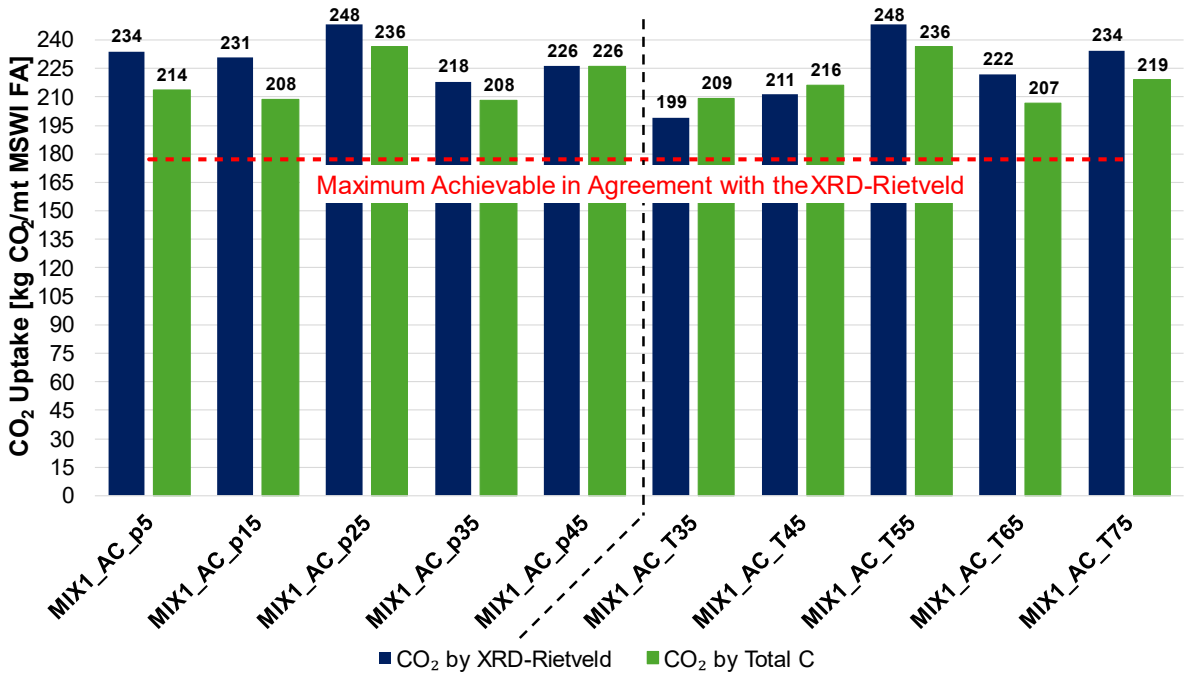

***Figure 34**: CO_2 uptake of AC samples from pressure-variation (AC_p5 to AC_p45) and temperature variation trials (AC_T35 to AC_T75).*

The carbonation process, optimized with mechanical agitation, reached completion within 25–71 min. The best results were obtained at a constant pressure of 25 bar and a temperature of 55 °C, consistent with literature values of 130-280 kg CO_2/mt residue [9]. As elucidated in Section 2.3.1.2, these conditions are well-suited for industrial applications, particularly because carbonation reactions are exothermic. The generated heat can be harnessed to reduce energy consumption, enhancing the overall cost-effectiveness of ACT.

For context, the WtE plant in Brescia (Italy), operated by A2A S.p.A, produced around 34.8 kt MSWI FA in 2023 [95]. Implementing this ACT could prevent the release of approx. 6.8-8.2 kt CO_2/yr. On a larger scale, in China, where MSWI FA production is projected to reach 13 Mt by 2025 [235], the averted CO_2 release could possibly exceed 2.4-3.1 Mt CO_2/yr.

6.4.4 Stabilization Results

The role of carbonation in stabilizing MSWI FA was assessed using ICP-OES to analyze the elemental composition of the leachates from the carbonated samples, complemented with IC analyses to measure the chloride content, as detailed in Section 4.6.5 and 4.6.6, respectively. The primary goal was to determine whether carbonation could reliably help stabilize Pb and Zn, in addition to the pozzolanic and cementitious reactions. The results are summarized in **Table 16** and **Figure 35**. The initial leachate concentrations of Pb and Zn from MSWI FA were approx. 36.45 mg/L and 4.65 mg/L, respectively (see Section 5.3.1).

***Table 16**: pH-values and elemental concentrations of the leachates from MSWI FA, MIX1, MIX1_OS, and MIX1_AC samples from pressure-variation (AC_p5, AC_15p, and AC_p45) and temperature-variation trials (AC_T45, AC_T55, and AC_T75).*

Elements	MSWI FA	MIX1	MIX1_OS	MIX1_ AC_p5	MIX1_ AC_p15	MIX1_ AC_p45	MIX1_ AC_T45	MIX1_ AC_T55	MIX1_ AC_T75
	pH = 12.5	pH = 12.0	pH = 12.4	pH =8.0	pH =7.9	pH =7.9	pH =8.0	pH =7.8	pH =8.0
					[mg/L]				
Ca	7761.94	5142.61	4709.40	4109.29	3953.73	3777.31	3598.93	4054.75	4070.85
Mg	< 0.003	< 0.002	< 0.002	200.17	289.21	312.62	374.85	354.67	313.64
Pb	36.45	11.41	8.85	0.06	0.07	0.08	0.15	0.10	0.15
Zn	4.65	2.62	1.62	0.28	0.34	0.32	0.52	0.55	0.21
Mn	< 0.001	< 0.001	< 0.001	0.82	0.98	0.73	0.75	0.99	1.07
As	< 0.007	0.15	0.15	0.18	0.19	0.16	0.13	0.16	0.14
Be	< 0.001	< 0.001	< 0.001	< 0.001	< 0.001	< 0.001	< 0.001	< 0.001	< 0.001
Cd	< 0.001	< 0.001	< 0.001	0.32	0.28	0.20	0.19	0.30	0.30
Co	< 0.001	0.02	0.02	0.03	0.04	0.04	0.03	0.04	0.02
Cr	0.12	0.11	0.03	< 0.001	< 0.001	< 0.001	< 0.001	< 0.001	< 0.001
Cu	0.13	0.08	0.09	0.08	0.10	0.07	0.04	0.07	0.05
Mo	0.14	0.25	0.26	0.44	0.67	0.20	0.98	0.74	0.95
Ni	< 0.002	< 0.002	< 0.002	0.03	0.04	0.04	0.03	0.03	0.01
Sb	< 0.009	0.10	0.10	0.44	0.45	0.32	0.39	0.41	0.29
Se	0.01	0.14	0.13	0.22	0.29	0.27	0.20	0.22	0.21

Ti	< 0.001	0.01	0.01	0.03	0.03	0.02	0.004	0.01	0.01
V	< 0.003	< 0.003	< 0.003	< 0.003	0.01	< 0.003	< 0.003	< 0.003	< 0.003
K	2214.24	1027.49	1024.15	1256.90	1043.68	1127.67	1094.24	1209.65	885.33
Na	2361.61	941.43	944.26	1334.11	1103.73	1185.20	1145.30	1297.71	912.99
Fe	< 0.002	0.02	< 0.002	< 0.002	< 0.002	< 0.002	< 0.002	< 0.002	< 0.002
Al	< 0.001	< 0.001	< 0.001	< 0.001	< 0.001	0.01	< 0.001	< 0.001	< 0.001
P	0.28	0.40	0.54	0.41	0.46	0.44	0.52	0.40	0.46
Cl	16069.61	9090.79	8870.94	8753.67	8274.88	8145.85	8096.59	8791.05	8383.65

As discussed in Section 6.2.4, the concentrations of the elements were reduced due to the dilution of MSWI FA through adding other industrial residues. Moreover, previous studies have shown that drying alone can have a mild stabilizing effect on heavy metals, making it necessary to distinguish drying from carbonation effects [17,23]. To account for this, a control trial (OS) was conducted, whereby the sample was dried at 105 °C overnight, immediately after water addition without undergoing AC. In this trial, Pb and Zn concentrations in the leachates dropped to 8.85 and 1.62 mg/L, respectively.

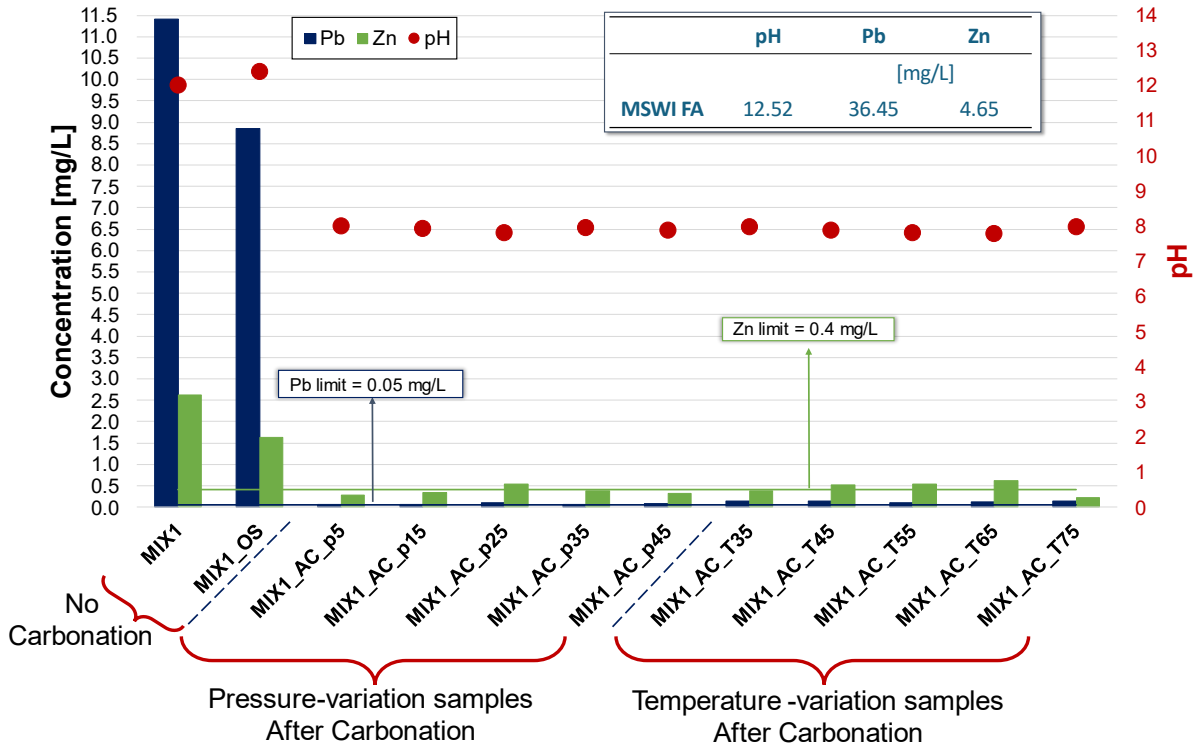

***Figure 35**: Pb and Zn concentrations and pH-values MSWI FA, MIX1, MIX1_OS, and MIX1_AC samples from pressure-variation (AC_p5 to AC_p45) and temperature variation trials (AC_T35 to AC_T75).*

By contrast, AC trials showed a significant reduction, with Pb concentrations decreasing by approx. two orders of magnitude (< 0.15 mg/L) and Zn by one order of magnitude (< 0.55 mg/L). These results are consistent with those performed in NC trials (Section 6.2.4), indicating that carbonation significantly enhances heavy metals stabilization, as supported by

SEM-EDS analyses (Section 6.3.2). No clear trend was observed with varying pressure or temperature, as all trials yielded comparable results.

A notable decrease in pH-levels to 7.8-8.0 was observed in the leachates, indicating titration due to CO_2 insertion. The positive impact of carbonation on heavy metals leaching can be attributed to chemical and mineralogical changes induced by the process [9,104]. Three mechanisms likely contribute to the stabilization of Pb and Zn: (i) the shift towards a near-neutral pH-value, where many heavy metals generally exhibit lower solubility [236]; (ii) the formation and precipitation of less soluble compounds such as heavy metal carbonates [75,104]; and (iii) the potential physical incorporation of these metals into carbonaceous agglomerates, as reported in the literature [237] and supported by prior SEM-EDS findings discussed in Section 6.3.2. Additionally, the affinity of Pb for calcite suggests possible sorption onto $CaCO_3$ and/or coprecipitation with newly formed minerals such as complexes with Fe and Al (hydr)oxides [104,238]. Moreover, decreased Pb leaching may be attributed to the reduction in its amphoteric behavior caused by the formation of sparingly soluble $PbCO_3$ [239,240]. The absence of these carbonates in XRD-Rietveld data is likely due to their quantity being below the detection limit of the instrument. These observations underscore the critical role of pH control in enhancing both carbonation efficiency and heavy metal stabilization.

It should be noted that these trials specifically focused on the stabilizing effect of AC, without considering pozzolanic reactions, which typically require several days to manifest. The reaction time can vary depending on the type of residue, from 3 days for silica fume to 28 days for cement, waste bricks, and similar materials [22,241].

Moreover, carbonation reactions could also affect the mobility of other heavy metals. Indeed, a slight increase in antimony, selenium, and molybdenum concentrations was recorded after carbonation, albeit in much lower values than what has been studied in the literature [104]. Additionally, it was observed that carbonation did not affect chloride solubility. This is consistent with other studies that report no impact on the retention of chlorides and sulfates-critical species in MSWI FA, particularly concerning landfilling or reuse [104,242]. Nevertheless, this finding contrasts with a study on MSWI BA [237]. Lastly, the presence of Ca in the leachates indicates that the carbonation reaction may have continued, potentially sequestering more CO_2. Indeed, according to **Table 15**, the post-carbonated mixtures reached slightly acidic pH-values (i.e., 5.6-5.8), which is far from the optimal conditions for carbonation (see Section 2.3.1.2, **Figure 7**). This highlights the paramount importance of pH-control during the process.

6.4.5 Potential Reuse of the Carbonated Industrial Alkaline Residues

The potential for reusing the carbonated mixture was evaluated using XRF analysis (Section 4.6.8), and the ternary diagram (**Figure 36**) proposed by the literature [243]. For this purpose, the major oxide composition of the industrial alkaline residues (**Table 8**) used in this study and the carbonated sample MIX1_AC_p25 (**Table 17**) were considered and compared. No data is available for carbonated MIX2 samples. According to the diagram, materials are classified into four categories—K, S, C, and CK—based on their composition, with each category further divided by levels of acidity based on the silicon content [244]: high, medium, and low.

MSWI FA and FGD fall into the CK area, characterized by material with high water solubility, alkaline pH, and reactive compounds with a low melting point [243]. This area represents an intermediate composition between area K and area C. Specifically, area K is defined by the dominance of phosphates, sulfates, and chlorides, with smaller amounts of carbonates, silicates, and glass, whereas area C is characterized by the presence of carbonates, oxides-hydroxides, glass, and silicates, with fewer phosphates and sulfates [243]. MSWI BA and CkFA[18] are located in the C area. CFA falls within the S area, which is mainly composed of glass, silicates, and (Fe, Al, and Mn) oxides-hydroxides [243].

***Table 17**: XRF normalized major oxides data of carbonated sample MIX1_AC_p25.*

	Main Oxides											
	CaO	**MgO**	**MnO**	**TiO_2**	**K_2O**	**Na_2O**	**SiO_2**	**Fe_2O**	**Al_2O_3**	**P_2O_5**	**SO_3**	**Cl_2O**
	[%]											
MIX1_AC_p25	51.1	1.4	0.1	0.7	2.4	0.8	10.1	2.5	4.0	0.5	16.8	9.5

When analyzing the initial mixture (MIX1), it falls within the CK area, which aligns with the high content of MSWI FA (59 wt.%) and FGD (8 wt.%). MIX2 would likely fall into the C area. Upon carbonation, MIX1 shifts into the C area, consistent with the definition of that region. Although data for carbonated MIX2 is not available, it is reasonable to assume that it would also fall within the C area.

Based on **Figure 36**, several potential uses for carbonated mixtures can be proposed. Among the options suggested [243], construction-related applications, such as concrete, construction blocks, bricks, and cement (due to their pozzolanic minerals) are the most evident [245]. These applications could reduce land-use pressures, especially given that concrete is one

[18] [168]

of the most consumed resources globally, second only to water [246]. These materials could also have applications in fire resistance or as substitutes for activated carbons in pollutant adsorption [247,248]. Further exploration of these possibilities could enhance ACT using industrial alkaline residues and open up more opportunities for utilizing these recovered materials.

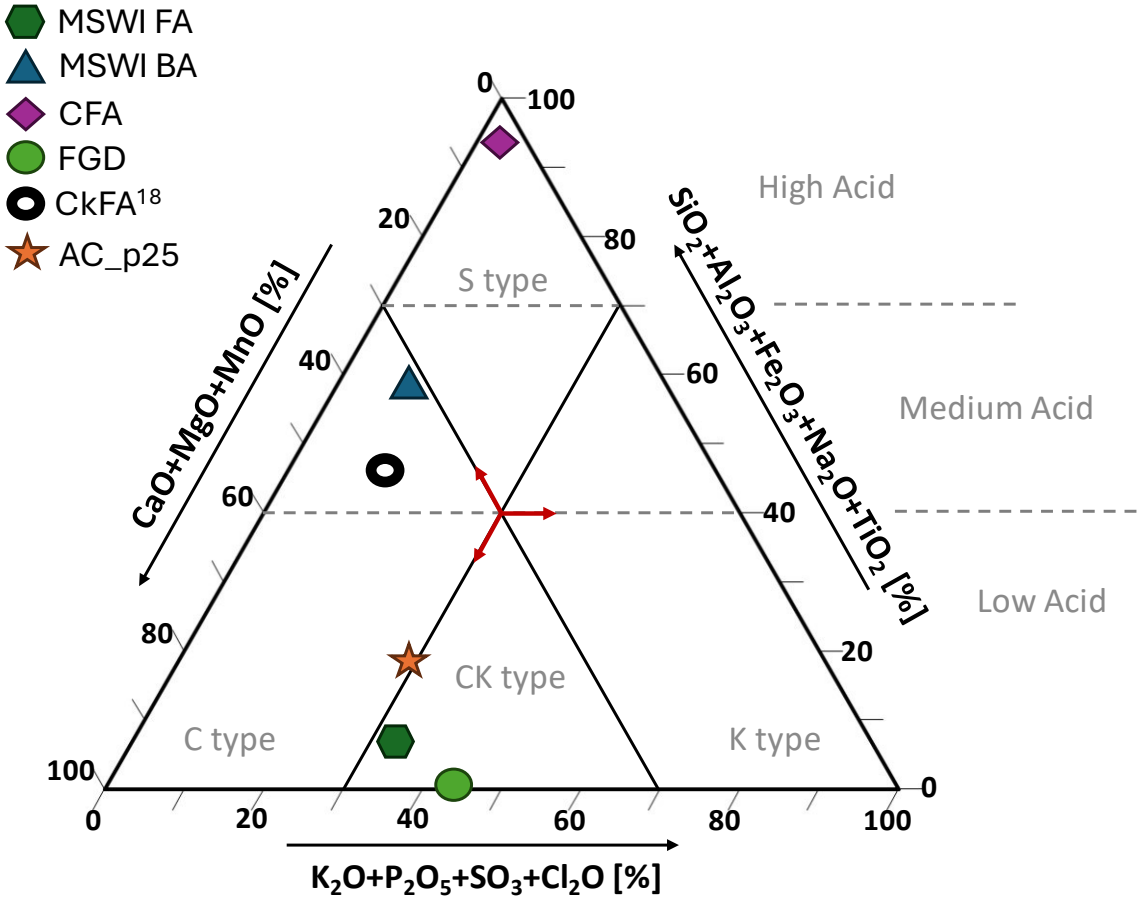

***Figure 36**: Normalized phase ternary diagram ($CaO+MgO+MnO$ – $K_2O+P_2O_5+SO_3+Cl_2O$ – $SiO_2+Al_2O_3+Fe_2O_3+Na_2O+TiO_2$) of the selected industrial alkaline residues and the carbonated sample (AC_p25) contextualized to the inorganic chemical group classification.*

6.4.6 Summary and Conclusions

This study explored the impact of pressure and temperature during the AC process for MIX1 (Section 4.5.1). The reaction mixture, with a water content of 1.2 L/kg, was agitated while varying CO_2 pressure from 5 bar to 45 bar with 10 bar increments, and temperature from 35 °C to 75 °C with 10 °C increments, for an experimental period of 90 min. A separate non-carbonation trial was conducted to better understand the role of carbonation in stabilizing heavy metals. The samples were characterized using XRD-Rietveld, Total C, and SEM-EDS analyses. The leachates were analyzed using ICP-OES, while XRF analysis was used to understand the potential reuse of the carbonated material.

The results showed that higher CO_2 pressures significantly increased CO_2 uptake and reaction rates, reducing reaction time to between 25-40 min, except at 5 bar, where the process took 71 min. The effect of the temperature on the reaction rate was complex, with higher temperatures reducing CO_2 solubility and $Ca(OH)_2$ dissolution but increasing other Ca-salts dissolution and potentially accelerating the carbonation reaction rate. The AC process caused a significant decrease in pH-values, dropping from 12.5 to 5.6-5.8, thereby indicating a strong neutralizing effect.

Post-carbonation trials showed a substantial increase in $CaCO_3$ content, from an initial 9 wt.% to 36-41 wt.%. The highest CO_2 uptake was recorded at 25 bar and 55 °C, representing a 355 % increase. The achieved CO_2 sequestration ranged from 199-248 kg CO_2/mt MSWI FA. Carbonation also effectively stabilized heavy metals, such as Pb and Zn, reducing their concentrations close to or within regulatory limits for safe landfill or recovery. This stabilization is attributed to the formation of heavy metal carbonates, carbonaceous agglomeration, and the reduced solubility of these compounds at lower pH-values.

The AC treatment demonstrated significant improvements in CO_2 sequestration, addressing calcium and heavy metal leaching while drastically shortening the operating time from months to less than 90 min. This technology can potentially avert the release of more than 2.4-3.1 Mt CO_2/yr. Moreover, utilizing industrial alkaline residues leverages cross-industry synergies; it reduces both transport and disposal costs and minimizes the need for additional chemical reactants. Additionally, the exothermic nature of the carbonation reaction could further diminish external energy requirements. The resulting carbonated material holds promise for various applications, including construction, fire resistance, and pollutant adsorption, in line with environmentally sustainable, circular economic principles.

Chapter 7: Conclusions and Future Outlook

Mitigating climate change requires effective short- to medium-term solutions, with accelerated carbonation technology (ACT) emerging as a promising technology, offering sustainable ways to both harness and minimize carbon dioxide (CO_2) emissions into the atmosphere. This cutting-edge technology also poses enormous opportunities to exploit the vast quantities of industrial alkaline residues incurred each year from the energy sector which hitherto have been landfilled due to their leachable elements such as salts, chlorinated and alkaline chemicals, and heavy metals. This study explores the utilization of such alkaline materials, rich in calcium (Ca) and magnesium (Mg), for CO_2 sequestration via ACT. Foremost, the primary goal is to advance ACT for industrial applications by better understanding and exploiting the varying conditions of pressure, temperature, agitation, and water content.

7.1 Selection of Industrial Alkaline Residues and their Characterization

The study primarily focused on a primary mixture of municipal solid waste incineration fly ash (MSWI FA), municipal solid waste incineration bottom ash (MSWI BA), coal fly ash (CFA), and flue gas desulfurization residues (FGD). These residues were selected based on their high alkalinity, Ca and Mg potential release, particle size, and specific surface area, all of which are paramount factors for effective carbonation. In this study, to further explore the potential versatility of ACT, an alternative mixture, formulated as MSWI FA, MSWI BA, and cork fly ash (CkFA), was also designed. This alternative was included as part of a feasibility study to investigate the potential of CkFA as a substitute for CFA and FGD, in light of the continuous decline in coal use for energy production.

A comprehensive characterization of each residue was conducted, including particle-size distribution, immediate soluble content, BET surface area measurements, magnetic and paramagnetic separation, chemical composition (ICP-OES, IC, and XRF), mineralogical studies (XRD-Rietveld and SEM-EDS), LOI and Total Carbon.

The investigated residues showed a low particle size, medium BET-SA, and low magnetic content, except for MSWI BA, which is identified as a coarse residue, thus requiring mechanical grinding and magnetic separation pretreatments. MSWI FA, FGD and CkFA are particularly notable for their alkalinity (pH-value 12-13) and high leachable Ca content—identified as

lime (CaO), calcium hydroxide ($Ca(OH)_2$), and calcium hydroxy chloride (CaClOH)—which are critical for the formation of carbonate ions (CO_3^{2-}) and subsequent precipitation as stable carbonates.

MSWI BA and CFA, being poor in leachable Ca content but alkaline at the same time (pH-value 12-13), were included to maintain an alkaline pH-level and improve reaction kinetics, indirectly contributing to carbonation. Moreover, by considering their pozzolanic properties, these residues could possibly facilitate reuse in construction applications, thus adding value to the carbonated materials.

The study also identified high levels of leachable heavy metals (e.g., Pb and Zn) and chlorides in MSWI FA, which require environmental safety considerations. Finally, CkFA emerged as a viable alternative to CFA and FGD due to their similar physical and chemical composition.

7.2 Accelerated Carbonation and Enhanced Stabilization of Leachable Alkaline Chemicals and Heavy Metals in Industrial Residues

After preliminary studies to assess the feasibility of ACT applied to both mixtures, further experiments were conducted to assess the influence of the water content and CO_2 pressure on carbonation reactions. ACT trials demonstrated significant improvements in CO_2 uptake under various conditions, with higher water content and stirring systems being critical for optimal CO_2 diffusion. Aiming to optimize the process, further experiments were carried out by stirring the primary reactive mixture with a water content of 1.2 L/kg, varying the CO_2 pressure from 5 bar to 45 bar with 10 bar increments, and temperatures from 35 °C to 75 °C with 10 °C increments, for an experimental period of 90 min.

Higher CO_2 pressures significantly increase uptake and reaction rates, reducing the required carbonation time to 25-40 min, except at 5 bar, which took 71 min. The effect of the temperature is not straightforward due to competing factors; higher temperatures reduce CO_2 solubility and $Ca(OH)_2$ dissolution but increase the dissolution of other Ca-salts and potentially increase the kinetics of carbonation reactions. The ACT also causes a significant reduction in pH-levels from 12.5 to 5.6-5.8, indicating effective neutralization. Post-carbonation analyses using XRD-Rietveld and Total C methods showed a significant increase in total $CaCO_3$ content (calcite and vaterite), from an initial 9 wt.% to 36-41 wt.%, with the highest CO_2 uptake observed at 25 bar and 55 °C, representing a 355% increase. The CO_2 sequestration achieved ranges from 199-248 kg CO_2/mt of MSWI FA, comparable to, or higher than the uptake obtained by a 1-month

natural carbonation period (182-211 kg CO_2/mt MSWI FA) applied on the same mixture, and higher than the data reported in the literature by using only MSWI FA. Applying ACT at the WtE plant operated by A2A S.p.A, which provided the MSWI FA, MSWI BA, CFA, and FGD for this study, could prevent the release of approx. 6.8-8.2 kt CO_2/yr. On a larger scale, in countries like China, this technology could possibly avert the release of more than 2.4-3.1 Mt CO_2/yr.

In addition, the ACT effectively stabilizes heavy metals, such as Pb and Zn, bringing their levels close to or within regulatory limits for safe disposal or recovery. SEM-EDS analysis revealed newly formed agglomerates of calcium carbonates and calcium aluminosilicate incorporating other particles. This suggests that carbonation contributes to heavy metal stabilization through mechanisms such as the trapping effect of carbonate agglomerates, the formation of heavy metal carbonates, and reduced solubility of heavy metals at slightly acidic to neutral pH-values. Notably, the rapid stabilization achieved through carbonation complements the slower, long-term stabilizing effects of pozzolanic and cementitious activities, which the mixture develops through natural curing over extended periods.

7.3 Utilization of Alternative Industrial Alkaline Residues

CkFA has emerged as a viable alternative to CFA and FGD in the residue mixture, offering similar carbonation and stabilization behaviors in both AC and NC processes, due to its high Ca content and additional benefits from higher Al and Si contents. These results point to promising opportunities to optimize the ACT process by mixing CkFA with other alkaline residues. As a by-product of biomass combustion, often considered carbon-neutral, CkFA is an attractive resource for reducing greenhouse gas emissions. The successful incorporation of CkFA in this study has demonstrated the versatility of ACT in using various industrial alkaline residues, highlighting its potential for resource-efficient and region-specific solutions.

7.4 Future Outlook

ACT applied to mixtures of industrial alkaline residues offers promising benefits: effective long-term CO_2 capture, rapid carbonation within minutes, and the stabilization of harmful leachable elements, such as alkaline chemicals and heavy metals. The exothermic nature of the carbonation process further enhances its economic viability by reducing energy requirements. Moreover, the proximity of residues to CO_2 emission sources lowers transportation costs. Using different alkaline residues will foster cross-industry collaborations

and mutual synergies, thereby reducing the need for additional commercial chemical reactants and lowering costs even further. Finally, the resulting carbonated materials have potential applications in several fields, such as the construction sector, in line with circular economic principles.

Built on established technologies, ACT represents a versatile approach to complement industrial carbon capture utilization and storage (CCUS) applications, offering a scalable and valuable solution for reducing industrial environmental impacts. The future of ACT lies in its continued refinement and broader application. Key areas for further research should include:

- **Optimization for diverse residues**: Continued exploration of new residues, such as other types of biomass ashes, could further enhance ACT's versatility. Tailoring the process to local industrial residue and wastewater streams may unlock even greater CO_2 sequestration potential.
- **Scaling and integration with existing infrastructure**: ACT could be integrated into industrial facilities, especially where CO_2 emissions are directly generated, reducing transportation costs and maximizing synergies.
- **Long-term stability and regulatory compliance**: Ensuring the long-term stability of carbonated materials, especially concerning leachable alkaline chemicals and heavy metals, will be crucial for regulatory approval and commercial application.
- **Economic feasibility and carbon pricing**: As carbon pricing schemes become more prevalent, ACT's economic viability will improve. Additional research into reducing costs and improving energy efficiency will be fundamental to maintaining its competitiveness.
- **Circular economy and material reuse**: Further investigation into the reuse of carbonated materials in construction and other industries could expand ACT's contribution to the circular economic objectives.

With these advancements, ACT will play a paramount role in mitigating climate change by reducing CO_2 emissions in the short- to medium-term and promoting farsighted and environmentally sustainable, industrial waste management.

References

1. IPCC, 2023: Climate Change 2023: Synthesis Report. Contribution of Working Groups I, II and III to the Sixth Assessment Report of the Intergovernmental Panel on Climate Change [Core Writing Team, H. Lee and J. Romero (Eds.)]. *IPCC, Geneva, Switzerland* **2023**, 1–184, doi:10.59327/IPCC/AR6-9789291691647.
2. Shayanmehr, S.; Rastegari Henneberry, S.; Sabouhi Sabouni, M.; Shahnoushi Foroushani, N. Climate Change and Sustainability of Crop Yield in Dry Regions Food Insecurity. *Sustainability* **2020**, *12*, 9890, doi:10.3390/su12239890.
3. Carleton, T.A.; Hsiang, S.M. Social and Economic Impacts of Climate. *Science (1979)* **2016**, *353*, doi:10.1126/science.aad9837.
4. Berchin, I.I.; Valduga, I.B.; Garcia, J.; de Andrade Guerra, J.B.S.O. Climate Change and Forced Migrations: An Effort towards Recognizing Climate Refugees. *Geoforum* **2017**, *84*, 147–150, doi:10.1016/j.geoforum.2017.06.022.
5. Yang, H.; Xu, Z.; Fan, M.; Gupta, R.; Slimane, R.B.; Bland, A.E.; Wright, I. Progress in Carbon Dioxide Separation and Capture: A Review. *Journal of Environmental Sciences* **2008**, *20*, 14–27, doi:10.1016/S1001-0742(08)60002-9.
6. Nieddu, A. Contenimento delle emissioni di anidride carbonica da sorgenti puntiformi. Doctoral dissertation, Università degli Studi di Cagliari, Italy: Cagliari, 2017.
7. Wang, F.; Harindintwali, J.D.; Yuan, Z.; Wang, M.; Wang, F.; Li, S.; Yin, Z.; Huang, L.; Fu, Y.; Li, L.; et al. Technologies and Perspectives for Achieving Carbon Neutrality. *The Innovation* **2021**, *2*, 100180, doi:10.1016/j.xinn.2021.100180.
8. Chiang, P.-C.; Pan, S.-Y. Introduction. In *Carbon Dioxide Mineralization and Utilization*; Springer Singapore: Singapore, 2017; pp. 1–6.
9. Pan, S.-Y.; Chang, E.E.; Chiang, P.-C. CO_2 Capture by Accelerated Carbonation of Alkaline Wastes: A Review on Its Principles and Applications. *Aerosol Air Qual Res* **2012**, *12*, 770–791, doi:10.4209/aaqr.2012.06.0149.
10. Bonenfant, D.; Kharoune, L.; Sauvé, S.; Hausler, R.; Niquette, P.; Mimeault, M.; Kharoune, M. Molecular Analysis of Carbon Dioxide Adsorption Processes on Steel Slag Oxides. *International Journal of Greenhouse Gas Control* **2009**, *3*, 20–28, doi:10.1016/j.ijggc.2008.06.001.
11. Gerdemann, S.J.; O'Connor, W.K.; Dahlin, D.C.; Penner, L.R.; Rush, H. Ex Situ Aqueous Mineral Carbonation. *Environ Sci Technol* **2007**, *41*, 2587–2593, doi:10.1021/es0619253.
12. Labande, A.; Debono, N.; Sournia-Saquet, A.; Daran, J.-C.; Poli, R. Oxidation-Promoted Activation of a Ferrocene C–H Bond by a Rhodium Complex. *Dalton Transactions* **2013**, *42*, 6531, doi:10.1039/c3dt50240f.
13. Ji, L.; Yu, H.; Zhang, R.; French, D.; Grigore, M.; Yu, B.; Wang, X.; Yu, J.; Zhao, S. Effects of Fly Ash Properties on Carbonation Efficiency in CO_2 Mineralisation. *Fuel Processing Technology* **2019**, *188*, 79–88, doi:10.1016/j.fuproc.2019.01.015.
14. Olajire, A.A. A Review of Mineral Carbonation Technology in Sequestration of CO_2. *J Pet Sci Eng* **2013**, *109*, 364–392, doi:10.1016/j.petrol.2013.03.013.
15. Gomes, H.I.; Mayes, W.M.; Rogerson, M.; Stewart, D.I.; Burke, I.T. Alkaline Residues and the Environment: A Review of Impacts, Management Practices and Opportunities. *J Clean Prod* **2016**, *112*, 3571–3582, doi:10.1016/j.jclepro.2015.09.111.
16. Chiang, P.-C.; Pan, S.-Y. *Carbon Dioxide Mineralization and Utilization*; Springer Singapore: Singapore, 2017; ISBN 978-981-10-3267-7.

17. Assi, A.; Bilo, F.; Zanoletti, A.; Ponti, J.; Valsesia, A.; La Spina, R.; Zacco, A.; Bontempi, E. Zero-Waste Approach in Municipal Solid Waste Incineration: Reuse of Bottom Ash to Stabilize Fly Ash. *J Clean Prod* **2019**, *245*, 118779, doi:10.1016/j.jclepro.2019.118779.
18. Quina, M.J.; Bontempi, E.; Bogush, A.; Schlumberger, S.; Weibel, G.; Braga, R.; Funari, V.; Hyks, J.; Rasmussen, E.; Lederer, J. Technologies for the Management of MSW Incineration Ashes from Gas Cleaning: New Perspectives on Recovery of Secondary Raw Materials and Circular Economy. *Science of The Total Environment* **2018**, *635*, 526–542, doi:10.1016/j.scitotenv.2018.04.150.
19. Levaggi, L.; Levaggi, R.; Marchiori, C.; Trecroci, C. Waste-to-Energy in the EU: The Effects of Plant Ownership, Waste Mobility, and Decentralization on Environmental Outcomes and Welfare. *Sustainability* **2020**, *12*, 5743, doi:10.3390/su12145743.
20. Lackner, K.S. A Guide to CO_2 Sequestration. *Science (1979)* **2003**, *300*, 1677–1678, doi:10.1126/science.1079033.
21. Xia, Y.; He, P.J.; Pu, H.X.; Lü, F.; Shao, L.M.; Zhang, H. Inhibitory Effect of High Calcium Concentration on Municipal Solid Waste Leachate Treatment by the Activated Sludge Process. *Waste Management & Research: The Journal for a Sustainable Circular Economy* **2017**, *35*, 508–514, doi:10.1177/0734242X16684943.
22. Assi, A.; Federici, S.; Bilo, F.; Zacco, A.; Depero, L.E.; Bontempi, E. Increased Sustainability of Carbon Dioxide Mineral Sequestration by a Technology Involving Fly Ash Stabilization. *Materials* **2019**, *12*, 2714, doi:10.3390/ma12172714.
23. Benassi, L.; Zanoletti, A.; Depero, L.E.; Bontempi, E. Sewage Sludge Ash Recovery as Valuable Raw Material for Chemical Stabilization of Leachable Heavy Metals. *J Environ Manage* **2019**, *245*, 464–470, doi:10.1016/j.jenvman.2019.05.104.
24. Al-Ghussain, L. Global Warming: Review on Driving Forces and Mitigation. *Environ Prog Sustain Energy* **2019**, *38*, 13–21, doi:10.1002/ep.13041.
25. Balat, M. Coal in the Global Energy Scene. *Energy Sources, Part B: Economics, Planning, and Policy* **2009**, *5*, 50–62, doi:10.1080/15567240701758927.
26. Karl, T.R.; Trenberth, K.E. Modern Global Climate Change. *Science (1979)* **2003**, *302*, 1719–1723, doi:10.1126/science.1090228.
27. UNFCCC *The Paris Agreement*; 2018;
28. Bontempi, E.; Sorrentino, G.P.; Zanoletti, A.; Alessandri, I.; Depero, L.E.; Caneschi, A. Sustainable Materials and Their Contribution to the Sustainable Development Goals (SDGs): A Critical Review Based on an Italian Example. *Molecules* **2021**, *26*, 1407, doi:10.3390/molecules26051407.
29. Chiang, P.-C.; Pan, S.-Y. Waste-to-Resource (WTR) Green Supply Chain. In *Carbon Dioxide Mineralization and Utilization*; Springer Singapore: Singapore, 2017; pp. 361–401.
30. Madurai Elavarasan, R.; Afridhis, S.; Vijayaraghavan, R.R.; Subramaniam, U.; Nurunnabi, M. SWOT Analysis: A Framework for Comprehensive Evaluation of Drivers and Barriers for Renewable Energy Development in Significant Countries. *Energy Reports* **2020**, *6*, 1838–1864, doi:10.1016/j.egyr.2020.07.007.
31. Vassilev, S. V.; Vassileva, C.G. Extra CO_2 Capture and Storage by Carbonation of Biomass Ashes. *Energy Convers Manag* **2020**, *204*, 112331, doi:10.1016/j.enconman.2019.112331.
32. Lackner, K.S. Carbonate Chemistry for Sequestering Fossil Carbon. *Annual Review of Energy and the Environment* **2002**, *27*, 193–232, doi:10.1146/annurev.energy.27.122001.083433.
33. Alivand, M.S.; Mazaheri, O.; Wu, Y.; Zavabeti, A.; Stevens, G.W.; Scholes, C.A.; Mumford, K.A. Water-Dispersible Nanocatalysts with Engineered Structures: The New

Generation of Nanomaterials for Energy-Efficient CO_2 Capture. *ACS Appl Mater Interfaces* **2021**, *13*, 57294–57305, doi:10.1021/acsami.1c17678.
34. Nnamdi, D.; Moghanloo, R.G. Embedding Existing Pipelines in Design of CO_2 Transportation Networks for Optimal Sequestration Economics. In Proceedings of the Day 2 Tue, October 17, 2023; SPE, October 9 2023.
35. Onyebuchi, V.E.; Kolios, A.; Hanak, D.P.; Biliyok, C.; Manovic, V. A Systematic Review of Key Challenges of CO_2 Transport via Pipelines. *Renewable and Sustainable Energy Reviews* **2018**, *81*, 2563–2583, doi:10.1016/j.rser.2017.06.064.
36. Becattini, V.; Gabrielli, P.; Antonini, C.; Campos, J.; Acquilino, A.; Sansavini, G.; Mazzotti, M. Carbon Dioxide Capture, Transport and Storage Supply Chains: Optimal Economic and Environmental Performance of Infrastructure Rollout. *International Journal of Greenhouse Gas Control* **2022**, *117*, 103635, doi:10.1016/j.ijggc.2022.103635.
37. Kampman, N.; Maskell, A.; Bickle, M.J.; Evans, J.P.; Schaller, M.; Purser, G.; Zhou, Z.; Gattacceca, J.; Peitre, E.S.; Rochelle, C.A.; et al. Scientific Drilling and Downhole Fluid Sampling of a Natural CO_2 Reservoir, Green River, Utah. *Scientific Drilling* **2013**, *16*, 33–43, doi:10.5194/sd-16-33-2013.
38. Pawar, R.J.; Bromhal, G.S.; Carey, J.W.; Foxall, W.; Korre, A.; Ringrose, P.S.; Tucker, O.; Watson, M.N.; White, J.A. Recent Advances in Risk Assessment and Risk Management of Geologic CO_2 Storage. *International Journal of Greenhouse Gas Control* **2015**, *40*, 292–311, doi:10.1016/j.ijggc.2015.06.014.
39. Armor, J.N. Addressing the CO_2 Dilemma. *Catal Letters* **2007**, *114*, 115–121, doi:10.1007/s10562-007-9063-3.
40. Huesemann, M.H. Can Advances in Science and Technology Prevent Global Warming? *Mitig Adapt Strateg Glob Chang* **2006**, *11*, 539–577, doi:10.1007/s11027-006-2166-0.
41. Klinthong, W.; Yang, Y.-H.; Huang, C.-H.; Tan, C.-S. A Review: Microalgae and Their Applications in CO_2 Capture and Renewable Energy. *Aerosol Air Qual Res* **2015**, *15*, 712–742, doi:10.4209/aaqr.2014.11.0299.
42. Olivares-Marín, M.; Maroto-Valer, M.M. Development of Adsorbents for CO_2 Capture from Waste Materials: A Review. *Greenhouse Gases: Science and Technology* **2012**, *2*, 20–35, doi:10.1002/ghg.45.
43. Yang, Y.; Tang, S.; Chen, J.P. Carbon Capture and Utilization by Algae with High Concentration CO_2 or Bicarbonate as Carbon Source. *Science of The Total Environment* **2024**, *918*, 170325, doi:10.1016/j.scitotenv.2024.170325.
44. Bodor, M.; Santos, R.; Gerven, T.; Vlad, M. Recent Developments and Perspectives on the Treatment of Industrial Wastes by Mineral Carbonation — a Review. *Open Engineering* **2013**, *3*, doi:10.2478/s13531-013-0115-8.
45. Costa, G.; Baciocchi, R.; Polettini, A.; Pomi, R.; Hills, C.D.; Carey, P.J. Current Status and Perspectives of Accelerated Carbonation Processes on Municipal Waste Combustion Residues. *Environ Monit Assess* **2007**, *135*, 55–75, doi:10.1007/s10661-007-9704-4.
46. Huijgen, W.J.J.; Comans, R.N.J. Carbonation of Steel Slag for CO_2 Sequestration: Leaching of Products and Reaction Mechanisms. *Environ Sci Technol* **2006**, *40*, 2790–2796, doi:10.1021/es052534b.
47. Čančarevič, Ž.; Schön, J.C.; Jansen, M. Alkali Metal Carbonates at High Pressure. *Z Anorg Allg Chem* **2006**, *632*, 1437–1448, doi:10.1002/zaac.200600068.
48. Chiang, P.-C.; Pan, S.-Y. Principles of Accelerated Carbonation Reaction. In *Carbon Dioxide Mineralization and Utilization*; Springer Singapore: Singapore, 2017; pp. 71–96.

49. Haug, T.A.; Kleiv, R.A.; Munz, I.A. Investigating Dissolution of Mechanically Activated Olivine for Carbonation Purposes. *Applied Geochemistry* **2010**, *25*, 1547–1563, doi:10.1016/j.apgeochem.2010.08.005.
50. Seifritz, W. CO_2 Disposal by Means of Silicates. *Nature* **1990**, *345*, 486–486, doi:10.1038/345486b0.
51. Chiang, P.-C.; Pan, S.-Y. CO_2 Mineralization and Utilization via Accelerated Carbonation. In *Carbon Dioxide Mineralization and Utilization*; Springer Singapore: Singapore, 2017; pp. 35–49.
52. Sanna, A.; Uibu, M.; Caramanna, G.; Kuusik, R.; Maroto-Valer, M.M. A Review of Mineral Carbonation Technologies to Sequester CO_2. *Chem. Soc. Rev.* **2014**, *43*, 8049–8080, doi:10.1039/C4CS00035H.
53. Azdarpour, A.; Rahmani, O.; Junin, R.; Yeop, M.A. Use of Olivine for Carbon Dioxide Mineral Sequestration. In Proceedings of the 2013 IEEE Business Engineering and Industrial Applications Colloquium (BEIAC); IEEE, April 2013; pp. 561–564.
54. Bobicki, E.R.; Liu, Q.; Xu, Z.; Zeng, H. Carbon Capture and Storage Using Alkaline Industrial Wastes. *Prog Energy Combust Sci* **2012**, *38*, 302–320, doi:10.1016/j.pecs.2011.11.002.
55. Chiang, P.-C.; Pan, S.-Y. Post-Combustion Carbon Capture, Storage, and Utilization. In *Carbon Dioxide Mineralization and Utilization*; Springer Singapore: Singapore, 2017; pp. 9–34.
56. Lackner, K.S.; Wendt, C.H.; Butt, D.P.; Joyce, E.L.; Sharp, D.H. Carbon Dioxide Disposal in Carbonate Minerals. *Energy* **1995**, *20*, 1153–1170, doi:10.1016/0360-5442(95)00071-N.
57. Villain, G.; Thiery, M.; Platret, G. Measurement Methods of Carbonation Profiles in Concrete: Thermogravimetry, Chemical Analysis and Gammadensimetry. *Cem Concr Res* **2007**, *37*, 1182–1192, doi:10.1016/j.cemconres.2007.04.015.
58. Lekakh, S.N.; Rawlins, C.H.; Robertson, D.G.C.; Richards, V.L.; Peaslee, K.D. Kinetics of Aqueous Leaching and Carbonization of Steelmaking Slag. *Metallurgical and Materials Transactions B* **2008**, *39*, 125–134, doi:10.1007/s11663-007-9112-8.
59. Pan, S.-Y.; Liu, H.-L.; Chang, E.-E.; Kim, H.; Chen, Y.-H.; Chiang, P.-C. Multiple Model Approach to Evaluation of Accelerated Carbonation for Steelmaking Slag in a Slurry Reactor. *Chemosphere* **2016**, *154*, 63–71, doi:10.1016/j.chemosphere.2016.03.093.
60. Viadero, R. Principles of Gas Solubility in Water: Henry's Law. In *Encyclopedia of Water*; Wiley, 2019; pp. 1–7.
61. NIST NIST Chemistry WebBook, SRD 69 Available online: https://webbook.nist.gov/cgi/cbook.cgi?ID=C124389&Mask=10#Refs (accessed on 13 September 2024).
62. Al-Rawajfeh, A.E.; Al-Amaireh, M.N. The Influence of CO_2 Injection on the Carbonate Chemistry and Scaling in Multiple-Effect Distillers. *Desalination Water Treat* **2009**, *7*, 191–197, doi:10.5004/dwt.2009.700.
63. Morel, F.; Hering, J. Principles and Applications of Aquatic Chemistry. *Choice Reviews Online* **1993**, *31*, 31-0941-31–0941, doi:10.5860/CHOICE.31-0941.
64. Coto, B.; Martos, C.; Peña, J.L.; Rodríguez, R.; Pastor, G. Effects in the Solubility of $CaCO_3$: Experimental Study and Model Description. *Fluid Phase Equilib* **2012**, *324*, 1–7, doi:10.1016/j.fluid.2012.03.020.
65. Chiang, P.-C.; Pan, S.-Y. Carbonation Mechanisms and Modelling. In *Carbon Dioxide Mineralization and Utilization*; Springer Singapore: Singapore, 2017; pp. 127–158.

66. Eloneva, S.; Teir, S.; Salminen, J.; Fogelholm, C.-J.; Zevenhoven, R. Fixation of CO_2 by Carbonating Calcium Derived from Blast Furnace Slag. *Energy* **2008**, *33*, 1461–1467, doi:10.1016/j.energy.2008.05.003.
67. Teir, S.; Eloneva, S.; Fogelholm, C.-J.; Zevenhoven, R. Dissolution of Steelmaking Slags in Acetic Acid for Precipitated Calcium Carbonate Production. *Energy* **2007**, *32*, 528–539, doi:10.1016/j.energy.2006.06.023.
68. Park, A.A.; Jadhav, R.; Fan, L. CO_2 Mineral Sequestration: Chemically Enhanced Aqueous Carbonation of Serpentine. *Can J Chem Eng* **2003**, *81*, 885–890, doi:10.1002/cjce.5450810373.
69. Park, A.-H.A.; Fan, L.-S. CO_2 Mineral Sequestration: Physically Activated Dissolution of Serpentine and PH Swing Process. *Chem Eng Sci* **2004**, *59*, 5241–5247, doi:10.1016/j.ces.2004.09.008.
70. Kodoma, S.; Nishimoto, T.; Yamamoto, N.; Yogo, K.; Yamada, K. Development of a New PH-Swing CO_2 Mineralization Process with a Recyclable Reaction Solution. *Energy* **2008**, *33*, 776–784, doi:10.1016/j.energy.2008.01.005.
71. Eloneva, S.; Said, A.; Fogelholm, C.-J.; Zevenhoven, R. Preliminary Assessment of a Method Utilizing Carbon Dioxide and Steelmaking Slags to Produce Precipitated Calcium Carbonate. *Appl Energy* **2012**, *90*, 329–334, doi:10.1016/j.apenergy.2011.05.045.
72. Ding, W.; Yang, H.; Ouyang, J. Mineral Carbonation of a Desulfurization Residue for CO_2 Sequestration. *RSC Adv* **2015**, *5*, 67184–67194, doi:10.1039/C5RA10576E.
73. Koralegedara, N.H.; Pinto, P.X.; Dionysiou, D.D.; Al-Abed, S.R. Recent Advances in Flue Gas Desulfurization Gypsum Processes and Applications – A Review. *J Environ Manage* **2019**, *251*, 109572, doi:10.1016/j.jenvman.2019.109572.
74. Lim, M.; Han, G.-C.; Ahn, J.-W.; You, K.-S. Environmental Remediation and Conversion of Carbon Dioxide (CO_2) into Useful Green Products by Accelerated Carbonation Technology. *Int J Environ Res Public Health* **2010**, *7*, 203–228, doi:10.3390/ijerph7010203.
75. Fernandez Bertos, M.; Simons, S.; Hills, C.; Carey, P. A Review of Accelerated Carbonation Technology in the Treatment of Cement-Based Materials and Sequestration of CO_2. *J Hazard Mater* **2004**, *112*, 193–205, doi:10.1016/j.jhazmat.2004.04.019.
76. Van Gerven, T.; Van Keer, E.; Arickx, S.; Jaspers, M.; Wauters, G.; Vandecasteele, C. Carbonation of MSWI-Bottom Ash to Decrease Heavy Metal Leaching, in View of Recycling. *Waste Management* **2005**, *25*, 291–300, doi:10.1016/j.wasman.2004.07.008.
77. Li, X.; Bertos, M.F.; Hills, C.D.; Carey, P.J.; Simon, S. Accelerated Carbonation of Municipal Solid Waste Incineration Fly Ashes. *Waste Management* **2007**, *27*, 1200–1206, doi:10.1016/j.wasman.2006.06.011.
78. Polettini, A.; Pomi, R. The Leaching Behavior of Incinerator Bottom Ash as Affected by Accelerated Ageing. *J Hazard Mater* **2004**, *113*, 209–215, doi:10.1016/j.jhazmat.2004.06.009.
79. Stolaroff, J.K.; Lowry, G. V.; Keith, D.W. Using CaO- and MgO-Rich Industrial Waste Streams for Carbon Sequestration. *Energy Convers Manag* **2005**, *46*, 687–699, doi:10.1016/j.enconman.2004.05.009.
80. Shih, S.-M.; Ho, C.-S.; Song, Y.-S.; Lin, J.-P. Kinetics of the Reaction of $Ca(OH)_2$ with CO_2 at Low Temperature. *Ind Eng Chem Res* **1999**, *38*, 1316–1322, doi:10.1021/ie980508z.
81. Chang, E.-E.; Chiu, A.-C.; Pan, S.-Y.; Chen, Y.-H.; Tan, C.-S.; Chiang, P.-C. Carbonation of Basic Oxygen Furnace Slag with Metalworking Wastewater in a Slurry

Reactor. *International Journal of Greenhouse Gas Control* **2013**, *12*, 382–389, doi:10.1016/j.ijggc.2012.11.026.
82. Biava, G.; Zacco, A.; Zanoletti, A.; Sorrentino, G.P.; Capone, C.; Principallo, A.; Depero, L.E.; Bontempi, E. Accelerated Direct Carbonation of Steel Slag and Cement Kiln Dust: An Industrial Symbiosis Strategy Applied in the Bergamo–Brescia Area. *Materials* **2023**, *16*, 4055, doi:10.3390/ma16114055.
83. Bonenfant, D.; Kharoune, L.; Sauve´, S.; Hausler, R.; Niquette, P.; Mimeault, M.; Kharoune, M. CO_2 Sequestration Potential of Steel Slags at Ambient Pressure and Temperature. *Ind Eng Chem Res* **2008**, *47*, 7610–7616, doi:10.1021/ie701721j.
84. Klansky, J. Hardness Testing. In *Characterization of Materials*; Wiley, 2002; pp. 316–323.
85. Zhang, D.; Li, C.; Jia, D.; Zhang, Y. Investigation into Engineering Ceramics Grinding Mechanism and the Influential Factors of the Grinding Force. *International Journal of Control and Automation* **2014**, *7*, 19–34, doi:10.14257/ijca.2014.7.4.03.
86. Mehta, P.K. Studies on Blended Portland Cements Containing Santorin Earth. *Cem Concr Res* **1981**, *11*, 507–518, doi:10.1016/0008-8846(81)90080-6.
87. Zaman, A. A Strategic Framework for Working toward Zero Waste Societies Based on Perceptions Surveys. *Recycling* **2017**, *2*, 1, doi:10.3390/recycling2010001.
88. Chimenos, J.M.; Segarra, M.; Fernández, M.A.; Espiell, F. Characterization of the Bottom Ash in Municipal Solid Waste Incinerator. *J Hazard Mater* **1999**, *64*, 211–222, doi:10.1016/S0304-3894(98)00246-5.
89. The Economist Global Waste Generation Will Nearly Double by 2050 Available online: https://www.economist.com/graphic-detail/2018/10/02/global-waste-generation-will-nearly-double-by-2050 (accessed on 22 September 2024).
90. Paul Hockenos EU Climate Ambitions Spell Trouble for Electricity from Burning Waste Available online: https://www.cleanenergywire.org/news/eu-climate-ambitions-spell-trouble-electricity-burning-waste (accessed on 18 September 2024).
91. UNEP Guidelines on Best Available and Provisional guidance on Best Environmental Practices to Article 5 and Annex C of the Stockholm Convention on Persistent Organic Pollutants. *Secretariat of the Stockholm Convention on Persistent Organic Pollutants* **2007**.
92. Rendek, E.; Ducom, G.; Germain, P. Influence of Waste Input and Combustion Technology on MSWI Bottom Ash Quality. *Waste Management* **2007**, *27*, 1403–1407, doi:10.1016/j.wasman.2007.03.016.
93. Xiao, Y.; Zhou, B. Does the Development of Delivery Industry Increase the Production of Municipal Solid Waste?—An Empirical Study of China. *Resour Conserv Recycl* **2020**, *155*, 104577, doi:10.1016/j.resconrec.2019.104577.
94. Li, J. Four Years of Waste Sorting Leaves China's Incinerators Short of Fuel Available online: https://chinadialogue.net/en/cities/four-years-of-waste-sorting-leaves-chinas-incinerators-short-of-fuel/ (accessed on 22 September 2024).
95. A2A Ambiente *Il Termoutilizzatore Di Brescia Ambientale*; 2024;
96. Zacco, A.; Borgese, L.; Gianoncelli, A.; Struis, R.P.W.J.; Depero, L.E.; Bontempi, E. Review of Fly Ash Inertisation Treatments and Recycling. *Environ Chem Lett* **2014**, *12*, 153–175, doi:10.1007/s10311-014-0454-6.
97. Zhu, F.; Xiong, Y.; Wang, Y.; Wei, X.; Zhu, X.; Yan, F. Heavy Metal Behavior in "Washing-Calcination-Changing with Bottom Ash" System for Recycling of Four Types of Fly Ashes. *Waste Management* **2018**, *75*, 215–225, doi:10.1016/j.wasman.2018.01.032.
98. Diliberto, C.; Meux, E.; Diliberto, S.; Garoux, L.; Marcadier, E.; Rizet, L.; Lecomte, A. A Zero-Waste Process for the Management of MSWI Fly Ashes: Production of

Ordinary Portland Cement. *Environ Technol* **2020**, *41*, 1199–1208, doi:10.1080/09593330.2018.1525434.
99. Husgafvel, R.; Karjalainen, E.; Linkosalmi, L.; Dahl, O. Recycling Industrial Residue Streams into a Potential New Symbiosis Product – The Case of Soil Amelioration Granules. *J Clean Prod* **2016**, *135*, 90–96, doi:10.1016/j.jclepro.2016.06.092.
100. Abebe, S.; Sisay, A.; Abebe, W. Characterization and Optimization of Incinerated Municipal Solid Waste Fly Ash as a Cement Substitute Material in Concrete at Reppie Waste to Energy Plant, Ethiopia, East Africa. *Advances in Environmental Studies* **2021**, *5*, doi:10.36959/742/235.
101. Zhao, K.; Hu, Y.; Tian, Y.; Chen, D.; Feng, Y. Chlorine Removal from MSWI Fly Ash by Thermal Treatment: Effects of Iron/Aluminum Additives. *Journal of Environmental Sciences* **2020**, *88*, 112–121, doi:10.1016/j.jes.2019.08.006.
102. Bakalár, T.; Pavolová, H.; Hajduová, Z.; Lacko, R.; Kyšeľa, K. Metal Recovery from Municipal Solid Waste Incineration Fly Ash as a Tool of Circular Economy. *J Clean Prod* **2021**, *302*, 126977, doi:10.1016/j.jclepro.2021.126977.
103. Huang, T.Y.; Chuieh, P.T. Life Cycle Assessment of Reusing Fly Ash from Municipal Solid Waste Incineration. *Procedia Eng* **2015**, *118*, 984–991, doi:10.1016/j.proeng.2015.08.539.
104. Cappai, G.; Cara, S.; Muntoni, A.; Piredda, M. Application of Accelerated Carbonation on MSW Combustion APC Residues for Metal Immobilization and CO_2 Sequestration. *J Hazard Mater* **2012**, *207–208*, 159–164, doi:10.1016/j.jhazmat.2011.04.013.
105. Allegrini, E.; Maresca, A.; Olsson, M.E.; Holtze, M.S.; Boldrin, A.; Astrup, T.F. Quantification of the Resource Recovery Potential of Municipal Solid Waste Incineration Bottom Ashes. *Waste Management* **2014**, *34*, 1627–1636, doi:10.1016/j.wasman.2014.05.003.
106. Huber, F.; Blasenbauer, D.; Aschenbrenner, P.; Fellner, J. Complete Determination of the Material Composition of Municipal Solid Waste Incineration Bottom Ash. *Waste Management* **2020**, *102*, 677–685, doi:10.1016/j.wasman.2019.11.036.
107. Assi, A.; Bilo, F.; Federici, S.; Zacco, A.; Depero, L.E.; Bontempi, E. Bottom Ash Derived from Municipal Solid Waste and Sewage Sludge Co-Incineration: First Results about Characterization and Reuse. *Waste Management* **2020**, *116*, 147–156, doi:10.1016/j.wasman.2020.07.031.
108. Jurič, B.; Hanžič, L.; Ilić, R.; Samec, N. Utilization of Municipal Solid Waste Bottom Ash and Recycled Aggregate in Concrete. *Waste Management* **2006**, *26*, 1436–1442, doi:10.1016/j.wasman.2005.10.016.
109. Loginova, E.; Volkov, D.S.; van de Wouw, P.M.F.; Florea, M.V.A.; Brouwers, H.J.H. Detailed Characterization of Particle Size Fractions of Municipal Solid Waste Incineration Bottom Ash. *J Clean Prod* **2019**, *207*, 866–874, doi:10.1016/j.jclepro.2018.10.022.
110. Joy, A.; Bouchbinder, E.; Procaccia, I. Cooling-Rate Dependence of the Shear Modulus of Amorphous Solids. *Phys Rev E* **2013**, *87*, 042310, doi:10.1103/PhysRevE.87.042310.
111. Alterary, S.S.; Marei, N.H. Fly Ash Properties, Characterization, and Applications: A Review. *J King Saud Univ Sci* 2021, *33*.
112. Assi, A.; Bilo, F.; Zanoletti, A.; Borgese, L.; Depero, L.E.; Nenci, M.; Bontempi, E. Stabilization of Municipal Solid Waste Fly Ash, Obtained by Co-Combustion with Sewage Sludge, Mixed with Bottom Ash Derived by the Same Plant. *Applied Sciences* **2020**, *10*, 6075, doi:10.3390/app10176075.

113. Mininni, G.; Santori, M. Problems and Perspectives of Sludge Utilization in Agriculture. *Agric Ecosyst Environ* **1987**, *18*, 291–311, doi:10.1016/0167-8809(87)90096-X.
114. Canpolat, F.; Yılmaz, K.; Köse, M.M.; Sümer, M.; Yurdusev, M.A. Use of Zeolite, Coal Bottom Ash and Fly Ash as Replacement Materials in Cement Production. *Cem Concr Res* **2004**, *34*, 731–735, doi:10.1016/S0008-8846(03)00063-2.
115. Al-Rawas, A.A.; Wahid Hago, A.; Taha, R.; Al-Kharousi, K. Use of Incinerator Ash as a Replacement for Cement and Sand in Cement Mortars. *Build Environ* **2005**, *40*, 1261–1266, doi:10.1016/j.buildenv.2004.10.009.
116. Puma, S.; Marchese, F.; Dominijanni, A.; Manassero, M. Reuse of MSWI Bottom Ash Mixed with Natural Sodium Bentonite as Landfill Cover Material. *Waste Management & Research: The Journal for a Sustainable Circular Economy* **2013**, *31*, 577–584, doi:10.1177/0734242X13477722.
117. Šyc, M.; Simon, F.G.; Hykš, J.; Braga, R.; Biganzoli, L.; Costa, G.; Funari, V.; Grosso, M. Metal Recovery from Incineration Bottom Ash: State-of-the-Art and Recent Developments. *J Hazard Mater* **2020**, *393*, 122433, doi:10.1016/j.jhazmat.2020.122433.
118. Hjelmar, O.; Holm, J.; Crillesen, K. Utilisation of MSWI Bottom Ash as Sub-Base in Road Construction: First Results from a Large-Scale Test Site. *J Hazard Mater* **2007**, *139*, 471–480, doi:10.1016/j.jhazmat.2006.02.059.
119. Stabile, P.; Bello, M.; Petrelli, M.; Paris, E.; Carroll, M.R. Vitrification Treatment of Municipal Solid Waste Bottom Ash. *Waste Management* **2019**, *95*, 250–258, doi:10.1016/j.wasman.2019.06.021.
120. Chen, C.-H.; Chiou, I.-J. Distribution of Chloride Ion in MSWI Bottom Ash and De-Chlorination Performance. *J Hazard Mater* **2007**, *148*, 346–352, doi:10.1016/j.jhazmat.2007.02.046.
121. Zhu, Y.; Zhao, Y.; Zhao, C.; Gupta, R. Physicochemical Characterization and Heavy Metals Leaching Potential of Municipal Solid Waste Incinerated Bottom Ash (MSWI-BA) When Utilized in Road Construction. *Environmental Science and Pollution Research* **2020**, *27*, 14184–14197, doi:10.1007/s11356-020-08007-9.
122. Caviglia, C.; Confalonieri, G.; Corazzari, I.; Destefanis, E.; Mandrone, G.; Pastero, L.; Boero, R.; Pavese, A. Effects of Particle Size on Properties and Thermal Inertization of Bottom Ashes (MSW of Turin's Incinerator). *Waste Management* **2019**, *84*, 340–354, doi:10.1016/j.wasman.2018.11.050.
123. Fernández Bertos, M.; Li, X.; Simons, S.J.R.; Hills, C.D.; Carey, P.J. Investigation of Accelerated Carbonation for the Stabilisation of MSW Incinerator Ashes and the Sequestration of CO_2. *Green Chem.* **2004**, *6*, 428–436, doi:10.1039/B401872A.
124. Chang, E.-E.; Pan, S.-Y.; Yang, L.; Chen, Y.-H.; Kim, H.; Chiang, P.-C. Accelerated Carbonation Using Municipal Solid Waste Incinerator Bottom Ash and Cold-Rolling Wastewater: Performance Evaluation and Reaction Kinetics. *Waste Management* **2015**, *43*, 283–292, doi:10.1016/j.wasman.2015.05.001.
125. Society for Mining, M. and E. *Coal's Importance to the World*; 2021;
126. Pandurangan, B. Coal India Ltd: Role in India's Energy Transition. *The Management Accountant Journal* **2023**, *58*, 26, doi:10.33516/maj.v58i10.26-28p.
127. Balat, H. Role of Coal in Sustainable Energy Development. *Energy Exploration & Exploitation* **2007**, *25*, 151–174, doi:10.1260/014459807782009169.
128. Kitto, J.B..; Stultz, S.C.. *Steam, Its Generation and Use*; Kitto, J.B.., Stultz, S.C.., Eds.; 41st ed.; Babcock & Wilcox, 2005; ISBN 0963457012.

129. IEA Greenhouse Gas Emissions from Energy Data Explorer Available online: https://www.iea.org/data-and-statistics/data-tools/greenhouse-gas-emissions-from-energy-data-explorer (accessed on 12 September 2024).
130. Kim, A.G.; Hesbach, P. Comparison of Fly Ash Leaching Methods. *Fuel* **2009**, *88*, 926–937, doi:10.1016/j.fuel.2008.11.013.
131. EEA Greenhouse Gas Emissions under the EU Emissions Trading System Available online: https://www.eea.europa.eu/en/analysis/indicators/greenhouse-gas-emissions-under-the (accessed on 12 September 2024).
132. Eurostat Coal Production and Consumption See Rebound in 2021 Available online: https://ec.europa.eu/eurostat/web/products-eurostat-news/-/ddn-20220502-2 (accessed on 12 September 2024).
133. Kartal, M.T.; Kılıç Depren, S.; Ali, U.; Nurgazina, Z. Long-Run Impact of Coal Usage Decline on CO_2 Emissions and Economic Growth: Evidence from Disaggregated Energy Consumption Perspective for China and India by Dynamic ARDL Simulations. *Energy & Environment* **2024**, *35*, 2357–2381, doi:10.1177/0958305X231152482.
134. Kabeyi, M.J.B.; Olanrewaju, O.A. Sustainable Energy Transition for Renewable and Low Carbon Grid Electricity Generation and Supply. *Front Energy Res* **2022**, *9*, doi:10.3389/fenrg.2021.743114.
135. Jin, S.; Zhao, Z.; Jiang, S.; Sun, J.; Pan, H.; Jiang, L. Comparison and Summary of Relevant Standards for Comprehensive Utilization of Fly Ash at Home and Abroad. *IOP Conf Ser Earth Environ Sci* **2021**, *621*, 012006, doi:10.1088/1755-1315/621/1/012006.
136. Zhou, Q.; Huang, G.H.; Chan, C.W. Development of an Intelligent Decision Support System for Air Pollution Control at Coal-Fired Power Plants. *Expert Syst Appl* **2004**, *26*, 335–356, doi:10.1016/j.eswa.2003.09.005.
137. Singh, N.B.; Agarwal, A.; De, A.; Singh, P. Coal Fly Ash: An Emerging Material for Water Remediation. *Int J Coal Sci Technol* 2022, *9*.
138. Shoumkova, A.S. Magnetic Separation of Coal Fly Ash from Bulgarian Power Plants. *Waste Management and Research* **2011**, *29*, 1078–1089, doi:10.1177/0734242X10379494.
139. Ramezanianpour, A.A. *Cement Replacement Materials*; Springer Berlin Heidelberg: Berlin, Heidelberg, 2014; ISBN 978-3-642-36720-5.
140. Alegbe, J.; Ayanda, O.S.; Ndungu, P.; Alexander, N.; Fatoba, O.O.; Petrik, L.F. Chemical, Mineralogical and Morphological Investigation of Coal Fly Ash Obtained from Mpumalanga Province, South Africa. *Res J Environ Sci* **2018**, *12*, 98–105, doi:10.3923/rjes.2018.98.105.
141. Assi, A.; Bilo, F.; Zanoletti, A.; Ponti, J.; Valsesia, A.; Spina, R. La; Depero, L.E.; Bontempi, E. Review of the Reuse Possibilities Concerning Ash Residues from Thermal Process in a Medium-Sized Urban System in Northern Italy. *Sustainability (Switzerland)* 2020, *12*.
142. Sambandam, B.; Palanisami, E.; Abbugounder, R.; Prakhya, B.; Thiyagarajan, D. Characterizations of Coal Fly Ash Nanoparticles and Induced in Vitro Toxicity in Cell Lines. *Journal of Nanoparticle Research* **2014**, *16*, doi:10.1007/s11051-013-2217-x.
143. Akın, S.Ş.; Magalhães, D.; Kazanç, F. A Study on the Effects of Various Combustion Parameters on the Mineral Composition of Tunçbilek Fly Ash. *Fuel* **2020**, *275*, 117881, doi:10.1016/j.fuel.2020.117881.
144. Thomas, M.; Jewell, R.; Jones, R. Coal Fly Ash as a Pozzolan. In *Coal Combustion Products (CCP's)*; Elsevier, 2017; pp. 121–154.

145. Rashid, A.N.A.A.; Talib, M.K.A.; Yusoff, M.N.M. Utilization of Coir Fibre Ash (CFA) in Cement Stabilized Peat. *IOP Conf Ser Earth Environ Sci* **2023**, *1238*, 012014, doi:10.1088/1755-1315/1238/1/012014.
146. Nayak, D.K.; Abhilash, P.P.; Singh, R.; Kumar, R.; Kumar, V. Fly Ash for Sustainable Construction: A Review of Fly Ash Concrete and Its Beneficial Use Case Studies. *Cleaner Materials* 2022, *6*.
147. Panda, L.; Dash, S. Characterization and Utilization of Coal Fly Ash: A Review. *Emerging Materials Research* 2020, *9*, 921–934.
148. Santos, A.C.; Guedes, A.; French, D.; Futuro, A.; Valentim, B. Integrative Study Assessing Space and Time Variations with Emphasis on Rare Earth Element (REE) Distribution and Their Potential on Ashes from Commercial (Colombian) Coal. *Minerals* **2022**, *12*, doi:10.3390/min12020194.
149. Bontempi, E. *Raw Materials Substitution Sustainability*; SpringerBriefs in Applied Sciences and Technology; Springer International Publishing: Cham, 2017; ISBN 978-3-319-60830-3.
150. Cui, Z.; Hao, T.; Yao, S.; Xu, H. Preparation of Porous Mullite Ceramic Supports from High Alumina Fly Ash. *J Mater Cycles Waste Manag* **2023**, doi:10.1007/s10163-023-01598-8.
151. Luo, Y.; Wu, Y.; Ma, S.; Zheng, S.; Zhang, Y.; Chu, P.K. Utilization of Coal Fly Ash in China: A Mini-Review on Challenges and Future Directions. *Environmental Science and Pollution Research* 2021, *28*, 18727–18740.
152. Yadav, V.K.; Gacem, A.; Choudhary, N.; Rai, A.; Kumar, P.; Yadav, K.K.; Abbas, M.; Khedher, N. Ben; Awwad, N.S.; Barik, D.; et al. Status of Coal-Based Thermal Power Plants, Coal Fly Ash Production, Utilization in India and Their Emerging Applications. *Minerals* 2022, *12*.
153. Sanjuán, M.Á.; Suárez-Navarro, J.A.; Argiz, C.; Mora, P. Assessment of Natural Radioactivity and Radiation Hazards Owing to Coal Fly Ash and Natural Pozzolan Portland Cements. *J Radioanal Nucl Chem* **2020**, *325*, 381–390, doi:10.1007/s10967-020-07263-w.
154. Chen, Z.; Wu, S.; Li, F.; Chen, J.; Qin, Z.; Pang, L. Recycling of Flue Gas Desulfurization Residues in Gneiss Based Hot Mix Asphalt: Materials Characterization and Performances Evaluation. *Constr Build Mater* **2014**, *73*, 137–144, doi:10.1016/j.conbuildmat.2014.09.049.
155. Bigham, J.M.; Kost, D.A.; Stehouwer, R.C.; Beeghly, J.H.; Fowler, R.; Traina, S.J.; Wolfe, W.E.; Dick, W.A. Mineralogical and Engineering Characteristics of Dry Flue Gas Desulfurization Products. *Fuel* **2005**, *84*, 1839–1848, doi:10.1016/j.fuel.2005.03.018.
156. Liu, S.; Yang, H.; Zhang, Z.; Chen, J.; Chen, C.; Guo, T.; Cao, Y.; Jia, W. Emission Characteristics of Fine Particles from Wet Flue Gas Desulfurization System Using a Cascade of Double Towers. *Aerosol Air Qual Res* **2018**, *18*, 1901–1909, doi:10.4209/aaqr.2017.11.0480.
157. Baligar, V.C.; Clark, R.B.; Korcak, R.F.; Wright, R.J. *Flue Gas Desulfurization Product Use on Agricultural Land*; Advances in Agronomy.; 2011; Vol. 111;.
158. Caillahua, M.C.; Moura, F.J. Technical Feasibility for Use of FGD Gypsum as an Additive Setting Time Retarder for Portland Cement. *Journal of Materials Research and Technology* 2018, *7*, 190–197.
159. Yrjas, P.; Hupa, M.; Iisa, K. Pressurized Stabilization of Desulfurization Residues from Gasification Processes. *Energy & Fuels* **1996**, *10*, 1189–1195, doi:10.1021/ef960013r.
160. Panday, D.; Ferguson, R.B.; Maharjan, B. Flue Gas Desulfurization Gypsum as Soil Amendment. In *Soil Amendments for Sustainability*; CRC Press, 2018; pp. 191–200.

161. Wang, J.; Yang, P. Potential Flue Gas Desulfurization Gypsum Utilization in Agriculture: A Comprehensive Review. *Renewable and Sustainable Energy Reviews* **2018**, *82*, 1969–1978, doi:10.1016/j.rser.2017.07.029.
162. Kabeyi, M.J.B.; Olanrewaju, O.A. Biogas Production and Applications in the Sustainable Energy Transition. *Journal of Energy* **2022**, *2022*, 1–43, doi:10.1155/2022/8750221.
163. Associação Portuguesa da Cortiça (APCOR) *Cork Yearbook 2020*; 2020;
164. Guimarães, R.; Guedes, A.; Valentim, B. Identification and Characterization of Ti-Spheres (Titanspheres) in Cork Powder Fly Ash. *Waste Biomass Valorization* **2020**, *11*, 2905–2923, doi:10.1007/s12649-019-00609-w.
165. Gil, L. Cork Powder Waste: An Overview. *Biomass Bioenergy* **1997**, *13*, 59–61, doi:10.1016/S0961-9534(97)00033-0.
166. Matos, A.M.; Nunes, S.; Sousa-Coutinho, J. Cork Waste in Cement Based Materials. *Mater Des* **2015**, *85*, 230–239, doi:10.1016/j.matdes.2015.06.082.
167. Ghonjizade-Samani, F.; Haurie, L.; Malet, R.; Realinho, V. The Components' Roles in Thermal Stability and Flammability of Cork Powder. *Materials* **2023**, *16*, 3829, doi:10.3390/ma16103829.
168. Guimarães, R. Reciclagem de resíduos de incineração de pó de cortiça para recuperação de titânio e carbono e utilização na correção de solos. Doctoral Dissertation, Universidade do Porto, Portugal: Porto, 2023.
169. Gil, L. Cork: Sustainability and New Applications. *Front Mater* **2015**, *1*, doi:10.3389/fmats.2014.00038.
170. Sadr, M.; Esmaeili Aliabadi, D.; Avşar, B.; Thrän, D. Assessing the Impact of Seasonality on Bioenergy Production from Energy Crops in Germany, Considering Just-in-time Philosophy. *Biofuels, Bioproducts and Biorefining* **2024**, *18*, 883–898, doi:10.1002/bbb.2602.
171. Nussbaumer, T. Combustion and Co-Combustion of Biomass: Fundamentals, Technologies, and Primary Measures for Emission Reduction. *Energy & Fuels* **2003**, *17*, 1510–1521, doi:10.1021/ef030031q.
172. Guimarães, R.; Guedes, A.; Valentim, B.R.V. Characterization, Concentration of Biochar and Titanspheres and Heavy Metals Assessment of Quercus Suber Cork Powder Fly Ash Fractions. *The Journal of Solid Waste Technology and Management* **2021**, *47*, 605–618, doi:10.5276/JSWTM/2021.605.
173. Knapp, B.A.; Insam, H. Recycling of Biomass Ashes: Current Technologies and Future Research Needs. In *Recycling of Biomass Ashes*; Springer Berlin Heidelberg: Berlin, Heidelberg, 2011; pp. 1–16.
174. Ramos, T.; Matos, A.M.; Sousa-Coutinho, J. Strength and Durability of Mortar Using Cork Waste Ash as Cement Replacement. *Materials Research* **2014**, *17*, 893–907, doi:10.1590/S1516-14392014005000092.
175. Wang, Q.; Lai, Z.; Mu, J.; Chu, D.; Zang, X. Converting Industrial Waste Cork to Biochar as Cu (II) Adsorbent via Slow Pyrolysis. *Waste Management* **2020**, *105*, 102–109, doi:10.1016/j.wasman.2020.01.041.
176. Ortega, J.M.; Branco, F.G.; Pereira, L. Long-Term Behavior Related to Water Ingress in Mortars Which Combine Expanded and Natural Cork Lightweight Aggregates and Eco-Friendly Cements. *Buildings* **2023**, *13*, 1651, doi:10.3390/buildings13071651.
177. Dong, F.; Kirk, D.W.; Tran, H. Biomass Ash Alkalinity Reduction for Land Application via CO_2 from Treated Boiler Flue Gas. *Fuel* **2014**, *136*, 208–218, doi:10.1016/j.fuel.2014.07.059.

178. Trivedi, N.S.; Mandavgane, S.A.; Mehetre, S.; Kulkarni, B.D. Characterization and Valorization of Biomass Ashes. *Environmental Science and Pollution Research* **2016**, *23*, 20243–20256, doi:10.1007/s11356-016-7227-7.
179. Wang, W.; Zheng, Y.; Liu, X.; Wang, P. Characterization of Typical Biomass Ashes and Study on Their Potential of CO_2 Fixation. *Energy & Fuels* **2012**, *26*, 6047–6052, doi:10.1021/ef300781e.
180. UNI EN 12457-2 Characterisation of waste - leaching - compliance test for leaching of granular waste materials and sludges - part 2: one stage batch test at a liquid to solid ratio of 10 l/kg for materials with particle size below 4 mm (without or with size reduction). **2004**.
181. Bontempi, E.; Zacco, A.; Borgese, L.; Gianoncelli, A.; Ardesi, R.; Depero, L.E. A New Method for Municipal Solid Waste Incinerator (MSWI) Fly Ash Inertization, Based on Colloidal Silica. *Journal of Environmental Monitoring* **2010**, *12*, 2093, doi:10.1039/c0em00168f.
182. ISO 7404–2 Methods for the Petrographic Analysis of Coals—Part 2: Methods of Preparing Coal Samples. **2009**.
183. EN 15149-2 *Solid Biofuels – Determination of Particle Size – Part 2: Vibrating Screen Method Using Apertures of 3,15 Mm and Below.*; 2010;
184. ISO 9277 *Determination of the Specific Surface Area of Solids by Gas Adsorption-BET Method*; 2022;
185. ISO 10304-1 *Water Quality —Determination of Dissolved Anions by Liquid Chromatography of Ions — Part 1: Determination of Bromide,Chloride, Fluoride, Notrate, Nitrite, Phosphate and Sulfate*; 2007;
186. Colombi, P.; Agnihotri, D.K.; Asadchikov, V.E.; Bontempi, E.; Bowen, D.K.; Chang, C.H.; Depero, L.E.; Farnworth, M.; Fujimoto, T.; Gibaud, A.; et al. Reproducibility in X-Ray Reflectometry: Results from the First World-Wide Round-Robin Experiment. *J Appl Crystallogr* **2008**, *41*, 143–152, doi:10.1107/S0021889807051904.
187. del Valle-Zermeño, R.; Gómez-Manrique, J.; Giro-Paloma, J.; Formosa, J.; Chimenos, J.M. Material Characterization of the MSWI Bottom Ash as a Function of Particle Size. Effects of Glass Recycling over Time. *Science of The Total Environment* **2017**, *581–582*, 897–905, doi:10.1016/j.scitotenv.2017.01.047.
188. Doebelin, N.; Kleeberg, R. *Profex*: A Graphical User Interface for the Rietveld Refinement Program *BGMN*. *J Appl Crystallogr* **2015**, *48*, 1573–1580, doi:10.1107/S1600576715014685.
189. ISO 11722 *Solid Mineral Fuels-Hard Coal-Determination of Moisture in the General Analysis Test Sample by Drying in Nitrogen*; 2013;
190. ASTM C25-19 Standard Test Methods for Chemical Analysis of Limestone, Quicklime, and Hydrated Lime. *Book of Standards Volume 04.01. Pages 40* **2019**, doi:10.1520/C0025-19.
191. Walker, R.; Pavía, S. Physical Properties and Reactivity of Pozzolans, and Their Influence on the Properties of Lime–Pozzolan Pastes. *Mater Struct* **2011**, *44*, 1139–1150, doi:10.1617/s11527-010-9689-2.
192. Wypych, G. Physical Properties of Fillers and Filled Materials. In *Handbook of Fillers*; Elsevier, 2016; pp. 303–371.
193. Veetil, S.P.; Mercier, G.; Blais, J.-F.; Cecchi, E.; Kentish, S. Magnetic Separation of Serpentinite Mining Residue as a Precursor to Mineral Carbonation. *Int J Miner Process* **2015**, *140*, 19–25, doi:10.1016/j.minpro.2015.04.024.
194. Horák, J.; Kuboňová, L.; Bajer, S.; Dej, M.; Hopan, F.; Krpec, K.; Ochodek, T. Composition of Ashes from the Combustion of Solid Fuels and Municipal Waste in

Households. *J Environ Manage* **2019**, *248*, 109269, doi:10.1016/j.jenvman.2019.109269.
195. Beikmohammadi, M.; Yaghmaeian, K.; Nabizadeh, R.; Mahvi, A.H. Analysis of Heavy Metal, Rare, Precious, and Metallic Element Content in Bottom Ash from Municipal Solid Waste Incineration in Tehran Based on Particle Size. *Sci Rep* **2023**, *13*, 16044, doi:10.1038/s41598-023-43139-1.
196. Wei, Y.; Shimaoka, T.; Saffarzadeh, A.; Takahashi, F. Mineralogical Characterization of Municipal Solid Waste Incineration Bottom Ash with an Emphasis on Heavy Metal-Bearing Phases. *J Hazard Mater* **2011**, *187*, 534–543, doi:10.1016/j.jhazmat.2011.01.070.
197. Speight, J.G. Sources and Types of Organic Pollutants. In *Environmental Organic Chemistry for Engineers*; Elsevier, 2017; pp. 153–201.
198. Hörold, S. Phosphorus-Based and Intumescent Flame Retardants. In *Polymer Green Flame Retardants*; Elsevier, 2014; pp. 221–254.
199. Kalmykova, Y.; Karlfeldt Fedje, K. Phosphorus Recovery from Municipal Solid Waste Incineration Fly Ash. *Waste Management* **2013**, *33*, 1403–1410, doi:10.1016/j.wasman.2013.01.040.
200. Roskosch, A.; Mitwirkende, P.H.; Bannick, C.-G.; Brandt, S.; Bernicke, M.; Dienemann, C.; Gast, M.; Hofmeier, M.; Kabbe, C.; Schwirn, K.; et al. *Klärschlamm-entsorgung in Der Bundesrepublik Deutschland*; 2018;
201. Sommers, L.E. Chemical Composition of Sewage Sludges and Analysis of Their Potential Use as Fertilizers. *J Environ Qual* **1977**, *6*, 225–232, doi:10.2134/jeq1977.00472425000600020026x.
202. Le Forestier, L.; Libourel, G. Characterization of Flue Gas Residues from Municipal Solid Waste Combustors. *Environ Sci Technol* **1998**, *32*, 2250–2256, doi:10.1021/es980100t.
203. Ferreira, C.; Ribeiro, A.; Ottosen, L. Heavy Metals in MSW Incineration Fly Ashes. *Journal de Physique IV (Proceedings)* **2003**, *107*, 463–466, doi:10.1051/jp4:20030341.
204. Li, Y.; Ma, J.; Ren, Y.; Li, Y.; Yue, D. Calcium Leaching Characteristics in Landfill Leachate Collection Systems from Bottom Ash of Municipal Solid Waste Incineration. *J Environ Manage* **2021**, *280*, 111729, doi:10.1016/j.jenvman.2020.111729.
205. Shan, R.; Zhao, C.; Lv, P.; Yuan, H.; Yao, J. Catalytic Applications of Calcium Rich Waste Materials for Biodiesel: Current State and Perspectives. *Energy Convers Manag* **2016**, *127*, 273–283, doi:10.1016/j.enconman.2016.09.018.
206. Hassan, M.L.; Hassan, E.A.; Elseoud, W.S.A.; Moustafa, A.M. Utilization of Paper Sludge in Preparation of High-Purity Calcium Formate. *Biomass Convers Biorefin* **2023**, doi:10.1007/s13399-023-05216-3.
207. Wan, Z.; Li, J.; Yang, D.; Hou, S. Microstructural and Mechanical Properties Characterization of Graphene Oxide-Reinforced Ti-Matrix Composites. *Coatings* **2022**, *12*, 120, doi:10.3390/coatings12020120.
208. Alam, Q.; Hendrix, Y.; Thijs, L.; Lazaro, A.; Schollbach, K.; Brouwers, H.J.H. Novel Low Temperature Synthesis of Sodium Silicate and Ordered Mesoporous Silica from Incineration Bottom Ash. *J Clean Prod* **2019**, *211*, 874–883, doi:10.1016/j.jclepro.2018.11.173.
209. Golewski, G.L. Combined Effect of Coal Fly Ash (CFA) and Nanosilica (NS) on the Strength Parameters and Microstructural Properties of Eco-Friendly Concrete. *Energies (Basel)* **2022**, *16*, 452, doi:10.3390/en16010452.
210. Golewski, G.L. The Effect of the Addition of Coal Fly Ash (CFA) on the Control of Water Movement within the Structure of the Concrete. *Materials* **2023**, *16*, 5218, doi:10.3390/ma16155218.

211. D.M. 03/08/2005 *Definizione Dei Criteri Di Ammissibilità Dei Rifiuti in Discarica (Tabella 2)*;
212. D.M. 05/02/1998 *Individuazione Dei Rifiuti Non Pericolosi Sottoposti Alle Procedure Semplificate Di Recupero Ai Sensi Degli Articoli 31 e 33 Del Decreto Legislativo 5 Febbraio 1997, n. 22 (Allegato 3)*;
213. Sorrentino, G.P.; Guimaraes, R.; Cornelio, A.; Zanoletti, A.; Valentim, B.; Bontempi, E. Mitigating CO_2 Emissions through an Industrial Symbiosis Approach: Leveraging Cork Ash Carbonation. *Heliyon* **2024**, *10*, doi:10.1016/j.heliyon.2024.e32893.
214. Allal, K.M.; Dolignier, J.-C.; Martin, G. *Reaction Mechanism of Calcium Hydroxide with Gaseous Hydrogen Chloride*; 1998; Vol. 53;.
215. Shi, X.; Xie, N.; Fortune, K.; Gong, J. Durability of Steel Reinforced Concrete in Chloride Environments: An Overview. *Constr Build Mater* **2012**, *30*, 125–138, doi:10.1016/j.conbuildmat.2011.12.038.
216. Allal, K.M.; Dolignier, J.C.; Martin, G. Determination of Thermodynamical Data of Calcium Hydroxichloride. *Revue de l'Institut Français du Pétrole* **1997**, *52*, 361–368, doi:10.2516/ogst:1997046.
217. Galan, I.; Glasser, F.P.; Andrade, C. Calcium Carbonate Decomposition. *J Therm Anal Calorim* **2013**, *111*, 1197–1202, doi:10.1007/s10973-012-2290-x.
218. Ishida, T.; Maekawa, K. Modeling of PH Profile in Pore Water Based on Mass Transport and Chemical Equilibrium Theory. *Doboku Gakkai Ronbunshu* **2000**, *2000*, 203–215, doi:10.2208/jscej.2000.648_203.
219. Black, L.; Breen, C.; Yarwood, J.; Garbev, K.; Stemmermann, P.; Gasharova, B. Structural Features of C–S–H(I) and Its Carbonation in Air—A Raman Spectroscopic Study. Part II: Carbonated Phases. *Journal of the American Ceramic Society* **2007**, *90*, 908–917, doi:10.1111/j.1551-2916.2006.01429.x.
220. Han, Y.S.; Hadiko, G.; Fuji, M.; Takahashi, M. Factors Affecting the Phase and Morphology of $CaCO_3$ Prepared by a Bubbling Method. *J Eur Ceram Soc* **2005**, *26*, 843–847, doi:10.1016/j.jeurceramsoc.2005.07.050.
221. Zhao, Y.; Wen, L.; Zhang, Y.; Wang, J.; Yang, Z. Study on the Pyro-Hydrolysis of $CaCl_2$ with Steam and CO_2 by Experiments and DFT Calculation. *Colloids Surf A Physicochem Eng Asp* **2024**, *683*, 133075, doi:10.1016/j.colsurfa.2023.133075.
222. Zhang, X.; Asselin, E.; Li, Z. $CaCO_3$ Precipitation Kinetics in the System $CaCl_2$ –CO_2 –$Mg(OH)_2$ –H_2 O for Comprehensive Utilization of Soda Production Wastes. *ACS Sustain Chem Eng* **2021**, *9*, 398–410, doi:10.1021/acssuschemeng.0c07467.
223. Watanabe, H.; Mizuno, Y.; Endo, T.; Wang, X.; Fuji, M.; Takahashi, M. Effect of Initial PH on Formation of Hollow Calcium Carbonate Particles by Continuous CO_2 Gas Bubbling into $CaCl_2$ Aqueous Solution. *Advanced Powder Technology* **2009**, *20*, 89–93, doi:10.1016/j.apt.2008.10.004.
224. Baciocchi, R.; Costa, G.; Di Bartolomeo, E.; Polettini, A.; Pomi, R. The Effects of Accelerated Carbonation on CO_2 Uptake and Metal Release from Incineration APC Residues. *Waste Management* **2009**, *29*, 2994–3003, doi:10.1016/j.wasman.2009.07.012.
225. Brück, F.; Schnabel, K.; Mansfeldt, T.; Weigand, H. Accelerated Carbonation of Waste Incinerator Bottom Ash in a Rotating Drum Batch Reactor. *J Environ Chem Eng* **2018**, *6*, 5259–5268, doi:10.1016/j.jece.2018.08.024.
226. Pan, S.-Y.; Chang, E.-E.; Kim, H.; Chen, Y.-H.; Chiang, P.-C. Validating Carbonation Parameters of Alkaline Solid Wastes via Integrated Thermal Analyses: Principles and Applications. *J Hazard Mater* **2016**, *307*, 253–262, doi:10.1016/j.jhazmat.2015.12.065.
227. Hover, K.C. The Influence of Water on the Performance of Concrete. *Constr Build Mater* **2011**, *25*, 3003–3013, doi:10.1016/j.conbuildmat.2011.01.010.

228. Garbev, K.; Stemmermann, P.; Black, L.; Breen, C.; Yarwood, J.; Gasharova, B. Structural Features of C–S–H(I) and Its Carbonation in Air—A Raman Spectroscopic Study. Part I: Fresh Phases. *Journal of the American Ceramic Society* **2007**, *90*, 900–907, doi:10.1111/j.1551-2916.2006.01428.x.
229. Slegers, P.A.; Rouxhet, P.G. Carbonation of the Hydration Products of Tricalcium Silicate. *Cem Concr Res* **1976**, *6*, 381–388, doi:10.1016/0008-8846(76)90101-0.
230. Salminen, J.; Prausnitz, J. Carbon Dioxide in Chemical Processes. In *Developments and Applications in Solubility*; Royal Society of Chemistry: Cambridge, 2007; pp. 337–349.
231. Häusler, F.; Schmidt, H.; Freyer, D. Calcium Hydroxide Chlorides: The Ternary System $Ca(OH)_2$-$CaCl_2$-H_2O at 25, 40, and 60°C, Phase Stoichiometry and Crystal Structure. *Z Anorg Allg Chem* **2019**, *645*, 723–731, doi:10.1002/zaac.201900051.
232. Ali, S.; Ali S, A. Determination of Thermodynamic Parameters from the Dissolution of Calcium Hydroxide in Mixed Solvent Systems by PH-Metric Method. *J Phys Chem Biophys* **2013**, *03*, doi:10.4172/2161-0398.1000116.
233. Brady, P. V. *Physics and Chemistry of Mineral Surfaces*; Brady, P. V., Ed.; CRC Press, 2020; ISBN 9781003068945.
234. Ropp, R.C. *Encyclopedia of the Alkaline Earth Compounds*; Elsevier, 2013; ISBN 9780444595508.
235. Liang, D.; Wang, F.; Lv, G. The Resource Utilization and Environmental Assessment of MSWI Fly Ash with Solidification and Stabilization: A Review. *Waste Biomass Valorization* **2024**, *15*, 37–56, doi:10.1007/s12649-023-02275-5.
236. Benassi, L.; Pasquali, M.; Zanoletti, A.; Dalipi, R.; Borgese, L.; Depero, L.E.; Vassura, I.; Quina, M.J.; Bontempi, E. Chemical Stabilization of Municipal Solid Waste Incineration Fly Ash without Any Commercial Chemicals: First Pilot-Plant Scaling Up. *ACS Sustain Chem Eng* **2016**, *4*, 5561–5569, doi:10.1021/acssuschemeng.6b01294.
237. Fernández Bertos, M.; Li, X.; Simons, S.J.R.; Hills, C.D.; Carey, P.J. Investigation of Accelerated Carbonation for the Stabilisation of MSW Incinerator Ashes and the Sequestration of CO_2. *Green Chem.* **2004**, *6*, 428–436, doi:10.1039/B401872A.
238. Rendek, E.; Ducom, G.; Germain, P. Carbon Dioxide Sequestration in Municipal Solid Waste Incinerator (MSWI) Bottom Ash. *J Hazard Mater* **2006**, *128*, 73–79, doi:10.1016/j.jhazmat.2005.07.033.
239. Van Gerven, T.; Moors, J.; Dutré, V.; Vandecasteele, C. Effect of CO_2 on Leaching from a Cement-Stabilized MSWI Fly Ash. *Cem Concr Res* **2004**, *34*, 1103–1109, doi:10.1016/j.cemconres.2003.11.022.
240. Sanchez, F.; Gervais, C.; Garrabrants, A.C.; Barna, R.; Kosson, D.S. Leaching of Inorganic Contaminants from Cement-Based Waste Materials as a Result of Carbonation during Intermittent Wetting. *Waste Management* **2002**, *22*, 249–260, doi:10.1016/S0956-053X(01)00076-9.
241. Weng, J.K.; Langan, B.W.; Ward, M.A. Pozzolanic Reaction in Portland Cement, Silica Fume, and Fly Ash Mixtures. *Canadian Journal of Civil Engineering* **1997**, *24*, 754–760, doi:10.1139/l97-025.
242. Wang, L.; Jin, Y.; Nie, Y. Investigation of Accelerated and Natural Carbonation of MSWI Fly Ash with a High Content of Ca. *J Hazard Mater* **2010**, *174*, 334–343, doi:10.1016/j.jhazmat.2009.09.055.
243. Vassilev, S. V.; Baxter, D.; Andersen, L.K.; Vassileva, C.G. An Overview of the Composition and Application of Biomass Ash..: Part 2. Potential Utilisation, Technological and Ecological Advantages and Challenges. *Fuel* **2013**, *105*, 19–39, doi:10.1016/j.fuel.2012.10.001.

244. Park, C. *A Dictionary of Environment and Conservation*; Oxford University Press, 2007; ISBN 9780198609957.
245. Zacco, A.; Gianoncelli, A.; Ardesi, R.; Sacrato, S.; Guerini, L.; Bontempi, E.; Tomasoni, G.; Alberti, M.; Depero, L.E. Use of Colloidal Silica to Obtain a New Inert from Municipal Solid Waste Incinerator (MSWI) Fly Ash: First Results about Reuse. *Clean Technol Environ Policy* **2012**, *14*, 291–297, doi:10.1007/s10098-011-0401-1.
246. Waters, C.N.; Zalasiewicz, J.; Summerhayes, C.; Barnosky, A.D.; Poirier, C.; Gałuszka, A.; Cearreta, A.; Edgeworth, M.; Ellis, E.C.; Ellis, M.; et al. The Anthropocene Is Functionally and Stratigraphically Distinct from the Holocene. *Science (1979)* **2016**, *351*, doi:10.1126/science.aad2622.
247. Zanoletti, A.; Ciacci, L. The Reuse of Municipal Solid Waste Fly Ash as Flame Retardant Filler: A Preliminary Study. *Sustainability* **2022**, *14*, 2038, doi:10.3390/su14042038.
248. Fahimi, A.; Zanoletti, A.; Federici, S.; Assi, A.; Bilo, F.; Depero, L.E.; Bontempi, E. New Eco-Materials Derived from Waste for Emerging Pollutants Adsorption: The Case of Diclofenac. *Materials* **2020**, *13*, 3964, doi:10.3390/ma13183964.
249. Jones, M.W.; Peters, G.P.; Gasser, T.; Andrew, R.M.; Schwingshackl, C.; Gütschow, J.; Houghton, R.A.; Friedlingstein, P.; Pongratz, J.; Le Quéré, C. National Contributions to Climate Change Due to Historical Emissions of Carbon Dioxide, Methane, and Nitrous Oxide since 1850. *Sci Data* **2023**, *10*, 155, doi:10.1038/s41597-023-02041-1.
250. Yan, L.; Hu, J.; Fang, Q.; Xia, X.; Lei, B.; Deng, Q. Eco-Development of Oil and Gas Industry: CCUS-EOR Technology. *Front Earth Sci (Lausanne)* **2023**, *10*, doi:10.3389/feart.2022.1063042.
251. Metz, B.; Davidson, O.; de Coninck, H.; Loos, M.; Meyer, L. *IPCC, 2005: IPCC Special Report on Carbon Dioxide Capture and Storage. Prepared by Working Group III of the Intergovernmental Panel on Climate Change*; Cambridge University Press, Cambridge, United Kingdom and New York, NY, USA, 2005;
252. UNEP *Waste to Energy Considerations for Informed Decision-Making*; 2019;
253. Liu, W.; Shi, H.; He, X.; Pan, S.; Ye, Z.; Wang, Y. An Application of Optimized Otsu Multi-Threshold Segmentation Based on Fireworks Algorithm in Cement SEM Image. *J Algorithm Comput Technol* **2019**, *13*, 174830181879702, doi:10.1177/1748301818797025.
254. Usta, M.C.; Yörük, C.R.; Uibu, M.; Hain, T.; Gregor, A.; Trikkel, A. CO_2 Curing of Ca-Rich Fly Ashes to Produce Cement-Free Building Materials. *Minerals* **2022**, *12*, 513, doi:10.3390/min12050513.